University of Nevada, Reno

Towards Development and Implementation of eco^2-UHPC: Material Characterization and Applications to Structural Precast Columns

A dissertation submitted in partial fulfillment of the

requirements for the degree of Doctor of Philosophy

in

Civil and Environmental Engineering

by

Allan Joseph Romero

Dr. Mohamed A. Moustafa / Dissertation Advisor

May 2024

THE GRADUATE SCHOOL

We recommend that the dissertation
prepared under our supervision by

Allan Joseph Romero

entitled

**Towards Development and Implementation of eco²-UHPC:
Material Characterization and Applications to Structural Precast
Columns**

be accepted in partial fulfillment of the
requirements for the degree of

Doctor of Philosophy

Mohamed Moustafa
Advisor

Keri Ryan
Committee Member

David McCallen
Committee Member

Floriana Petrone
Committee Member

Mustafa Hadj-Nacer
Graduate School Representative

Markus Kemmelmeier, Ph.D., Dean
Graduate School

May, 2024

ABSTRACT

Ultra-high performance concrete (UHPC) is a rapidly growing construction material with excellent mechanical properties and enhanced ductility, making it a leading material for future infrastructure projects. Currently, UHPC is mainly used in architectural facades and small-scale structural applications, mostly for bridges such as field joints and overlays. One of the main challenges hindering the use of UHPC in large-scale applications is the high material and construction costs associated with the proprietary nature of the robust commercial UHPC mixtures and consequential logistical issues. Moreover, a significant amount of experimental work and research is still needed to fully understand the structural performance and behavior of UHPC and develop the proper design guidelines and codes. To contribute towards addressing some of these challenges, the goal of this doctoral study is to develop a scalable, economical- and ecological-friendly (eco^2) UHPC that enables the use of locally sourced along with sustainable components like recycled steel fibers for large-scale production and precast applications. The outcome of this study is new knowledge on eco^2-UHPC that stems from upscaling the use of local and recycled material with large-scale production mixing, for the first time, to perform both comprehensive material variability and characterization testing with structural prototyping and showcasing using axial and seismic precast eco^2-UHPC columns.

This doctoral study aims to demonstrate the viability and feasibility of eco^2-UHPC with the following research objectives: (1) perform a comprehensive mechanical characterization of eco^2-UHPC with recycled steel fibers by investigating the effects of fiber aspect ratio, fiber ratio by volume, and different production methods; (2) examine the scalability of eco^2-UHPC with wide range of locally sourced and sustainable materials, first through a material variability and

mechanical characterization testing, then application to five full-scale axial eco^2-UHPC columns that vary in reinforcement detailing, fiber type, and fiber ratio; (3) demonstrate large-scale mixing and production of eco^2-UHPC using actual precast practices and equipment to fabricate and test four eco^2-UHPC bridge columns with different ABC connections under combined axial and quasi-static lateral cyclic loading; and finally, (4) perform shake table tests to investigate the dynamic behavior of eco^2-UHPC bridge columns with ABC grouted duct connections. The doctoral study is concluded with key observations and findings with regard to the design, construction, and detailing of UHPC columns that can be the basis for future design guideline documents and specifications.

This Doctoral study is dedicated to my parents

(Remedios Romero and Arturo Romero)

and my brothers

(Alvin and Adrian Romero)

for their unconditional support and love

throughout this journey.

ACKNOWLEDGMENTS

I want to express my deepest appreciation to everyone who supported me throughout my journey, both in my successes and failures, as it has made me the person I am today.

I would like to express my sincere gratitude to my advisor, Dr. Mohamed Moustafa, who has been my mentor since my undergraduate studies. Your guidance and mentorship have played a pivotal role in shaping me into the person I am today. Your unwavering belief in my abilities has always been a source of inspiration for me, especially during moments of self-doubt. While I may not always express it, I truly appreciate your kindness and thoughtfulness, not just as a mentor but also as a friend.

I am grateful to the members of my committee, Dr. Keri Ryan, Dr. Floriana Petrone, Dr. David McCallen, and Dr. Mustafa Hadj Nacer, for their support and guidance throughout my research work. Their constructive feedback proved invaluable in shaping my research significantly.

I want to express my gratitude to the industry mentors and collaborators who supported me throughout my project. I would like to extend a special thank you to Ms. Ruth Lehmann of PCI West for always believing in my work. I am also grateful to Mr. Brent Koch and Mr. Eric Jensen for providing me with tremendous support during the construction of my project. I am also grateful to CorTuf leadership, who generously supplied all the UHPC components needed for my project. I would like to extend my appreciation to Dr. Amarnath Kasalanati and Dr. Arpit Nema for assisting me in the PEER Laboratory. A special thank you to the EEL Staff headed by Dr. Patrick Laplace, Chad Lyttle, and Todd Lyttle for their patience and understanding throughout my experimental work.

I would like to express my gratitude for the tremendous support I received from my colleagues: Dr. Milana Cimesa, Dr. Rolando Grijalva, Sammelan Pokharel, and Junfei Huang. They have been excellent companions throughout this journey. I would also like to thank my dear friends Princess Goldstein, Elizabeth Goldstein, and Allan Marquez, who have stood by me through both happy and difficult times.

To my dear brothers, Alvin and Adrian Romero, thank you for your unwavering support throughout the years. Your presence has been a great comfort during the difficult moments of my life. To my beloved aunt, Adelaida Dela Cruz, you have been like a second mother to me since I was a child. I am forever grateful for your love and guidance.

I would also like to express my heartfelt gratitude to my father, Arturo Romero. I admire and adore him for his understanding and patience toward me despite also the challenges he is facing. To my dear mother, Remedios Romero, you are my inspiration in all that I do. Your unconditional love has shaped me into the person that I am today. I hope that I have made you proud.

Lastly, I would like to offer my gratitude to almighty God. Without His presence and kindness, none of this would be possible. To God be the glory!

<div align="right">

Sincerely,

Allan Joseph Romero

</div>

TABLE OF CONTENTS

LIST OF TABLES

LIST OF FIGURES

1   INTRODUCTION

1.1   Ultra-High Performance Concrete

Ultra-high performance concrete, commonly known as UHPC, is an emerging cementitious material with exceptional mechanical properties and high durability. UHPC is a superior cementitious material with low water-to-binder ratio, typically less than 0.2, optimized granular particles based on particle packing theory, and steel fibers that enhance ductility and durability. UHPC has been utilized in numerous infrastructure projects due to its favorable service life attributes and ability to be shaped in thin and curved shapes of aesthetic appearance. Figure 1-1 shows the constructed Seonyu footbridge cast with UHPC. The Seoul Seonyu footbridge, an arch pedestrian bridge with a span length of around 400 ft, was one of the early implementations of UHPC [1]. Other notable projects include the first UHPC highway in the United States, the Mars Hill Bridge constructed in 2006, and the recently completed Delaware Memorial Bridge deck overlay project, which required more than 300 cubic yards of UHPC and was the most extensive UHPC construction and rehabilitation project in Northern America to date. It can be noticed that most of the full UHPC systems projects (like bridges in Malaysia or the footbridge example above) have been carried out elsewhere outside the United States, and the focus in the United States remains to be limited only to bridge joints and overlays that are also geographically concentrated on the East Coast side of the country. Few UHPC projects have been implemented on the West Coast, and only few UHPC projects have been considered in high-seismic regions like California and Nevada, where existing

structures are in need of seismic retrofitting or replacement. Thus, the demand for a sustainable and cost-effective UHPC for large-scale infrastructure systems in the region will increase and become more challenging in the next few years.

Despite the many superior qualities of UHPC, the implementation of UHPC in large-scale projects is hindered by the high cost related to the materials and production. According to Graybeal [2], commercial UHPC costs around $2,000/yd^3$, significantly higher than the normal strength concrete of only $100/yd^3$ [2]. Table 1-1 shows a sample cost estimate of some commercial UHPC in the market [3]. While UHPC is a reliable option for small-scale projects, the high cost makes it less attractive for larger infrastructure projects such as full structural members in high-rise buildings or highway bridges. One of the aspects that makes UHPC expensive is the logistics, including the procurement and delivery of the UHPC components. Currently, commercial UHPC vendors supply all UHPC components, which can be financially and logistically challenging, especially for large-scale projects. Additionally, commercial UHPC limits precast producers from utilizing locally sourced materials like cement and aggregate. Moreover, steel fibers used in UHPC increase the cost significantly and contribute to UHPC's already high carbon footprint. Thus, more research that focuses on addressing the economic and sustainable challenges of UHPC is timely and is the focus of this doctoral study.

Many researchers have recently prioritized efforts to develop economical UHPC. One approach is to incorporate locally sourced and recycled materials. Several State Departments of Transportation (DOT) have developed guidelines for developing and

using non-proprietary UHPC (NP-UHPC), allowing producers to formulate their UHPC using locally sourced materials [2,4-5]. Likewise, individual research studies, e.g., Alsalman et al. [3], showed the feasibility of using locally sourced materials in the mechanical performance of UHPC. Regarding recycled materials, Mosquera et al. [6] conducted experimental work on replacing cementitious components like quartz powder with recycled glass powder for UHPC mixtures. Recycled coarse aggregate from demolished bridge structures was used as an alternative to replace common aggregate for UHPC [7]. A few studies have also shown the potential of using recycled steel fibers (RSF) to enhance the tensile and flexural properties of normal-strength concrete (NSC) and UHPC [8-9]. The experimental results of using locally sourced and recycled materials suggest a promising potential for future structural applications.

1.2   Precast construction: Application to buildings and bridges

Over the past decades, precast structures have become attractive because of their reliability and efficiency in delivering construction. Prefabricated components that comprise precast structures are commonly both structural and non-structural components, including but not limited to piles, girders, columns, void slabs, and wall panels. Many research efforts have investigated conventional precast structures, and technical communities and institutions such as the Precast/Prestressed Concrete Institute (PCI) have already established, and continue to update, guidelines for implementing precast around the United States for the past decades. However, implementing UHPC in precast applications is still limited, and further research and experimental prototyping and testing are necessary.

Efforts to investigate UHPC in precast applications have increased in the past years, as reflected by the different initiatives of several agencies. Federal Highway Administration (FHWA) has published different reports on developing UHPC in precast and prestressed structures, focusing on bridge applications such as I-girders and deck panels [10-11]. Recently, the PCI joined the efforts in establishing a guideline for using UHPC in precast and prestressed concrete flexural members like girders and slabs [12]. Figure 1-2 shows one of the precast facilities that participated in establishing the PCI guidelines for UHPC [13]. These initiatives have precedented that UHPC can be the next conventional concrete in precast applications. Future projects have considered applying UHPC in bridge superstructures for accelerated bridge construction (ABC). However, only limited studies have been conducted, particularly on this topic. In addition, since current UHPC costs are still expensive, convincing precast producers to go for UHPC is still a long path, which motivates further studies to develop economical UHPC that can attract more precast facilities in the future.

1.3   Why ABC?

Rapid development with increased population has demanded that future infrastructures be resilient and safer in extreme events such as earthquakes. Infrastructures, particularly bridges, require special attention because bridges serve a crucial role in the economy, primarily for the mobility of goods and people. However, recent studies conducted by the American Road and Transportation Builders Association have shown that one out of three (1/3) bridges in the United States is structurally deficient, with an average of 5% identified in the West Coast region [14]. In addition, 35% of more than 200,000

American bridges that are due for urgent repair, might need full bridge replacement, which is foreseen to cost the DOT around $58 billion [14]. Since most of these structurally deficient bridges are candidates for complete replacement, new construction methods have been introduced to potentially address this problem. ABC provides a fast and reliable way of bridge construction that aims to reduce construction and labor costs, minimize downtime, and lessen traffic interruptions.

In ABC, bridge structure components such as columns and footings are typically prefabricated and cast remotely and are only connected on-site through special types of connections and field joints. These connections linking the structural members are designed with minimal reinforcement to avoid any congestion in the joint and allow for faster placement of the structural components and subassemblies. Two common types of ABC connections for column-to-footing or column-to-bent cap connections, which are relevant for this study, are: (1) grouted duct connections, and (2) pocket connections, which are designed differently but serve similar purposes. Figure 1-3 shows the difference in the design of pocket and grouted duct connections [15]. In grouted duct connections, precast columns have extended reinforcements inserted through corrugated ducts placed on another precast member. In pocket connections, precast footings or bent cap beams are designed to have pockets that allow a portion of the precast columns to be inserted uninhibited. However, the performance of both connections could be of a concern in high seismic regions, and further studies should still be pursued.

Although ABC can provide efficient and reliable bridge construction, it demonstrates a need for improvement, particularly in the connections or more on the prefabricated

elements like columns if new materials were to be used. Many studies investigating ABC bridges have shown damage formed in the column, particularly in the plastic hinge zone. Thus, ABC research focused on improving the connection and improving the damage in the columns, typically within the plastic hinge regions. However, these ABC studies focus mainly on the seismic performance of conventional concrete [14-15], which is not ideal for longevity and future low-damage resilient infrastructure systems. The life cycle of bridges made of conventional concrete lasts mostly around 50 years, which is a conservative estimate as bridges undergo repetitive fatigue, leading to concrete cracks and steel corrosion. Emerging research on improving concrete material has led to the development of UHPC. However, research efforts related to UHPC are still limited to small applications, and the need to investigate the behavior of UHPC in larger structural applications is warranted.

1.4   Research Motivation and Problem Statement

With the increase in extreme events and the growing number of aging infrastructure systems, UHPC has been gaining attention to become the concrete material for future infrastructures. Many researchers have proposed using UHPC in buildings or bridges to make our infrastructure stronger and more resilient. A recent study by Aboukifa and Moustafa [18, 19] tested full-scale non-slender and slender UHPC building columns. The study shows that UHPC in full-scale columns can deliver superior performance with lesser damage than NSC due to the combined effect of proper reinforcement detailing and the steel fibers providing additional confinement. In addition, current ACI 318 equations reveal an overestimation of the UHPC's axial load capacity by approximately 13% and

9% for non-slender and slender columns, respectively. Thus, the performance of UHPC in full-scale columns does not reflect the current ACI equation, proving a need for more experimental work regarding large structural applications of UHPC so that dedicated UHPC-sensible design guidelines can be developed for the various applications.

However, state agencies and industries still have reservations about implementing UHPC in precast structures, particularly for ABC, mainly because of the high cost and lack of proper experience in producing and handling UHPC at a larger scale. These valid concerns have motivated several researchers to find practical ways of reducing the cost of UHPC, such as optimizing components through economical materials. Thus, the motivation of this doctoral study is to develop and improve a sustainable, economical, and ecologically friendly (eco^2) UHPC as a new emerging type of UHPC suitable for large-scale precast applications.

This doctoral study performed several trials and tests to understand the mechanical and structural performance of using eco^2-UHPC. The first phase of this study stems down to developing and improving eco^2-UHPC by optimizing the recycled steel fibers (RSF) through different production methods with varying fiber aspect ratios and fiber ratios. Different mechanical characterization procedures were performed to determine the limitations of RSF that can affect the fundamental properties of UHPC and promote opportunities for RSF in structural applications. The study's second phase investigates the application of eco^2-UHPC with a wide variety of locally sourced and sustainable components for full-scale axially loaded columns. Since most literature investigated UHPC columns under axial loading are either small-scale or with full commercial UHPC,

no studies have been performed to incorporate locally sourced and sustainable components at scale in full-scale UHPC columns. A part of this study investigates the combined effect of using locally sourced material and RSF, and several parameters were varied, such as aggregate source and gradation, moisture content, and mixing procedures. Furthermore, the study provides experimental test work of full-scale columns that varied in reinforcement ratio and were cast with different UHPC design mixes, such as varying fiber ratios and the use of RSF. In the end, the significance of this phase is to promote eco^2-UHPC in precast applications and provide guidelines for future implementation.

The third phase of the study is to investigate the seismic performance of ABC precast bridge columns using eco^2-UHPC. Most ABC studies only used UHPC in the connection acting as a bond between two precast substructures. No studies have implemented full UHPC in ABC bridge columns, let alone implementing eco^2-UHPC using locally sourced and recycled materials. The motivation of this study is to verify if the seismic performance of ABC bridge columns is still valid for UHPC columns and provide recommendations for future design guidelines using the experimental data. The specific research objective and methodology are outlined in the next sections.

1.5   Research Objectives

The overall goal of this study is to investigate the performance of eco^2-UHPC using local and sustainable materials for large-scale precast applications. In this section, the specific and detailed research objectives for this dissertation are presented.

Objective #1: Develop and validate the use of recycled steel fibers (RSF) for future eco^2-UHPC

The aim is to integrate RSF into eco^2-UHPC and demonstrate its potential by investigating the mechanical properties and exploring the scalability of RSF for various structural applications. By applying diverse mixing methods, the mechanical performance of MSF and RSF were compared by varying the aspect and fiber ratios. The samples underwent testing at different ages using established ASTM standard specifications for UHPC, including axial compression, direct tensile tests, and flexural tests. Following the optimal fiber ratio for RSF, the batch was reproduced for the large-scale mixing of UHPC columns. Additionally, suggestions for optimizing RSF for use in precast applications were presented.

Objective #2: Experimentally validate the use of eco^2-UHPC that incorporates local and sustainable components for full-scale axial UHPC columns

The primary aim is to use local and sustainable materials like recycled steel fibers and demonstrate scalability by testing full-scale axial UHPC columns. A material variability study was conducted first with the parameters tested varied from aggregate type, gradation, moisture conditions, cement type, and mixing protocol. Several small trials were conducted utilizing a high-shear mixer, and samples were subjected to pure axial compression, direct tension, and flexural testing. Based on the results, the most effective aggregate, cement, and mixing techniques were chosen and utilized to cast full-scale columns. The secondary phase of the study furthers a deeper understanding of the

structural behavior of five full-scale eco^2-UHPC columns subjected to axial loading. The columns had varying transverse configurations, fiber types, and fiber ratios. The columns were subjected to concentric axial loading until failure, and results were analyzed based on axial force-strain, strain capacity in the reinforcement, and the impact of the aforementioned parameters.

Objective #3: Comparatively assess the structural response of full precast eco^2-UHPC columns utilizing upcycled recycled steel wires and fibers

The aim is to implement and understand the structural response, for the first time, of a large upcycling application of recycled steel wires and fibers for precast eco^2-UHPC columns. Two sets of identical bridge column-footing specimens with different ABC connections were constructed at two precast plants located in California and Nevada, using standard production equipment such as a truck mixer. The specimens were subjected to a combined axial and lateral loading using a displacement-based control actuator placed at the loading head of the column. The specimens were subjected to increasing drift ratios until the column failed. At the end of the test, a comparative assessment was conducted to evaluate the performance of the UHPC column based on the damage achieved, force-drift hysteresis, ductility, energy dissipation, and moment-curvature.

Objective #4: Investigate the dynamic behavior of eco^2-UHPC precast bridge columns with both MSF and RSF and ABC grouted duct connection with different grouting material

The aim of this study is to examine the dynamic seismic performance of full precast UHPC columns that utilize economical and scalable UHPC mixtures with RSF. Three scaled eco^2-UHPC columns with ABC grouted duct connections were constructed and tested on a shake table at the Earthquake Engineering Laboratory of UNR. Several parameters were investigated, such as comparing the dynamic behavior of UHPC columns with MSF and RSF and examining the connection performance using conventional grout and UHPC. The study was the first dynamic testing of large-scale UHPC columns, which aimed to provide new insights into the behavior of UHPC columns subjected to earthquake ground motions. Moreover, the result of this study contributes to the lack of experimental tests regarding seismic UHPC columns and can be used to verify future UHPC analytical models.

1.6   Research Methodology and Scope of Work

While the scope of work and adopted heavily experimental methodology used in this study can be implied from the discussion in previous section, a more detailed and formal statement of such aspects is provided next. This doctoral study aimed to develop eco^2-UHPC and test it through a series of substantial experimental works, from mechanical characterization to large-scale testing of UHPC columns. The work was divided into four smaller standalone projects or phases throughout the study, where each project is presented as a separate chapter (Chapters 2-5) in this dissertation. The methodology of this doctoral study was formulated based on each objective and the availability of mixing and testing equipment. The first and second objectives focused on a comprehensive material characterization of RSF, and the results were used to implement large-scale

mixing for the remaining objectives. Based on these characterization results, the last two objectives, including the axial columns in the second objective, successfully implemented eco^2-UHPC for large or full-scale columns by examining the overall performance using a series of quasi-static and dynamic loading tests.

During the study, eco^2-UHPC was mechanically characterized by using locally sourced and sustainable materials like RSF. Throughout the study, a total of 40 UHPC batches were mixed for material testing only, where 1765 cylinder samples, 655 dog bone samples, and 126 prisms were obtained and tested under compression, direct tensile, and flexure, respectively. Each batch was unique, with variations in aggregate source, cement type, fiber type, fiber aspect ratio, curing condition, and mixing methodologies. The aggregate was sourced from local quarries, construction supply stores, and a precast facility and carefully graded using standard sieving procedures to determine the percentage distribution of the aggregate size. The study examined two cement types: general cement (Type I) and high-sulfate resistance cement (Type V). Different unrefined raw RSF fibers and aspect ratios were considered to gain insight into their behavior on the material and large-scale levels. Lastly, the study documented the effects of curing conditions and mixing equipment to determine if existing precast practices were still applicable.

Based on the resulting mixture, a large-scale experiment was conducted using five full-scale columns under axial loading. The study focused on the effects of fiber type (MSF and RSF), fiber ratio (1% and 2% by volume), and confinement ratio (0.6% and 1.2%). These columns were constructed at the UNR Earthquake Engineering Laboratory (EEL)

fabrication yard and cast using multiple high-shear mixers. Afterward, the columns were transported to the Pacific Earthquake Engineering Research (PEER) Center at the University of California, Berkeley, where they underwent testing using the 4000-kip big press machine. Each column was heavily instrumented with LVDTs and strain gauges to measure the global and local behavior.

The next large-scale experiment was conducted to test seven scaled ABC column specimens under combined axial and lateral forces, focusing on understanding the behavior of UHPC columns. The study examined the impact of connection detailing (pocket and grouted duct), fiber type (MSF and RSF), and loading rate (quasi-static and dynamic). The columns were constructed by ConFab Precast LLC, a precast producer in California, using a production truck mixer, with footings constructed by Jensen Precast in Sparks, Nevada. Both columns and footings were transported and assembled at the EEL fabrication yard. The experiment involved four UHPC columns tested under quasi-static cyclic lateral loading with increasing drift demands. The columns had pocket connections with MSF and RSF and grouted duct connections with MSF or RSF. A 110-kip servo-hydraulic actuator and an axial spreader beam were placed at the loading head to subject the column to combined axial and lateral loading. Furthermore, three columns were tested at one of UNR's uniaxial shake tables with a similar setup as quasi-static columns, except that the actuator was replaced with a rigid link connected to a mass rig to simulate the inertial force during dynamic testing under increasing ground motion intensities. All columns were heavily instrumented using load cells, accelerometers, and string potentiometers to measure global behavior, including acceleration, relative drifts, force-

drift hysteresis, and energy dissipation. LVDTs and strain gauges were used to measure local behavior, such as strain profile and moment-curvature.

1.7   Dissertation Outline and Paper Submission

The dissertation is structured in a paper-based format comprising of four standalone papers in four chapters, along with two chapters for an overall introduction and final concluding remarks.

- Chapter 1: *Introduction*

  The chapter introduces the feasibility of eco^2-UHPC and its potential applications in precast columns, along with the research motivation, objectives, and methodology.

- Chapter 2: *Effect of Recycled Tires Steel Fibers Characteristics on Mechanical Properties of Scalable Ultra-Economical UHPC*

  This chapter is the first standalone paper that presents the mechanical characterization of eco^2-UHPC with RSF for potential future precast columns. This chapter performed a comprehensive variability study on recycled steel fibers and the effect of aspect ratio, fiber ratio, and different mixing techniques on mechanical properties such as compressive, tensile, and flexural strength. In addition, the study provided recommendations on the scalability of UHPC mixes with recycled steel fibers, which were the basis of large-scale production and experimental tests performed on the rest of the dissertation study. This chapter has been submitted to the Journal of Cement and Concrete Composites.

- Chapter 3: *Towards Scalable Economical UHPC: Material Characterization and Application to Full-Scale Axial Columns*

  This chapter discusses a material variability study and the application and experimental testing of full-scale axial eco^2-UHPC columns. This chapter demonstrated several large-scale experimental tests of full-scale axial UHPC columns that utilized locally sourced and sustainable materials. This chapter has been submitted to the Journal of Construction and Building Materials.

- Chapter 4: *Upcycling of Recycled Tires Wires at Scale: Application to Full Precast Economic Ultra-High Performance Concrete Bridge Columns*

  This chapter focuses on the structural response and evaluation of full precast UHPC bridge columns with RSF and different ABC connections. This chapters demonstrates the full-scale precast production of UHPC columns that utilizes locally sourced and sustainable materials. Additionally, the chapter compares the application of manufactured and recycled steel fibers in UHPC bridge columns for different ABC column connections and assesses them in various damage states. This chapter has been submitted to the Journal of Cleaner Production.

- Chapter 5: *Shake Table Tests of Economical Precast UHPC Columns with Different Fibers Types and Seismic Joint Materials*

  This chapter focuses on experimental shake table testing of precast UHPC columns with different steel fibers and grouting materials for the ABC seismic joint. Moreover, this chapter presents new information on the dynamic response

and plastic hinge behavior of UHPC columns. This chapter has been submitted to the Journal of Composites Structures

- Chapter 6: *Summary, Conclusions, and Recommendations for Future Work*

  This chapter provides an overall summary, key findings and conclusions, and recommendations for future work.

References

[1]   Behloul, M., & Lee, K. C. (2003). Ductal® Seonyu Footbridge. Structural Concrete, 4(4), 195-201.

[2]   Graybeal, B. (2013.). Development of non-proprietary ultra-high performance concrete for use in the highway bridge sector.

[3]   Alsalman, A., Dang, C. N., Martí-Vargas, J. R., & Micah Hale, W. (2020). Mixture-proportioning of economical UHPC mixtures. Journal of Building Engineering, 27, 100970.

[4]   Abokifa, M., & Moustafa, M. A. (2021). Full-scale testing of non-proprietary ultra-high performance concrete for deck bulb tee longitudinal field joints. Engineering Structures, 243, 112696.

[5]   El-Tawil, S., Alkaysi, M., Naaman, A. E., Hansen, W., & Liu, Z. (2016). Development, characterization, and applications of a non-proprietary ultra-high

performance concrete for highway bridges (No. RC-1637). Michigan. Dept. of Transportation.

[6] Redondo-Mosquera, J. D., Sánchez-Angarita, D., Redondo-Pérez, M., Gómez-Espitia, J. C., & Abellán-García, J. (2023). Development of high-volume recycled glass ultra-high-performance concrete with high C3A cement. Case Studies in Construction Materials, 18, e01906.

[7] Leng, Y., Rui, Y., Zhonghe, S., Dingqiang, F., Jinnan, W., Yonghuan, Y., Qiqing, L., & Xiang, H. (2023). Development of an environmental Ultra-High Performance Concrete (UHPC) incorporating carbonated recycled coarse aggregate. Construction and Building Materials, 362, 129657.

[8] Isa, M. N., Pilakoutas, K., Guadagnini, M., & Angelakopoulos, H. (2020). Mechanical performance of affordable and eco-efficient ultra-high performance concrete (UHPC) containing recycled tyre steel fibres. Construction and Building Materials, 255, 119272.

[9] Yang, J., Peng, G.-F., Shui, G.-S., & Zhang, G. (2019). Mechanical properties and anti-spalling behavior of ultra-high performance concrete with recycled and industrial steel fibers. Materials, 12(5), 783.

[10] Graybeal, B. (2006). Structural behavior of ultra-high performance concrete prestressed I-girders.

[11] Graybeal, B. (2006). Development of an ultra-high performance concrete precast bridge deck element.

[12] Guidelines for the use of ultra-high-performance concrete (UHPC) in precast and prestressed concrete. (2022).

[13] Lawler, J., Wagner, E., & Tadros, M. (2021). Ultra-high-performance concrete is ready to revolutionize precast, prestressed concrete.

[14] ARTBA Bridge Report. ARTBA,

[15] Chan, T. (2019). Ultra-High Performance Concrete for Precast Seismic Bridge Column Connection.

[16] Tazarv, M., and Saiidi, M. S. (2014). "Next generation of bridge columns for accelerated bridge construction in high seismic zones." Rep. No. CCEER-14-06, Center for Civil Engineering Earthquake Research, Dept. of Civil and Environmental Engineering, Univ. of Nevada, Reno, NV.

[17] Tazarv, M., & Saiidi, M. S. (2015). UHPC-filled duct connections for accelerated bridge construction of RC columns in high seismic zones. Engineering Structures, 99, 413-422.

[18] Aboukifa, M., & Moustafa, M. A. (2022). Reinforcement detailing effects on axial behavior of full-scale UHPC columns. Journal of Building Engineering, 49, 104064.

[19] Aboukifa, M., & Moustafa, M. A. (2022). Structural and buckling behavior of full-scale slender UHPC columns. Engineering Structures, 255, 113928.

Table 1-1 – Cost estimate of commercial UHPC (adopted from [3])

Commercially available UHPC mixtures.

Component	Ductal®	BSI®	CEMTEC ®	CRC®	BCV®	Cor-Tuf ®
Premix					2,115[c]	
Binder	1,154	1,283	1,318	920–940[b]	n/a	1,550
Cement	712	1114	1,050	n/a	n/a	758
Fine sand	1,020	1072	514	1,300–1,350	n/a	733
Silica fume	231	169	268	n/a	n/a	497
Ground Quartz	211	n/a	n/a	n/a	n/a	295
HRWRA	31	40	44	n/a	21	13
Accelerator	30	n/a	n/a	n/a	n/a	n/a
Steel fibers	156	234	470	150–300	156	140
Water	109	209	180	145–155		158
w/b	0.10	0.16	0.14	0.16	0.25	0.10
Price (dollar/m^3)	$2,600[a]	$1,632	$2,843	n/a	n/a	$1,496

Figure 1-1. Completed Seonyu footbridge using Ductal UHPC [1]

Figure 1-2. Placement of UHPC for precast applications [9]

Socket Connection   Grouted Duct Connection
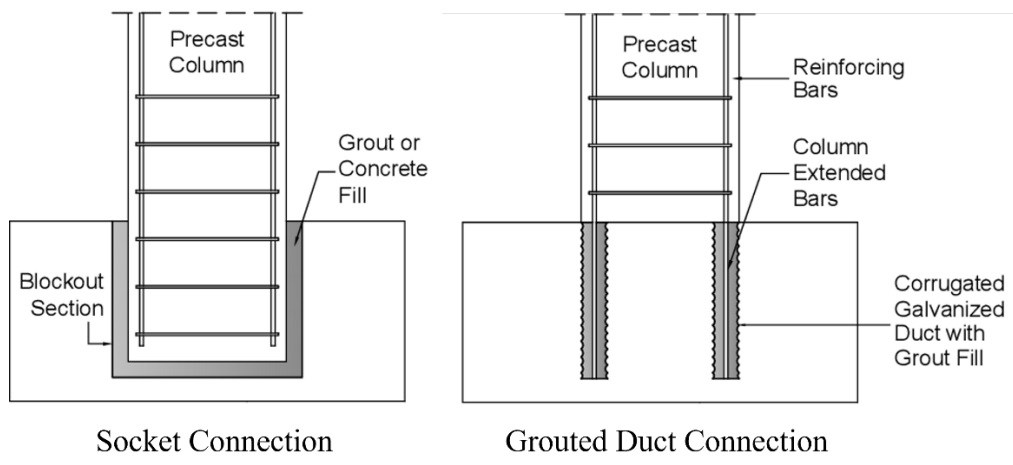
Figure 1-3. Layout view of socket/pocket connection vs. grouted duct connection [11]

2 EFFECT OF RECYCLED TIRES STEEL FIBERS CHARACTERISTICS ON MECHANICAL PROPERTIES OF SCALABLE ULTRA-ECONOMICAL UHPC

This chapter is a standalone paper that is ready to be submitted to the Journal of Cement and Concrete Composites

Abstract

Ultra-high performance concrete (UHPC) is gaining popularity for large-scale applications due to its superior mechanical performance and durability. However, the extent of large applications remains limited because of the high cost and carbon footprint of UHPC components like steel fibers. This study aims to incorporate different types of recycled steel fibers (RSF) from landfill tires as an alternative to manufactured steel fibers (MSF), specifically in semi- or non-proprietary UHPC mixtures, to realize and validate an ultra-economical UHPC solution. A base UHPC mixture with locally sourced materials is used to produce a total of 13 batches with varying steel fiber types (including different RSF), fiber ratios, and mixing mechanism and scalability. The study specifically focuses on understanding the effects of MSF and raw RSF characteristics, i.e., fibers diameter, length, and aspect ratio, on flowability and mechanical properties of UHPC using hundreds of compression, modulus of elasticity, direct tension, and flexural tests. Overall, the study outlines the opportunities and challenges of using RSF in scalable UHPC but also demonstrates, for the first time, the validity of RSF with a high aspect ratio and recommends the proper RSF dosage for comparable mechanical behavior as using high-end MSF.

Keywords: recycled steel fibers, economical UHPC, strain localization, cracking behavior

2.1   Introduction

The continuous demand for advanced construction materials has led to a rapidly growing market for robust and durable cementitious composites like ultra-high performance concrete (UHPC). Nonetheless, such growth directly calls for researching practical and ready-to-adopt solutions economy and sustainability aspects of scalable UHPC mixtures to allow for large applications and implementations. Compared to ordinary normal strength concrete (NSC), UHPC comprises finer components with a low water-cement ratio and steel fibers that bridge micro-cracks, leading to a more ductile response. Because of its superior mechanical characteristics, UHPC is currently used in some structural applications such as bridge deck field joints and overlays [1-2], and is continuously researched for new and larger applications such as structural beams and piles [3, 4]. Since UHPC is expected to increase in demand in the next decade, the high cost of UHPC tied to its proprietary nature or expensive critical constituents like steel fibers limits becomes a major concern that hinders mass production and construction industries from expanding into full structural systems and implementation at scale. Manufactured steel fibers (MSF), an essential UHPC component, constitute most of the total UHPC material cost. For example, adding 1.5% steel fiber by volume for a low-cost UHPC increases the price by $470/yd^3, making up 63% of the overall cost [5]. In addition, MSF significantly increases the carbon footprint in UHPC unless adequate reinforcements with reduced-cross sections are implemented to offset the increase in CO_2 by-product [6]. Ongoing research aims to reduce the cost and carbon footprint by

searching for alternative steel fibers that can perform effectively with UHPC but, more importantly, are practical and can be readily adopted if deemed acceptable for maintaining all the essential UHPC mechanical properties. Cheaper and more sustainable steel fibers, such as recycled steel fibers (RSF) from landfill tires, can be a viable solution that, when combined with non-proprietary or semi-proprietary mixtures with locally sourced materials, can produce an ultra-economical and sustainable UHPC as proposed and demonstrated in this study.

RSF is generated mostly from worn-out tires, typically as waste products of automobiles. Tires contain more than 50% rubber with 12-21% of high-performance quality steel wires, which helps increase stiffness and durability, resisting repetitive fatigue and stress [7]. At its end, a tire remains in waste facilities such as landfills, and about 300 million tires in the United States end up in these facilities yearly [8]. The overwhelming amount of disposed tires in these landfills can significantly increase the environmental pollutants and increase health risks [9]. Recycling steel fibers and wires is an effective and eco-friendly way of reducing the amount of tires that are in landfills. Standard techniques in recycling tires are shredding and mechanical recycling, while advanced processes such as pyrolysis and cryogenic are also effective in obtaining RSF [10]. Depending on the degree of the recycling procedure, RSF does not have uniform geometry, tensile strength, and homogeneity (presence of rubber residue) compared to MSF. These factors can potentially affect the workability and mechanical performance of UHPC. Therefore, there is a need for a full investigation to understand and implement the RSF in UHPC at scale.

Several studies have investigated the effects of RSF in NSC and UHPC. Workability is one of the identified challenges in using RSF in concrete. In NSC, several research studies have shown that a higher dosage of RSF can adversely affect the workability of fresh NSC mixes due to the interlocking of fibers [10]. Likewise, Abdolpour et al. [11] showed that distorted RSF creates interlocking issues within the fibers, causing a balling effect in the fresh UHPC concrete. Mixing RSF with other types of fibers also has an impact on workability. Isa et al. [12] found that increasing RSF dosage with recycled steel cords decreased the workability of UHPC. However, Zhong et al. [13] proved that increasing RSF fiber dosage mixed with MSF helped improve the workability in UHPC [13]. Overall, the workability of RSF in concrete mainly depends on the fiber dosage; a higher fiber dosage increases the chance of segregation and balling. As such, one investigation aspect of this study is to find the right RSF dosage that strikes a balance between acceptable workability and reserved mechanical superiority.

Another challenge of using RSF in concrete is its effect on the mechanical properties. In NSC, sufficient RSF dosage improved the mechanical performance regarding compressive, tensile, and flexural strength [14-16]. However, increasing or decreasing the RSF relative to the optimum dosage can negatively affect the mechanical performance, especially for flexural strength [17-19]. In UHPC, traces of rubber residue in RSF showed a decreasing trend in compressive strength [11-12]. In contrast, rubbers in RSF can benefit the UHPC by improving its splitting tensile strength and static elastic modulus [20]. Combining specific dosages of RSF with MSF improved the uniaxial and splitting tensile strength of UHPC [13]. Meanwhile, utilizing longer steel cords, tire

fibers greater than 9 mm long, and sorted tire fibers showed better flexural strength performance in UHPC as it efficiently benefits in bridging both micro and macro cracks [12]. In general, RSF at sufficient fiber dosage has promising results that can potentially replace MSF in fiber-reinforced concrete and UHPC.

Based on the above summary, previous RSF UHPC initiatives have demonstrated great potential but have the following limitations: (1) involved mainly small-scale mixing and trial UHPC mixtures that are not necessarily robust and scalable, (2) studied limited aspects of mechanical behavior without tying the properties to important fibers characteristics like RSF size and aspect ratio, (3) used mostly processed RSF with further processing (i.e., sorting and refining) that can increase the fiber cost due to the addition of cleaning equipment [22], and (4) RSF has been used in hybrid blends with MSF. None of the previous studies considered unrefined or raw RSF as a full replacement of MSF for economic scalability for large-scale structures and significantly reducing production costs and carbon footprint. None of the previous work also considered economic UHPC mixtures that allow the use of local sand, cement, and admixtures as the main matrix for such RSF trials. Moreover, guidelines for properly implementing RSF in UHPC are still lacking.

This study addresses the major knowledge gaps identified above and aims to implement and optimize the use of unrefined raw RSF for robust, economical UHPC mixtures that are scalable for large-scale applications. To be specific, the objectives of this study are to: (1) investigate the effects of two different types of RSF with varying characteristics and aspect ratios on workability and mechanical properties of UHPC, (2) demonstrate the

viability of producing RSF UHPC for mass production by using different mixing procedures and equipment including actual precast concrete practices, and (3) determine and quantify the comparative effect of RSF type, dosage, and mixing techniques on the mechanical performance of RSF UHPC with respect to reference MSF UHPC. This particular study involved 13 batches that span different variations of three parameters: fibers types, fibers dosage, and mixing method. Each batch was characterized for workability, compressive, tensile, and flexural performance. The paper provides the experimental program details, test results and discussions, and concludes with challenges and opportunities for implementation of RSF for future ultra-economical UHPC.

2.2   Materials and Experimental Program

This section provides the comparative characteristics of MSF and RSF along with the details of the utilized economic UHPC mixture, mixing procedures and material sampling, and overview of the flow and mechanical testing procedure.

2.2.1   Comparative Properties of MSF and RSF

To properly understand the fibers effect on the behavior of UHPC, the physical and mechanical characteristics of MSF and RSF were first determined in accordance to ASTM A820/A820M-16; the Standard Specification for Steel Fibers for Fibers Reinforced Concrete [23]. The experiments tested two types of RSF, Type I and II, and one standard type of MSF for comparison. Figure 2-1 shows visual samples of all three types of fibers used in this study. Type I and II RSF were sourced from two different tire recycling companies, and MSF was obtained from a standard steel fiber vendor for

UHPC. Both RSF types were not processed (e.g., no sorting and cleaning), and rubber residue remained on some fibers. A sample of 100 individual RSF was randomly selected to determine the nominal fiber length, diameter, and aspect ratio. Table 2-1 shows the summary of the full fibers geometric and mechanical properties for this experiment. The nominal fiber length (l_n) was measured based on the end-to-end length of the deformed RSF. The diameter of each fiber (d) was assumed to be the same across the fiber; thus, the effective diameter was not calculated. Measuring the nominal fiber length and diameter of RSF can provide a general idea of how the fibers interact with UHPC in terms of mixing and strength characterization.

Figure 2-2 shows the frequency and cumulative frequency of the nominal fiber length, diameter, and aspect ratio for Type I and II RSF. Note that due to MSF uniformity, there is no variation in fibers geometry and average values listed directly in Table 2-1. The nominal fiber length of Type I RSF varies from 0.3-1.7 in (8-42 mm), while Type II RSF ranges from 0.4-3.2 in (10-82 mm). Most of the Type I RSF has nominal fiber length skewed left, indicating that 98% of the fibers were less than 1.2 in (30 mm) with largest frequency 64% in the 0.4-0.8 in (10-20 mm) range. The result differs for Type II RSF, which has a more gaussian distributed nominal fiber length in the 0.4-2.0 in (10-50 mm) range with largest frequency of 28% in the 1.2-1.6 in (30-40 mm) range. The average nominal fiber length of Type I RSF was determined to be 0.62 in (16 mm) with a standard deviation of 0.24 in (6.1 mm), slightly above the typical length for MSF of 0.51 in (13 mm). However, Type II RSF have longer fibers with an average length of 1.27 in (32 mm) and a standard deviation of 0.54 in (13.7 mm).

Similar analysis was done for the fibers diameter and shown in Figure 2-2. As shown, the diameter of Type I RSF varies from 0.005-0.040 in (0.13-1.02 mm), and Type II RSF ranges from 0.008-0.077 in (0.2-1.96 mm). Different from the nominal fiber length, the diameter for both types of RSFs was skewed left, indicating that 98% and 83% of the steel fiber diameter for Type I and Type II were below 0.020 in (0.5 mm), respectively. About 55% and 53% of Types I and II RSF, respectively, have a 0.01-0.02 in (0.25-0.5 mm) diameter, followed closely by 43% and 30% less than 0.01 in (0.25 mm) for the two types, respectively. The calculated average diameter of Type I RSF was 0.011 in. (0.28 mm) with a standard deviation of 0.005 in. (0.12 mm), slightly higher than MSF diameter of 0.008 in (0.20 mm). Moreover, Type II RSF has thicker fibers with an average diameter of 0.018 in (0.46 mm) and a standard deviation of 0.016 in (0.41 mm).

Measuring the nominal fiber length and diameter of the fibers provides a general idea of the type of RSF in hand. However, the relationship between the fiber length and diameter, as expressed in terms of aspect ratio, can provide more information. For example, a shorter fiber with a thicker diameter can respond better to early cracking by bridging microcracks and sustaining more load. Meanwhile, a longer fiber with a thinner diameter can help bridge macrocracks but can potentially lose tensile strength rapidly. Figure 2-2 also shows the distribution of fibers aspect ratio for both types of RSF, which varies from 21-123 and 21-197 for Type I and II RSF, respectively. Considering the aspect ratio of 65 for typical MSF, 76% of the Type I RSF falls below 75, and only 37% of the Type II RSF of the same category. Furthermore, the average aspect ratio of Type I RSF was 60, with a standard deviation of 21.7, and Type II RSF has an aspect ratio of 93,

with a standard deviation of 46.5. Based on the samples collected, Type I RSF has a lower aspect ratio on average compared with the MSF. Meanwhile, Type II RSF has a higher aspect ratio than Type I RSF and MSF, indicating relatively longer and thinner fibers.

Other important properties of steel fibers are the tensile strength and density. Table 2-1 provides the average tensile strength and density of the MSF, Type I RSF, and Type II RSF. The average tensile strength of RSF was reported to be around 283 psi (1,948 MPa). The tensile strength of RSF is expected to be lower than that of MSF since the tires' life cycle and recycling process affect the fibers' quality and integrity. Moreover, the average density of Type I and II RSF was determined to be 313 lb/ft^3 (5,018 kg/m^3) and 300 lb/ft^3 (4,807 kg/m^3), respectively. The density of RSF was relatively lower than MSF because of heavier mass, larger volume, and presence of rubber impurities. In fiber reinforced concrete and UHPC, fibers density is used to calculate the volume of fibers in concrete mix; however, measurement of RSF in concrete can also be based on weight, which is preferred in field applications [24].

2.2.2   UHPC Mix Design and Proportions

One of the key contributions of this study is to tie the RSF implementation with an economic UHPC matrix to eventually achieve ultra-economic UHPC mixtures. As such, a semi-proprietary UHPC solution was adopted where a commerical UHPC premix from Cor-Tuf was used in conjunction with locally sourced cement, sand, admixtures, and fibers. A total of 13 batches were produced for this study where each UHPC batch differed in either steel fibers ratio, fibers type, or mixing scale and procedure as

summarized in Table 2-2. All batches were given a specific ID depending on the variations in the UHPC mixture. Since volume is difficult to measure in the field, each component was converted by its equivalent weight. The lines in the batch ID consecutively indicate the phase (P1, P2, or P3), fiber dosage by volume (0% to 6.3%), fiber type (M: MSF, R1: RSF Type I, R2: RSF Type II) and mixing procedure (S: high-shear mixer for small batches, T: truck mixer for production scale).

The mixing of the UHPC was divided into three phases. The first phase explored the application of Type I fibers and MSF at increasing fiber ratio. All first-phase batches were mixed using a high-shear Imer mixer. The amount of Type I RSF was initially determined by volume using the average density. The volume of the fibers varied from 0%-4% at increments of 1%. The calculated amount of Type I RSF fibers for fiber volume of 1%, 2%, 3%, and 4% was 3.1 lb., 6.3 lb., 9.4 lb., and 12.5 lb. per ft^3, respectively. The amount of Type I RSF was compared against the calculated amount of MSF for the same fiber volume and determined to be 4.9 lb., 9.8 lb., 14.7 lb., and 19.6 lb. per ft^3. Because of the lower density of Type I RSF, the amount of Type I RSF needed to match the MSF by the same volume was relatively lower. Since Type I RSF has an inherently lower aspect ratio and weaker tensile strength, the amount of RSF was adjusted by matching the weight of the RSF and MSF fibers (as reflected in Table 2-2). Thus, the resulting mixes of Type I RSF had 1.6%, 3.1%, 4.7%, and 6.3% fiber by volume. The effect of lower fiber amount for Type I RSF, even with adjusted weight, is discussed later as part of tests results.

The second and third phases investigated Type II RSF used in UHPC. The second phase batches were mixed using again same high-shear Imer mixer, while a typical precast plant concrete truck mixer was used for all the third-phase mixing. Initially, the goal was to compare Type II RSF with Type I RSF using the same volume of fibers from the first phase. However, mixing Type II RSF was more challenging and was not even possible for 3% or 4% fiber volumes. The density of the Type II RSF was also relatively lower than that of MSF; thus, the fiber amount of Type II RSF was adjusted precisely to the same amount of MSF by weight. Hence, the resulting mixes of Type II RSF that were possible to mix and realize had 1.6% and 3.2% fiber ratio by volume.

2.2.3   Mixing Protocol and Sample Preparations

Typical standard procedures for mixing UHPC were followed as illustraetd in Figure 2-3. Each batch in the first and second phases had an average volume of around 1.5 ft^3 (0.04 m^3), while the third phase for truck mixing had around 2.4 yd^3 (1.83 m^3). All the dry components except the steel fibers were added first to the mixer and mixed for about two minutes to homogenize. Next, the HRWRA and half of the water were added into the mixer. The remaining half of the water was placed after two minutes of additional mixing. Roughly after 10-15 mins, UHPC started formulating, and the steel fibers were then added. For the truck mixing, the RSF was dispersed manually. After mixing, UHPC was poured into molds, and samples were kept at room temperature and humidity. A total of 258 cylindrical molds, 223 dog bones, and 96 rectangular prisms were prepared for compression, direct tension, and flexure tests, respectively.

2.2.4   Testing Protocol

Several tests were comprehensively considered in this study. First, flowability tests were performed to assess the consistency and workability of the fresh UHPC mixture. Both static and dynamic flow tests were considered in accordance with the relevant standard ASTM procedure, i.e. ASTM C1437 and C230 modified by C1856 [25-27]. Static flowability tests were recorded within two minutes after the UHPC was released from the cone or when settled. Meanwhile, some batches were tested for dynamic flowability by applying 25 tapping/drops in 15 seconds. Both flowability tests calculated the average diameter based on two directions within flow table.

For compression testing, ASTM C1856 [25] was used to assess the UHPC compressive strength and obtain full stress-strain relationships as well as modulus of elasticity (MOE). The tests used 3 in $\times$ 6 in (75 mm $\times$ 150 mm) cylindrical specimens. Each cylinder was carefully prepared before testing by cutting the top 0.25 in (6.4 mm) weak crust, then both ends were ground for parallelness within a tolerance of 0.5° inclination. All cylinders were tested using a 500-kip SATEC compression machine and instrumented as shown in Figure 2-4. The samples were tested at a loading rate of 145 ± 7 psi/sec (1.0 ± 0.05 MPa/sec). All loading and strain output was recorded using a DAQ system, and a sample tested cylinder is also shown in Figure 2-4.

Direct tension tests (DTT) were considered in this study to estimate the UHPC tensile strength. The Federal Highway Administration (FHWA) in the US and several studies in the literature propose the use of DTT for UHPC because of its reliability in estimating the tensile response [28-30]. In this study, the DTT setup and adopted dog bone specimen

shape and size are shown in Figure 2-4. Two cross-section sizes were considered for the dog bone specimens: 1 in × 0.5 in (25 mm ×13 mm) or 1 in × 1 in (25 mm × 25 mm) An Instron machine with hydraulic grips was used to test the dog bone samples. Laser targets were placed in one specimen side at about 3 in (75 mm) apart, serving as the gauge length for measuring the strain using laser extensometer. The loading protocol followed a displacement-controlled loading with a loading rate that started at 0.005 in/min and increased to 0.08 in/min after peak. The average tensile strength and strain were determined using the recorded load and displacement data. Figure 2-4 shows an example of one of the tested dog bones and the cross-section after testing.

Another approach to assess the tensile strength of the UHPC is to perform four-point bending test. Several studies have performed inverse analysis to estimate tensile stress-strain from flexure tests [31-32]. The test setup for flexure testing is simpler than DTT and in turn, recommended by entities like the PCI to use for UHPC characterization. The four-point bending tests were performed following ASTM C1609 with modification from ATSM C1856 [25, 33]. The ASTM C1856 suggests that prism dimensions differ accordingly with the fiber length; however, the fiber length for both types of RSF varies significantly. Thus, the prism dimensions of 3 in × 3 in × 12 in (75 mm × 75 mm × 305 mm), based on MSF's fiber length, were kept similar for all samples of different fiber types. Figure 2-4 shows the flexure/bending test setup which also user laser targets along the prism midpoint to measure deflections. Figure 2-4 shows a sample UHPC prism after flexure testing. The bending stress was calculated using the recorded load and prism

dimensions, and modulus of rupture (MOR) was determined as per ASTM using maximum load.

2.3   Results and Discussion

2.3.1   *Flowability Test*

Using high range water reduction admixtures (HRWRA), UHPC achieves high flowability that ensures allow self-compactability and reaching to tight spaces within congested reinforcement without using any vibrating and compacting equipment. Acceptance flowability for UHPC has been recommended by different agencies, such as PCI (adapted from ASTM C1856), which requires flowability between 8-10 in (200-250 mm) [25, 34]. Several state and federal agencies reported flowability ranging from 7-11 in (178-280 mm), which is becoming the acceptable standard flow for UHPC [35-37]. Flowability reported in guidelines and literature considers only MSF, so more studies are needed to report flowability of RSF UHPC as provided here. Figure 2-5 shows the results from static flow tests conducted for the different UHPC batches, and Figure 2-6 summarizes the average spread diameter from static and dynamic tests.

Noticeably, for phase I batches, the average static flow decreased as the MSF fiber dosage increased. In addition, only P1-1%-M-S and P1-2%-M-S attained acceptable flowability of greater than 8 in (200 mm) according to the PCI guidelines. Meanwhile, all batches with Type I RSF showed good consistency without evidence of fiber clumping and segregation. The average spread diameter for Type I RSF ranged from 8.2-8.9 in (207-226 mm). The flowability improvement of Type I RSF, even with increased fiber

dosage, can be attributed to the lower aspect ratio than MSF. The lower aspect ratio of the Type I RSF reduces the chance for fibers to clump together or segregate. In the dynamic flow test, all batches in phase I recorded acceptable flow except P1-4%-M-S, which resulted in an average spread of 7.5 in (191 mm). Most dynamic flow tests for Type I RSF achieved more than 9 in (228 mm) spread, which agree with some case studies in the literature that also reported average spread of about 9 in (228 mm) [35, 38].

On the contrary, UHPC with Type II RSF demonstrated difficulty mixing after placing the fibers in the mixer. Fiber clumping and segregation was observed in the flow tests as illustrated in Figure 2-5 (see P2-3.2%-R2-S for instance). The fiber clumping and segregation can be attributed to the higher aspect ratio of Type II RSF. The resulting flow of P2-3.2%-R2-S prompted the reduction of fiber dosage. P2-1.6%-R2-S showed an acceptable static flow of 8.6 in (218 mm) with minor fiber clumping. Nevertheless, when similar mixture and RSF dosage was used in truck mixing (P3-1.6%-R2-T), fiber clumping and segregation were observed due to the reduced shearing power of the truck mixer which seems to be insufficient to disperse the fibers as well as the high-shear mixer. In general, the biggest limitation for RSF UHPC truck mixing was that steel fibers were not fairly distributed, causing the fibers to clump together.

2.3.2 *Compression Strength Gain and Stress-Strain Behavior*

The compressive strength gain of UHPC with MSF and RSF, for both the early and late ages, was recorded and shown in Figure 2-7. The mixing process for MSF and RSF fibers with similar fiber dosages underwent a same-day casting and curing regimen to ensure that no additional parameters (i.e., temperature and humidity) can affect the compressive

strength except for the fiber type. For completeness, Table 2-3 summarizes the peak compressive strength, strain, and MOE from the 7 and 28-day tests for all batches. Most batches gained more than 10 ksi (69 MPa) of compressive strength as early as Day 3. In addition, regardless of the fiber type, volume, and aspect ratio, early age results showed only a slight difference in the average compressive stress. The compressive strength of Type I RSF UHPC was slightly lower than that of MSF by ~10% on average, while that of Type II RSF was even lower. The decrease in compressive strength can be attributed to the high aspect ratio of Type II RSF, which caused fiber balling and clumping, leaving voids and traces of dry mix in the material samples.

At older ages, the difference in the compressive stress between RSF and MSF UHPC became more apparent. Using the samples from the 13 batches, the average compressive stress from both Type I and II RSF UHPC at 28-day age was 18.9 ksi (130.5 MPa) versus 21.8 ksi (142.2 MPa) for MSF UHPC. On Day 56, the compressive strength of Type I and II RSF reached 20 ksi (137.9 MPa), while MSF reached 22 ksi (152 MPa). The replacement of MSF with RSF caused the average compressive strength to decrease by around 13.3% and 9.1% at 28- and 56-day age, respectively. The decrease in compressive strength of RSF can be associated with many factors, such as the presence of rubber impurities in the steel fibers affecting the particle packing, higher aspect ratio, and mixing quality. Using results from average compressive strength, the predicted compressive strength gain was plotted in Figure 2-7 based on prediction model in [37]. Most MSF and RSF mixes showed a similar trend to the predicted compressive strength gain except for the early ages of Type II RSF and use of truck mixing.

As mentioned before, all compression tests were instrumented to obtain full stress-strain relationship. Figure 2-8 shows the average compressive stress-strain relationship of MSF and Type I RSF UHPC with varying fiber dosages and at different ages. The figure suggests that specific fiber dosages of RSF can be effective and comparable to MSF in UHPC. For instance, the stress-strain behavior of MSF at 1.0% and 2.0%, and Type I RSF at 1.6% and 3.1% RSF fiber dosages suggests minimal difference, with maximum stress differing by less than 3%. However, as the fiber dosage of Type I RSF increased to 4.7% and 6.3%, the compressive stress reduced by 5-15% at late ages. The decrease in compressive strength can be attributed to rubber in the fibers, increasing the air voids in the UHPC [11-12]. Although increasing the fiber content of Type I RSF reduced the compressive strength in general, the higher fiber content of Type I RSF does not significantly reduce the compressive strength, which can be helpful to improve other properties such as tensile and flexural as shown in next sections.

Similarly, Figure 2-9 shows the compressive stress-strain relationship of Type II RSF UHPC. The compressive strength of P2-1.6%-R2-S and P2-3.1%-R2-S decreased by 2-16% relative to P1-2%-M-S. However, the increase in fiber ratio does not significantly affect the peak compressive strength. Regarding using different mixers, P3-1.6%-R2-T showed a decrease in compressive strength by 6-11%. Unlike Type I RSF, reducing the volume to 1.6% Type II RSF can be suggested to improve the workability and increase the compressive strength; however, careful considerations should be followed in reducing the fiber ratio as it can negatively affect the tensile and flexural properties. Overall, since the compressive strength difference was minimal for both types of RSF, Type I RSF can

benefit from higher dosage (4.7-6.3%) while Type II RSF benefits from lower dosage (1.6%) and still be advantageous in obtaining acceptable compressive results.

2.3.3 Modulus of Elasticity (MOE) Assessment

The MOE was determined from the instrumented cylinder compression tests based on ASTM C469/C469M. Figure 2-10 shows the calculated MOE for every individual tested UHPC cylinder with MSF and RSF. The MOE was calculated using the best-fit linear approximation from 10-30% of the maximum compressive strength. The MOE of MSF UHPC ranged from 4,574-6,836 ksi (31.5-47.1 GPa), while Type I and II RSF UHPC altogether ranged from 4,740-6,421 ksi (32.7-44.3 GPa), for compressive strength greater than 20 ksi (138 MPa). The results from the MOE were compared to the newly proposed AASHTO equation (see Figure 2-10) for predicting UHPC MOE based on compressive strength [39]. In the AASHTO equation, the estimated MOE (E_c) is calculated using the compressive strength (f_c') and a K_1 factor, which can be adjusted based on experimental results or taken as a 1.0 default value. As observed, if $K_1 = 1.0$, the equation overestimates the MOE of the proposed and tested ultra-economical UHPC type. A fitting regression model was performed to calculate a new value of K_1. The calculated new K_1 for MSF and RSF UHPC are determined to be 0.81 and 0.79, respectively. Since the K_1 factor for both fibers was close, the K_1 factor is simplified, and a value of 0.8 is proposed for this UHPC type.

2.3.4 Tensile Behavior and Strain Localization

A distinct characteristic of UHPC compared to other concrete types is the capability to achieve and sustain relatively higher tensile strength through ductile behavior with large

strain capacity that is attributed to the help of steel fibers. Unlike NSC, the tensile response of UHPC can be characterized into three stages: the elastic region, the tension hardening, and the localized straining [40]. In the second phase when the tensile response transitions from linear elastic to tension hardening, the strain increases significantly with a slight increase in tensile strength and microcracks begin to transition to macrocracks. Steel fibers are observed to help bridge macrocracks and further increase the strain capacity. Subsequently, the tensile response reaches the localized strain wherein damage is concentrated in a single large crack develops where the steel fibers bridging effect come to an end as the fibers debond, slip, and separate.

Figure 2-11 shows the average tensile stress-strain response for different UHPC types where the first cracking stress, strain localization, and the corresponding stress are identified on the plots. The first cracking stress and strain were determined by the intersection of the recorded tensile stress-strain and a 0.02% offset linear line with a slope equal to the elastic modulus [40]. A summary of the first cracking stress and strain values for each batch are presented in Figure 2-12. Comparing the first cracking strength of MSF and Type I RSF shows up to 47% difference. In addition, as the fiber dosage increased, the difference in the first cracking strength decreased between MSF and Type I RSF. For Type II RSF, the first cracking strength of 3.2% fiber for Day 7 was relatively higher than 1.6%; however, no significant increase was noted at Day 28 for the 1.6% and 3.2 % RSF dosage. Furthermore, the first cracking strength of 2% MSF UHPC is shown to be 18.5% higher than the 1.6% Type II RSF UHPC (whether truck mixing or high-shear mixing were used).

Generally, when the fiber dosage was reduced, the first cracking strength decreased regardless of the fiber type. The lower fiber amount causes the micro-crack to grow rapidly, unlike the sample with an adequate amount of steel fibers. The cracking strength for RSF was lower than MSF, regardless of the fiber volume and mixing power. Moreover, the first cracking strain ranges from 0.05-0.09%, regardless of the fiber, which is expected as most of tensile strain is yet governed by the cementitious matrix at the instant. The third stage also identified the crack localization based on the tensile stress-strain response. Typically, the crack localization strain and corresponding stress are determined at the moment of visual detection of a single crack becoming evident in the sample. Although visual inspection can be utilized, it can result in bias and error and potentially underestimate or overestimate the localization stress. Since all samples exhibited tensile hardening after the first cracking strength, the crack localization stress was considered at the maximum recorded stress [40]. Once the crack localization was identified, the tensile response gradually decreased as observed for all the tested UHPC batches and types.

Figure 2-12 also summarizes the stress and strain localization for each batch. For Day 7, the stress localization of MSF UHPC ranged from 1.34-2.13 ksi [9.2-14.9 MPa] while Type I RSF UHPC ranged 1.09-2.01 ksi [7.5-13.9 MPa]. As the sample reached Day 28, the stress localization of MSF UHPC increased by up to 49.3%, while the Type I RSF UHPC increased by up to 32.6% relative to Day 7. Furthermore, the recorded stress localization of MSF and Type I RSF UHPC indicated a 30-54% difference for the 2% MSF (3.1% RSF) dosage. However, as the fiber dosage increased to 3% and 4% for MSF

(4.7% and 6.3% for RSF), the difference in maximum stress decreased to 8-11%. Hence, it is shown that a higher volume of Type I RSF was needed to offset the reduction of stress localization. Regarding Type II fibers, the stress localization of 1.6% and 3.2% fiber dosages on Day 7 was 1.53 ksi (10.5 MPa) and 1.86 ksi (12.8 MPa), respectively. However, the stress localization did not significantly increase on Day 28. Using a truck mixer, the stress localization of 1.6% Type II RSF UHPC decreased by 25% compared to the 2% MSF. Additionally, using truck mixer decreased the maximum observed stress by 14% compared to high-shear mixing methods, which confirms that the quality of mixing directly affects various aspects of the mechanical behavior associated with fibers distribution like tensile response.

In general, observing early and late ages, the crack localization stress slightly increased, indicating that the tensile strength of UHPC can reach at an early age regardless of the fiber type and volume. Furthermore, the trend shows that the stress localization of Type I and II RSF UHPC is lower than that of MSF. The result can be attributed to the mechanical deterioration and recycling procedure of RSF before application, which relatively reduce the tensile performance. Moreover, having fibers with a high aspect ratio, such as Type II RSF, improved the stress localization compared to Type I RSF, as evident from the 1.6% and 3.2% fiber dosages.

Unlike the first cracking strain, the strain localization significantly differs between MSF and RSF. The results show that Type I RSF lead to significantly lower UHPC localization strain than MSF except for 4% MSF/6.3% RSF case. For fiber dosage of 1% to 3% MSF (1.6% to 4.7% RSF), replacing MSF with Type I RSF decreases the strain localization by

about 30-53% for Day 7 and 39-44% for Day 28. The lower localization strain of Type I RSF UHPC can be attributed to reduced tensile hardening of RSF caused by weaker fiber or a smaller aspect ratio. On the contrary, when 4% fibers were used, the strain localization of MSF was relatively lower by 30% and 17% for Day 7 and 28, respectively. If an excessive amount of fiber dosage was used, the strain localization decreased in the case of the 4% MSF. Excess fibers can affect the synergism between the UHPC cementitious matrix and the fibers. However, the scenario differs for 6.3% Type I RSF, where the crack localization strain improved. Since the aspect ratio of Type I RSF was lower than MSF, increasing Type I RSF with up to 6.3% fiber dosage provides a better bridging effect in the UHPC and improves the tensile hardening. Regarding Type II RSF, the strain localization was relatively higher than Type I RSF and select MSF dosage. The improvement of strain localization with Type II RSF can be tied to the higher aspect ratio as it provides better anchorage when macro-cracks develop. Overall, the capabilities of UHPC using RSF to reach higher strain localization depend on the aspect ratio and adequate fiber dosage.

2.3.5 *Flexural Behavior*

Sometimes used as an alternative to DTT, four-point bending tests or simply flexural tests provide a simpler method to assess the tensile properties of UHPC (because it typically uses same equipment for compression testing) but in an indirect way. Figure 2-13 shows the comparative performance of the average flexural stress-deflection relationship of MSF and RSF UHPC. Based on the results, the flexural behavior of UHPC performs similarly to the tensile test. In the earlier stage, the flexural stress-deflection behaves

linearly around 40-50% of the MOR until the first cracking develops. As the prism reaches its first cracking, the fibers continue to engage and provide more rigidity that leads to strain hardening until maximum load or equivalent stress, i.e. MOR in this instant, is achieved. Afterwards, the bending stress gradually decreases while the main flexural crack widens and more steel fibers slip.

Figure 2-14 summarizes the MOR and the corresponding deflection when maximum load was achieved. The results show that the MOR of MSF UHPC significantly outperform the RSF UHPC for both early and late ages. On Day 7, the MOR of MSF UHPC ranged from 3.8-6.4 ksi, while Type I RSF attained up to 1.4-2.4 ksi. As samples reached Day 28, the MOR of MSF increased by 5-38%, while Type I RSF also increased by 5-15%. Moreover, as the fiber dosage was increased, both MSF and Type I RSF showed an increase in the MOR. However, an increase in the MOR was significant for MSF compared to RSF. Compared with similar dosages, the MOR of Type I RSF significantly decreased by 65-73% compared to MSF. In addition, the deflection at the MOR decreased by around 36-68% when Type I RSF was used. The significant decrease in MOR and deflection can be attributed to the lower aspect ratio and tensile strength of Type I RSF. As the samples reached the first cracking phase, the aspect ratio of Type I RSF (i.e., relatively short fibers) was inadequate to hold macro-cracks in place, limiting the sample to absorb energy from the applied force. In addition, if fibers are relatively short, debonding or slipping quickly takes place, which causes the cracks to grow rapidly in the prism.

Similar results were observed for Type II RSF, where the MOR is lower than MSF, but a slight improvement from Type I RSF. For phase II, 1.6% and 3.2% of Type II RSF showed a reduction in the MOR by around 42-59% and a decrease in the recorded deflection by around 7-45% when compared with 1% and 2% MSF, respectively. Using a truck mixer for 1.6% Type II RSF also decreased the MOR and the corresponding deflection by 54% and 19% compared to 2% MSF, respectively. In addition, the mixing method caused minimal difference in the MOR and deflection. Nevertheless, when the Type II fiber dosage doubled from 1.6% to 3.2%, the MOR and the corresponding deflection increased by 37% and 59%, respectively. Type II RSF showed improvement in MOR compared with Type I RSF. Given a similar fiber dosage, the MOR of 1.6% and 3.2% Type II RSF improved by 44% and 66% with respect to Type I RSF, while the deflection increased by almost 70 and 113%. The significant increase in MOR and deflection can be attributed to the higher aspect ratio of Type II RSF, which provides better crack resistance and allow for higher load and deformation.

2.3.6   Assessment of RSF UHPC Mechanical Performance and Fibers Synergism

Figure 2-15 shows the holistic and synergistic mechanical performance of Type I and II RSF using 28-day age tests to provide a concise summary and convenient visual comparisons that support the discussion summary in the next paragraphs. The result for each batch was evaluated and compared with typical UHPC mechanical performance as recommended by existing guidelines in using UHPC [34, 39]. Regarding flow requirements, most batches spread, except P2-3.2%-R2-S and P3-1.6%-R2-T, exceeded the recommended 8.0 in (203 mm) threshold. Flowability is mainly an issue with Type II

RSF because of the higher aspect ratio, causing the fibers to clump. It is suggested that the mixer mechanism be evaluated carefully, and less than 1.6% fiber dosage is recommended when RSF with high aspect ratios (like Type II in this study) is used. Regarding the compressive strength, all batches met the minimum required compressive strength of 17.5 ksi (120 MPa) as early as 7 days of age (except P3-1.6%-R2-T which only exceeds the threshold at or after 28 days age). Minimal difference in compressive strength shows that the fiber type and dosage do not play a crucial role in informing RSF dosage selection. As such, UHPC with raw RSF can be used for structural applications that perform as gravity load-carrying systems where mainly the compression behavior is of interest.

Unlike compressive strength, tensile and flexural performance are sensitive to the type of fiber, fibers aspect ratio, and applied dosage. Tensile stress localization of 1.6% dosage of Type I and II RSF underperformed compared to samples with higher RSF dosage. Increasing the fiber dosage can then help to achieve higher stress localization (as shown for Type I RSF), but could also lead to issues with flowability and fiber clumping (as seen for Type II RSF). To overcome this situation, a high-shear power mixer or improved fiber dispersal mechanism is recommended to deal with RSF of higher aspect ratio.

Another challenge with RSF is its lower tensile strain localization. Low strain localization for Type I RSF UHPC can be observed, even with higher fiber dosage up to the maximum viable ratio of 6.3% in this RSF type, when compared to MSF. This was quite the opposite with Type II RSF since the strain localization improved. Longer fibers from Type II RSF provide better crack control and ductility. Unlike Type I RSF,

increasing the fiber dosage of Type II RSF can be sensitive as it can negatively affect the flowability. It is suggested that the fiber dosage of raw RSF with higher aspect ratio (like Type II here) be kept to 1.6% or less.

RSF with low aspect ratio (like Type I here) is not recommended for applications with flexural requirements. Although fiber dosages above 3.1% achieve acceptable MOR, the deflection is significantly lower than the typical UHPC with MSF. The low aspect ratio of Type I RSF can limit the UHPC's ability to resist crack deformation and sustain higher loads, i.e. lower MOR and deflection than Type II RSF, which exhibits better crack resistance especially once macro-cracks develop as longer fibers engage well without any issue of slipping and debonding. Nonetheless, applications of UHPC with RSF should not heavily rely on fibers and rather continue to require proper mild reinforcement detailing to optimize the flexural performance.

2.3.7   Conclusions

This study presents the viability and mechanical performance of RSF as an alternative to MSF when used in conjunction with semi-proprierty UHPC mixtures with local materials to realize ultra-economical UHPC. With two different types of recycled tires fibers with varying fibers characteristics, along with comparative MSF and varying fiber dosage and mixing techniques, a total of 13 material batches were considered. Fresh and hardened UHPC samples were tested to fully characteritize the flowability, compressive, direct tensile, and flexural behavior of the proposed UHPC. The following key findings and conclusions can be drawn from test results:

- Experimental results suggest that RSF with higher aspect ratio can negatively affect UHPC flowability, and the maximum recommended dosage of this type of RSF should not exceed 1.6% to avoid fiber clumping and segregation. Nevertheless, RSF with lower aspect ratio do not pose any significant workability or flowability challenges for UHPC and dosages up to 6.3% by volume can be used.

- Truck mixing is demonstrated to be successful for mass production of scalable UHPC with 2% by volume MSF and economical UHPC with up to 1.6% of RSF of high aspect ratio. As such, high-shear mixers are recommended to use to properly disperse RSF if larger dosages are desired for in the UHPC mixture.

- UHPC with RSF maintains comparable compressive strength and modulus of elasticity as UHPC with highend MSF. Moreover, the RSF characteristics and dosage are shown not to cause any significant effect on the compressive behavior. To further extend the use of RSF UHPC in structural applications, the new AASHTO MOE prediction equation is calibrated and K_1 factor of 0.8 is proposed (instead of default value 1.0) to use for ultra-economical UHPC mixtures with RSF and semi-proprietary or non-proprieatry UHPC matrix.

- The first cracking and localization stress of RSF UHPC is comparatively lower than MSF, but in case of low dosage of RSF, stress localization can completely fall below the typical recommended value. Nonetheless, while first cracking strain of RSF and MSF UHPC are comparable, strain localization in case of RSF UHPC is significantly lower and only improve as fiber dosage increase.

- Flexural behavior of UHPC with RSF show similar trends as in tensile behavior stress and strain localization and strength, which requires increase in RSF dosage to compare with the typical 2% MSF UHPC. As such, the flexibility to use higher dosage of RSF should be granted and in turn, high-shear mixers should be used with raw RSF or further processing and sorting of RSF is needed to allow truck mixing of UHPC with high RSF dosage.

- Finally, and overall, RSF can be reliably used in UHPC but there is a need to engineer RSF UHPC and rather target specific applications. For instance, UHPC with low aspect ratio RSF can be used in axial members such as columns in gravity-load systems. Another example is that UHPC with high aspect ratio RSF can be suitable for applications that require higher tensile and flexural performance, but need to be disperse and mixed properly to overcome any fiber clumping or segregation

Acknowledgment

References

[1]   Abokifa, M., Moustafa, M. A., & Itani, A. M. (2021). Comparative Structural Behavior of Bridge Deck Panels With Polymer Concrete and UHPC Transverse Field Joints. *Engineering Structures*, *247*, 113195. doi:10.1016/j.engstruct.2021.113195

[2]   Haber, Z. B., Munoz, J. F., De la Varga, I., & Graybeal, B. A. (2018). Bond characterization of UHPC overlays for concrete bridge decks: Laboratory and field testing. *Construction and Building Materials*, *190*, 1056–1068. doi:10.1016/j.conbuildmat.2018.09.167

[3]   Morcous, G., & Tadros, M. K. (2023). UHPC Decked I-Beam for Accelerated Bridge Construction (FY21-005). https://rosap.ntl.bts.gov/view/dot/67210

[4]   Vande Voort, T. L., Suleiman, M. T., & Sritharan, S. (2008). Design and Performance Verification of UHPC Piles for Deep Foundations. (IHRB Project TR-558). https://rosap.ntl.bts.gov/view/dot/23880

[5]   Graybeal, B. A. (2013). Development of Non-Proprietary Ultra-High Performance Concrete for Use in the Highway Bridge Sector: Techbrief (United States. Federal Highway Administration, Ed.; FHWA-HRT-13-100). https://rosap.ntl.bts.gov/view/dot/34789

[6]   Shao, Y., Parks, A., & Ostertag, C. P. (2023). Carbon Footprint Between Steel-Reinforced Concrete and UHPC Beams. Journal of Structural Engineering, 149(3), 06023001.

[7]   What's in a Tire | U. S. Tire manufacturers association. (n.d.). Retrieved August 29, 2023, from https://www.ustires.org/whats-tire-0

[8]   Chesner, W. H., Collins, R. J., MacKay, M. H., & Emery, J. (2002). User Guidelines for Waste and By-Product Materials in Pavement Construction. https://rosap.ntl.bts.gov/view/dot/38365

[9]   Nadal, M., Rovira, J., Díaz-Ferrero, J., Schuhmacher, M., & Domingo, J. L. (2016). Human Exposure to Environmental Pollutants After A Tire Landfill Fire In Spain: Health Risks. Environment International, 97, 37–44.

[10] Liew, K. M., & Akbar, A. (2020). The Recent Progress of Recycled Steel Fiber Reinforced Concrete. Construction and Building Materials, 232, 117232.

[11] Abdolpour, H., Niewiadomski, P., & Sadowski, Ł. (2021). Recycling of Steel Fibres and Spent Equilibrium Catalyst in Ultra-High Performance Concrete: Literature Review, Research Gaps, and Future Development. Construction and Building Materials, 309, 125147.

[12] Isa, M. N., Pilakoutas, K., Guadagnini, M., & Angelakopoulos, H. (2020). Mechanical Performance of Affordable and Eco-Efficient Ultra-High Performance Concrete (UHPC) Containing Recycled Tyre Steel Fibres. Construction and Building Materials, 255, 119272.

[13] Zhong, H., Chen, M., & Zhang, M. (2023). Effect of Hybrid Industrial and Recycled Steel Fibres on Static and Dynamic Mechanical Properties of Ultra-High Performance Concrete. Construction and Building Materials, 370, 130691.

[14] Hu, H., Papastergiou, P., Angelakopoulos, H., Guadagnini, M., & Pilakoutas, K. (2018). Mechanical Properties Of SFRC Using Blended Recycled Tyre Steel Cords (RTSC) and Recycled Tyre Steel Fibres(RTSF). Construction and Building Materials, 187, 553–564. https://doi.org/10.1016/j.conbuildmat.2018.07.206

[15] Centonze, G., Leone, M., & Aiello, M. A. (2012). Steel Fibers from Waste Tires as Reinforcement in Concrete: A Mechanical Characterization. Construction and Building Materials, 36, 46–57.

[16] Sengul, O. (2016). Mechanical Behavior of Concretes Containing Waste Steel Fibers Recovered from Scrap Tires. Construction and Building Materials, 122, 649–658.

[17] Aghaee, K., Yazdi, M. A., & Tsavdaridis, K. D. (2015). Investigation into the Mechanical Properties of Structural Lightweight Concrete Reinforced with Waste Steel Wires. Magazine of Concrete Research, 67(4), 197–205.

[18] Papakonstantinou, C. G., & Tobolski, M. J. (2006). Use of Waste Tire Steel Beads in Portland Cement Concrete. Cement and Concrete Research, 36(9), 1686–1691.

[19] Leone, M., Centonze, G., Colonna, D., Micelli, F., & Aiello, M. A. (2018). Fiber-Reinforced Concrete with Low Content of Recycled Steel Fiber: Shear behaviour. Construction and Building Materials, 161, 141–155.

[20] Yang, J., Peng, G.-F., Shui, G.-S., & Zhang, G. (2019). Mechanical Properties and Anti-Spalling Behavior of Ultra-High Performance Concrete with Recycled And Industrial Steel Fibers. Materials, 12(5), 783.

[21] Graybeal, B. A. (2006). Material Property Characterization of Ultra-High Performance Concrete. FHWA."Ultra-High Performance Concrete." FHWA, https://www.fhwa.dot.gov/publications/research/infrastructure/structures/11038/.

[22] Markets for Wire and Fiber from Waste Tires (DRRR 2014-1513). (2014). California Department of Resources Recycling and Recovery.

[23] " Standard Specification for Steel Fibers for Fiber-Reinforced Concrete." ASTM International - Standards Worldwide, https://www.astm.org/standards/a820

[24] Zia, A., Pu, Z., Holly, I., Umar, T., Tariq, M. A. U. R., & Sufian, M. (2022). A Comprehensive Review of Incorporating Steel Fibers of Waste Tires in Cement Composites and Its Applications. Materials, 15(21), 7420.

[25] " Standard Practice for Fabricating and Testing Specimens of Ultra-High Performance Concrete." ASTM International - Standards Worldwide, https://www.astm.org/c1856_c1856m-17.html

[26] " Standard Test Method for Flow of Hydraulic Cement Mortar." ASTM International - Standards Worldwide, https://www.astm.org/c1437-20.html

[27] " Standard Specification for Flow Table for Use in Tests of Hydraulic Cement." ASTM International - Standards Worldwide, https://www.astm.org/c0230_c0230m-20.html

[28] Graybeal, B., & Baby , F. (2019). Tension Testing of Ultra-High Performance Concrete (FHWA-HRT-17-053). FHWA. https://www.fhwa.dot.gov

[29] Valentim, D., Aaleti, S., & Kreger, M. (2022). Evaluation of Test Methods to Characterize Tensile Strength of Ultra-High-Performance Concrete. *ACI Materials Journal*, *119*(4).

[30] Abokifa, M., & Moustafa, M. A. (2021). Mechanical Characterization and Material Variability Effects of Emerging Non-Proprietary UHPC Mixes for Accelerated Bridge Construction Field Joints. Construction and Building Materials, 308, 125064.

[31] Qian, S., & Li, V. C. (2007). Simplified Inverse Method for Determining the Tensile Strain Capacity of Strain Hardening Cementitious Composites. Journal of Advanced Concrete Technology, 5(2), 235–246.

[32] Method of Test for Bending Moment-Curvature Curve of Fiber-Reinforced Cementitious Composites. (2006). Journal of Advanced Concrete Technology, 4(1), 73–78.

[33] " Standard Test Method for Flexural Performance of Fiber-Reinforced Concrete (Using Beam with Third-Point Loading)." ASTM International - Standards Worldwide, https://www.astm.org/c1609_c1609m-12.html

[34] PCI Concrete Material Technology Committee. (2022). Guidelines for the Use of Ultra-High-Performance Concrete (UHPC) in Precast and Prestressed Concrete. Precast/Prestressed Concrete Institute.

[35] Riding, K. A., Ferraro, C. C., Hamilton, H. R., Voss, M. S., & Alrashidi, R. (2019). Requirements for Use of Field-Cast, Proprietary Ultra-High-Performance Concrete in Florida Structural Applications (University of Florida. Dept. of Civil and Coastal Engineering, Ed.; BDV31-977–94). https://rosap.ntl.bts.gov/view/dot/53965

[36] El-Tawil, S., Tai, Y.-S., Meng, B., Hansen, W., & Liu, Z. (2018). Commercial Production of Non-Proprietary Ultra High Performance Concrete (A. A. Regents of the University of Michigan, Ed.; RC-1670). https://rosap.ntl.bts.gov/view/dot/42751

[37] Russell, H. G., & Graybeal, B. A. (2013). Ultra-high Performance Concrete: A state-of-the-Art Report for the Bridge Community. (Inc. Henry G. Russell, Ed.; FHWA-HRT-13-060). https://rosap.ntl.bts.gov/view/dot/26387

[38] Ozyildirim, C. (2011). Evaluation of Fiber-Reinforced Concrete Ultra-High-Performance (VCTIR 12-R1). Virginia Center for Transportation Innovation and Research. https://www.virginiadot.org

[39] Graybeal, B. A., & El-Helou, R. (2023). Structural Design with Ultra-High Performance Concrete (United States. Department of Transportation. Federal Highway Administration. Office of Infrastructure Research and Development, Ed.; FHWA-HRT-23-077). https://rosap.ntl.bts.gov/view/dot/72525

[40] Haber, Z. B., De la Varga, I., Graybeal, B. A., Nakashoji, B., & El-Helou, R. (2018). Properties and Behavior of UHPC-Class Materials (FHWA-HRT-18-036). https://rosap.ntl.bts.gov/view/dot/37528

Table 2-1 − Physical properties of MSF, Type I RSF, and Type II RSF

Fiber Type	Length [mm]		Diameter [mm]		Aspect Ratio		Density [kg/m³]	Tensile Strength [MPa]
	Avg.	St. Div.	Avg.	St. Div.	Avg.	St. Div.		
MSF	13	0	0.2	0	65	0	7,850	3,000]
Type I RSF	16	6.1	0.28	0.12	60	21.7	5,018	1,948
Type II RSF	32	13.7	0.46	0.41	93	46.5	4,807	

Table 2-2 – Summary of different UHPC batches and mix design for MSF and RSF, lb/ft³ (kg/m³)

Batch ID	CorTuf Premix	Fine sand	Cement	Fibers	HRWRA	Water
P1-0%-//-S	40.8 (654)	51.7 (828)	49.5 (793)	0	7.4 (119)	10.2 (163)
P1-1%-M-S	40.4 (647)	51.2 (820)	49.0 (785)	4.9 (79)	7.4 (119)	10.1 (162)
P1-1.6%-R1-S	40.4 (647)	51.2 (820)	49.0 (785)	4.9 (79)	7.4 (119)	10.1 (162)
P1-2%-M-S	40.0 (641)	50.7 (812)	48.5 (777)	9.8 (157)	7.4 (119)	10.0 (160)
P1-3.1%-R1-S	40.0 (641)	50.7 (812)	48.5 (777)	9.8 (157)	7.4 (119)	10.0 (160)
P1-3%-M-S	39.6 (634)	50.2 (804)	48.0 (769)	14.7 (236)	7.4 (119)	9.9 (159)
P1-4.7%-R1-S	39.6 (634)	50.2 (804)	48.0 (769)	14.7 (236)	7.4 (119)	9.9 (159)
P1-4%-M-S	39.1 (626)	49.7 (796)	47.5 (761)	19.6 (314)	7.4 (119)	9.8 (157)
P1-6.3%-R1-S	39.1 (626)	49.7 (796)	47.5 (761)	19.6 (314)	7.4 (119)	9.8 (157)
P2-1.6%-R2-S	40.4 (647)	51.2 (820)	49.0 (785)	4.9 (79)	6.6 (106)	10.1 (162)
P2-3.2%-R2-S	40.0 (641)	50.7 (812)	48.5 (777)	9.8 (157)	6.6 (106)	10.0 (160)
P3-2%-M-T	40.0 (641)	50.7 (812)	48.5 (777)	9.8 (157)	6.6 (106)	10.0 (160)
P3-1.6%-R2-T	40.0 (641)	50.7 (812)	48.5 (777)	9.8 (157)	6.6 (106)	10.0 (160)

Table 2-3 − Compressive strength, strain, and modulus of elasticity of all batches for days 7 and 28

UHPC Batch ID	Age (Days)	Strength f'_c, ksi [MPa]	ε, %	MOE E_c, ksi [GPa]
P1-0%-//-S	7	16.1 [111]	0.46	5119 [35.3]
	28	21.2 [146]	0.49	5721 [39.4]
P1-1%-M-S	7	14.1 [97]	0.41	4963 [34.2]
	28	20.8 [143]	0.49	5583 [38.5]
P1-1.6%-R1-S	7	14.9 [102]	0.43	5055 [34.8]
	28	21.4 [147]	0.53	5822 [40.1]
P1-2%-M-S	7	14.3 [98]	0.38	5042 [34.7]
	28	22.4 [155]	0.50	6082 [41.9]
P1-3.1%-R1-S	7	14.2 [98]	0.41	5052 [34.8]
	28	21.5 [148]	0.50	6194 [42.7]
P1-3%-M-S	7	15.7 [108]	0.49	5145 [35.5]
	28	21.6 [149]	0.47	5846 [40.3]
P1-4.7%-R1-S	7	15.1 [104]	0.46	4868 [33.5]
	28	20.6 [142]	0.47	5439 [37.5]
P1-4%-M-S	7	16.9 [117]	0.45	5319 [36.6]
	28	22.2 [153]	0.51	5914 [40.7]
P1-6.3%-R1-S	7	15.8 [109]	0.45	5179 [35.7]
	28	18.8 [130]	0.47	5209 [35.9]
P2-1.6%-R2-S	7	12.9 [89]	0.49	3834 [26.4]
	28	19.6 [135]	0.53	4943 [34.1]
P2-2%-R2-S	7	12.8 [88]	0.49	4043 [27.9]
	28	18.6 [128]	0.52	5038 [34.7]
P3-2%-M-T	7	9.9 [68]	0.45	3703 [25.5]
	28	16.7 [115]	0.46	4831 [33.3]
P3-1.6%-R2-T	7	10.0 [69]	0.45	3202 [22.1]
	28	16.3 [112]	0.47	4408 [30.4]

Figure 2-1. Samples of MSF, Type I RSF, and Type II RSF
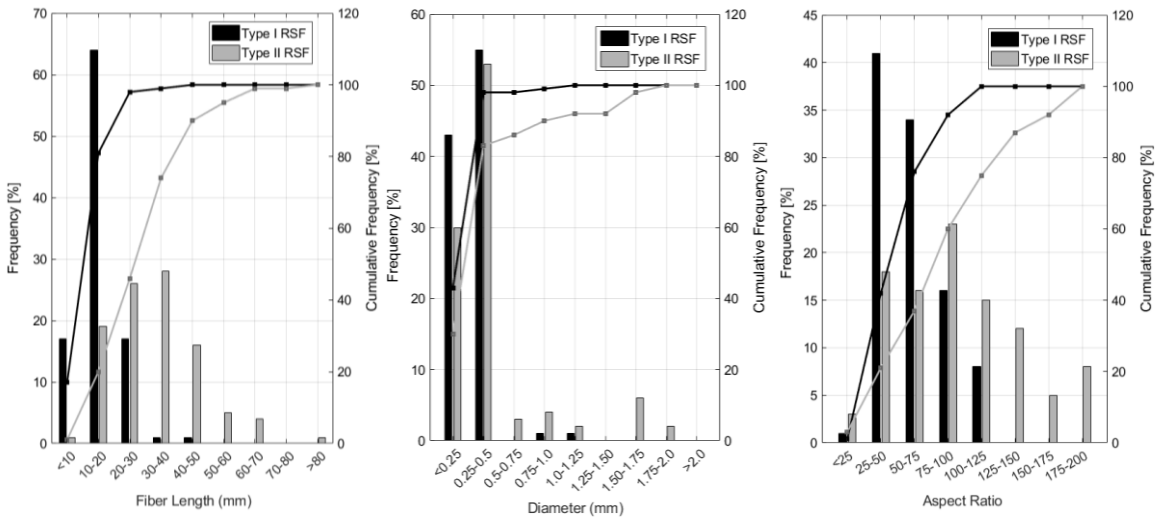
Figure 2-2. Frequency distribution of fiber length, diameter, and aspect ratio for Type I and II RSF

CorTuf premix (CT25)   Cement   Sand   HRWRA   Type I RSF

UHPC small-scale production using high-shear mixer

Application of CorTuf premix directly into truck mixer   Application of cement from silos into truck mixer

Sand application using conveyer belt   Admixtures pumping into mix   Manual application of Type II RSF

UHPC large-scale production at precast plant using truck mixer

Figure 2-3. Photographs of the different UHPC constituents and high-shear versus truck mixing

procedure
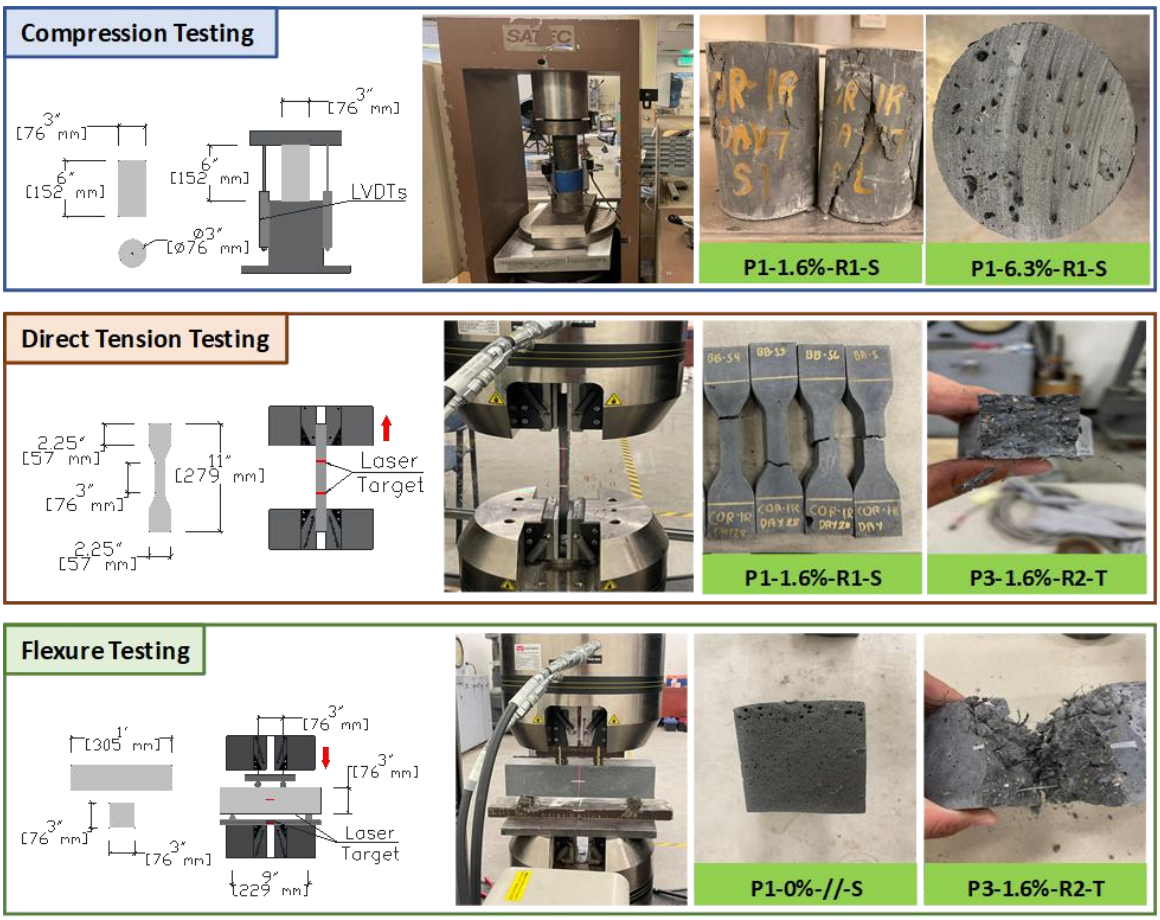
Figure 2-4. Illustration of different mechanical tests and photographs of sample tested specimens
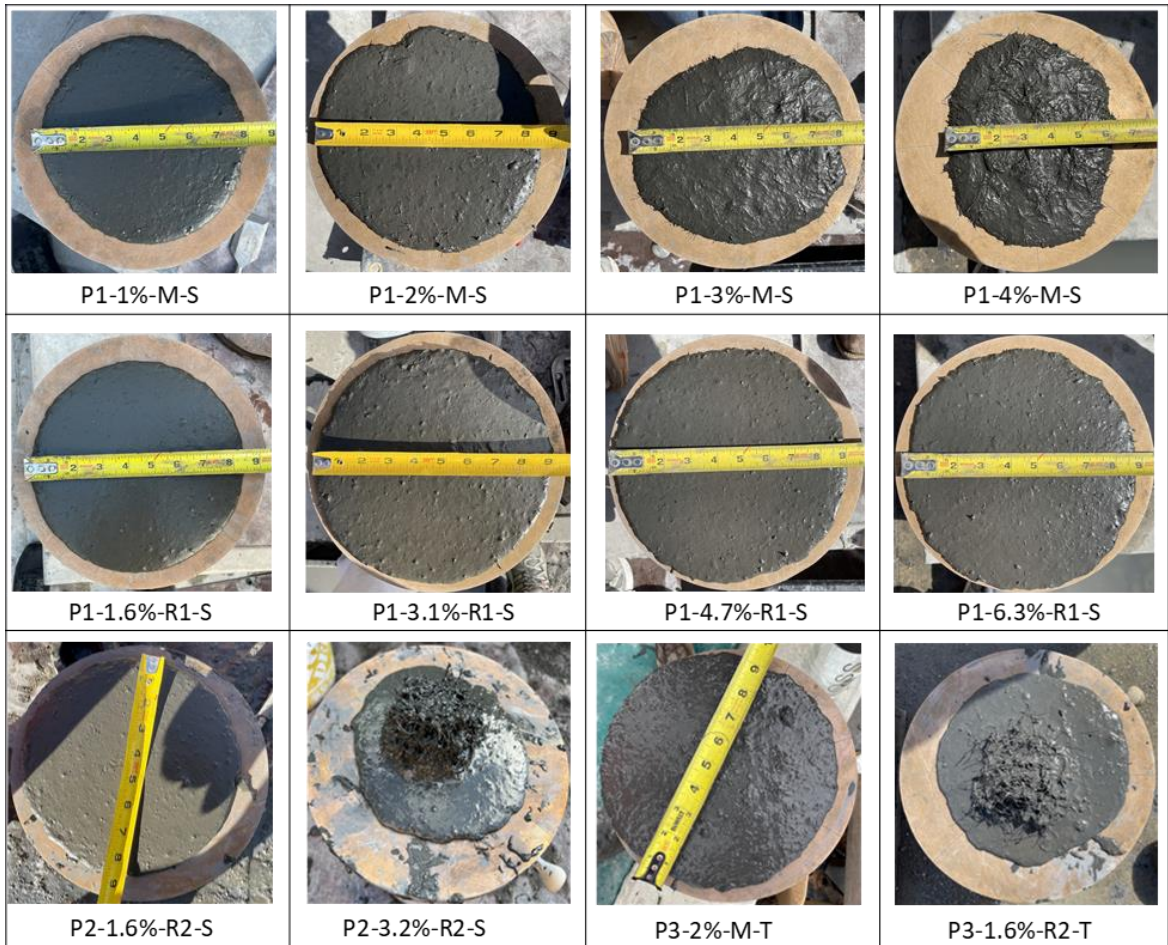
Figure 2-5. Representative UHPC spread after typical static flow tests for each batch
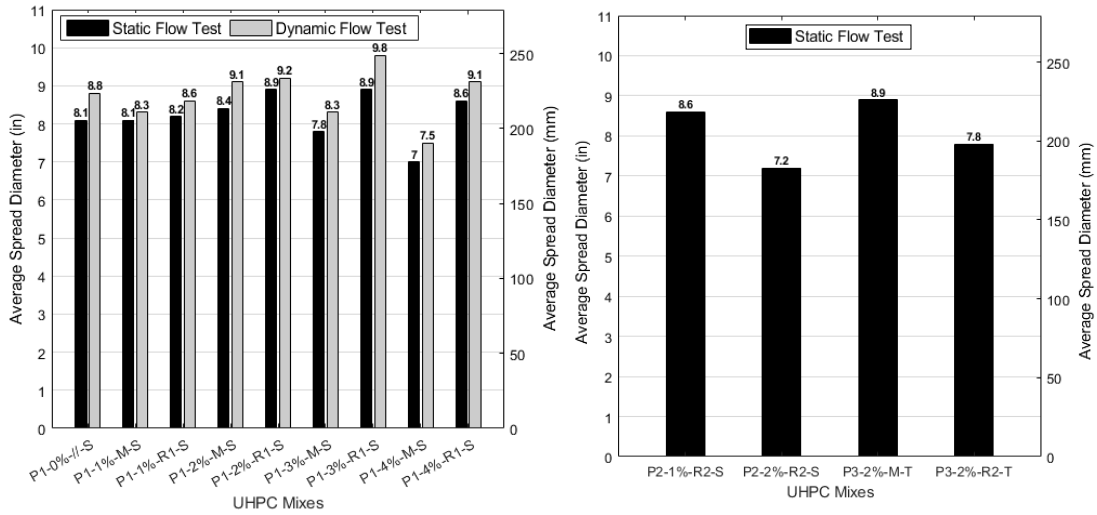
Figure 2-6. Average spread diameter of UHPC with MSF, Type I RSF, and Type II RSF
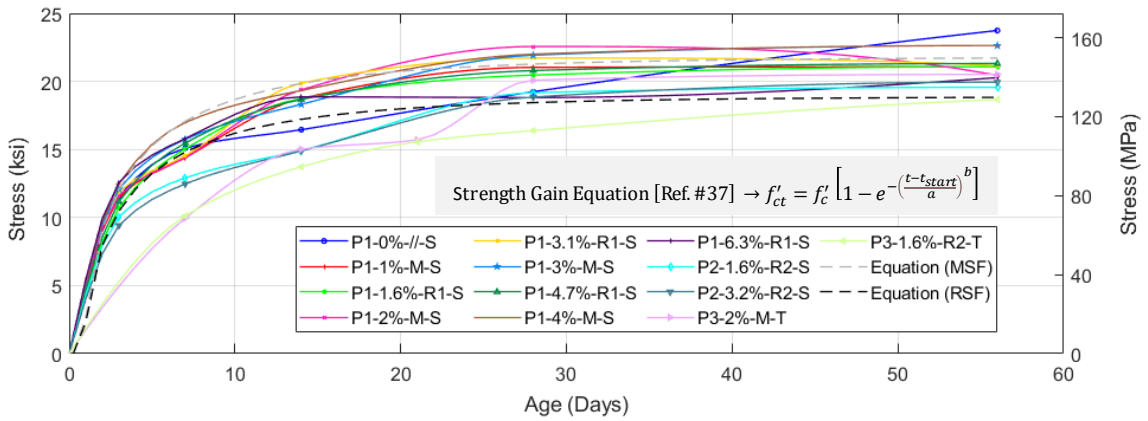
Figure 2-7. Compressive strength gain versus age (up to 56 days) for all tested UHPC batches and types
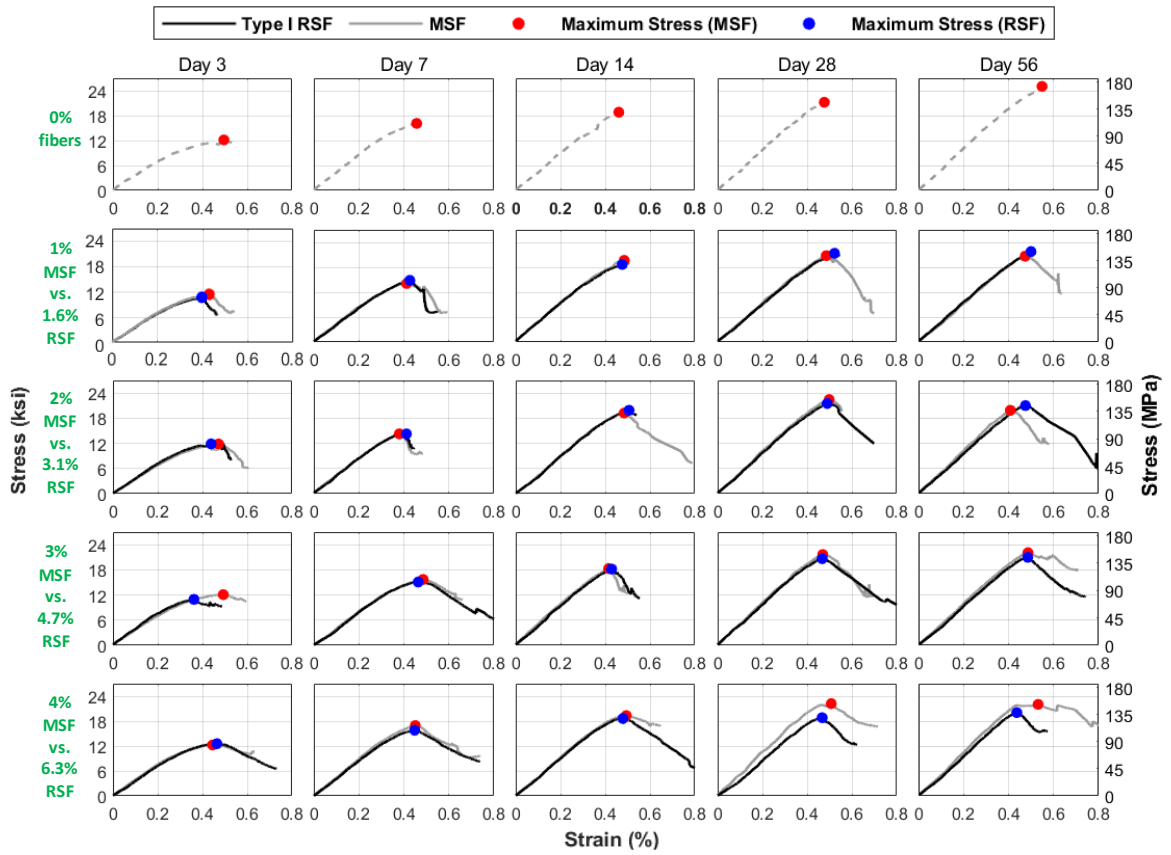
Figure 2-8. Average compressive stress-strain relationships of MSF and Type I RSF UHPC with varying fiber dosage at different ages (3, 7, 14, 28, and 56 days)
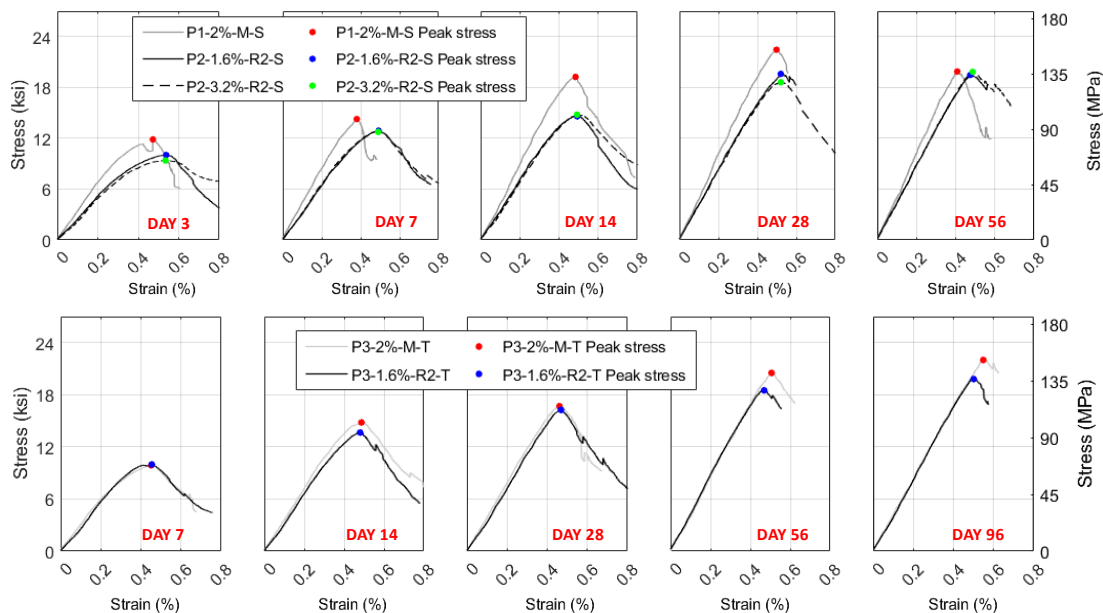
Figure 2-9. Compressive stress-strain relationships of Type II RSF UHPC with varying fiber dosages as obtained at different ages and from both mixing scales and procedures
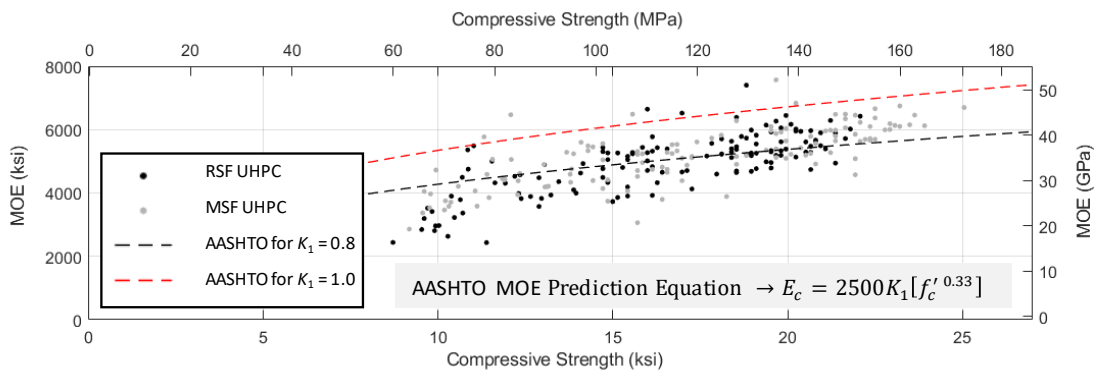
Figure 2-10. MOE experimental values of individual specimens of MSF and RSF UHPC and comparison against new AASHTO prediction equation with default and calibrated coefficient
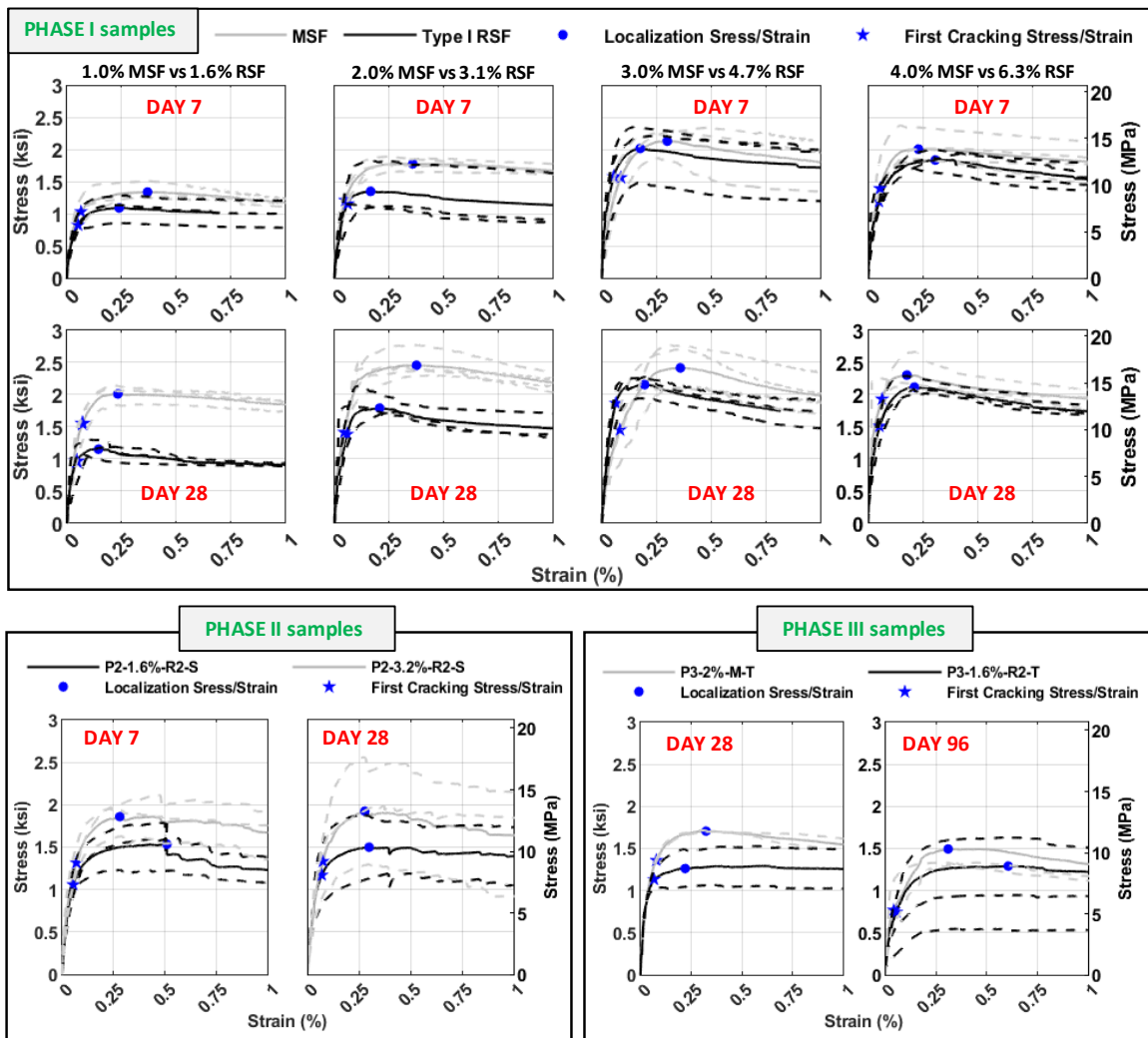
Figure 2-11. Average tensile stress-strain relationships at different ages for all tested UHPC batches with varying fibers type (MSF, Type I RSF, Type II RSF), fiber dosages, and mixing procedure
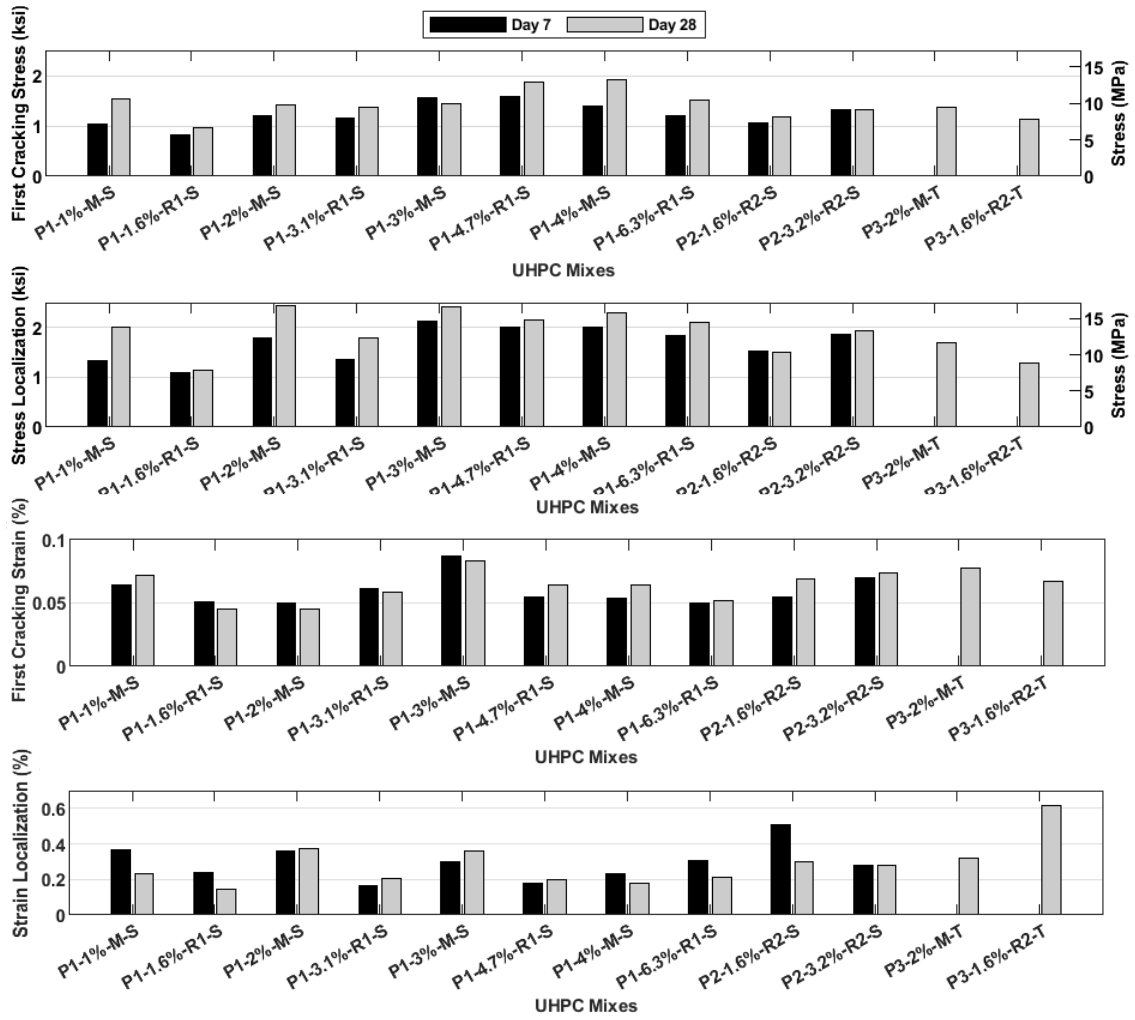
Figure 2-12. Summary of UHPC first cracking and localization stress and strain values from tension tests
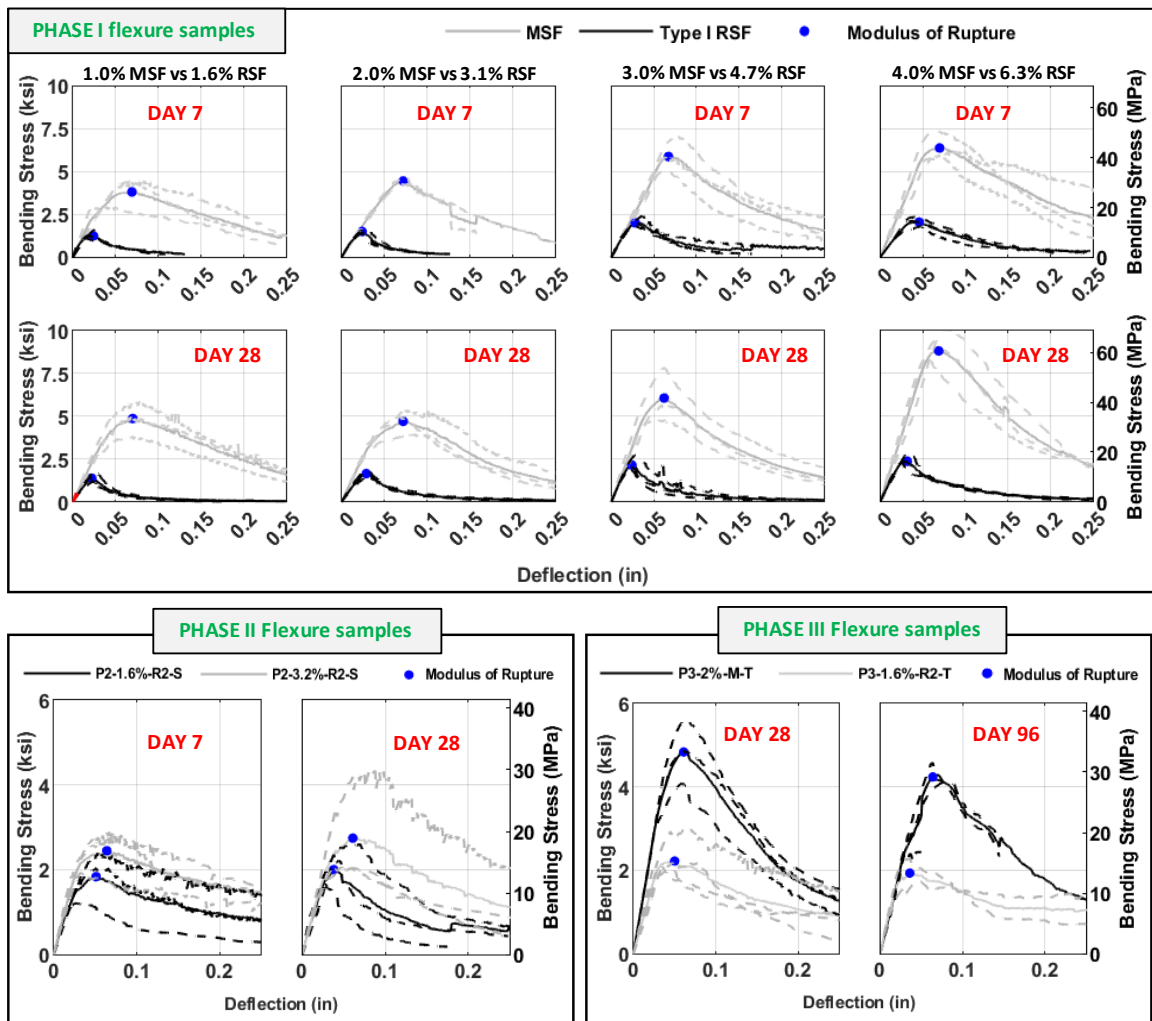
Figure 2-13. Average bending stress-deflection relationships at different ages for all tested UHPC batches with varying fibers type (MSF, Type I RSF, Type II RSF), fiber dosages, and mixing procedure
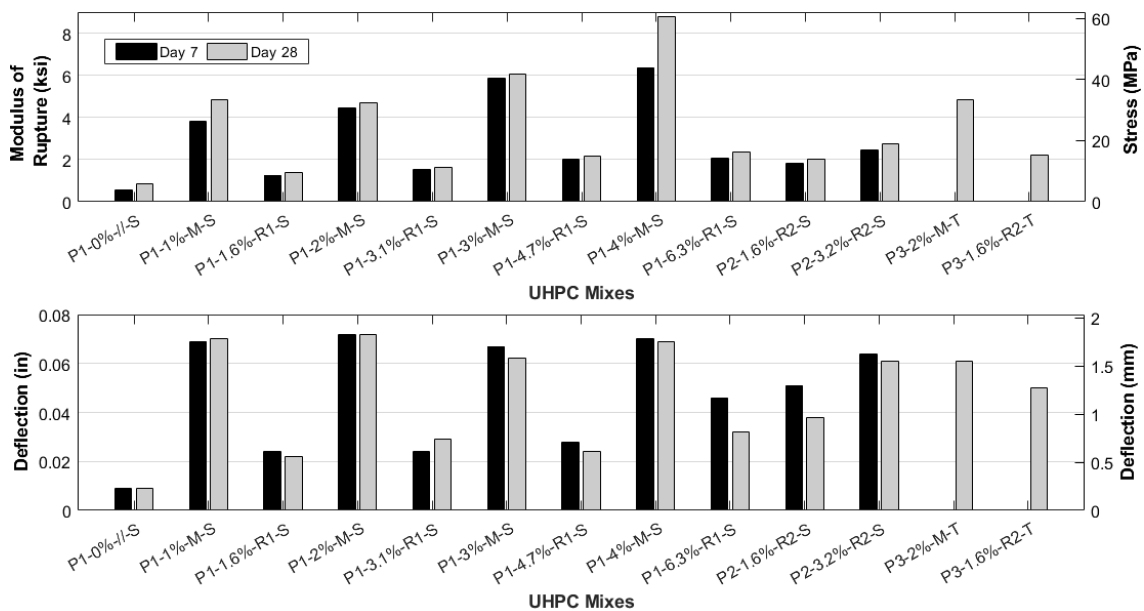
Figure 2-14. Summary results of modulus of rupture (MOR) and corresponding deflection from flexure tests of UHPC with different fibers types and dosages
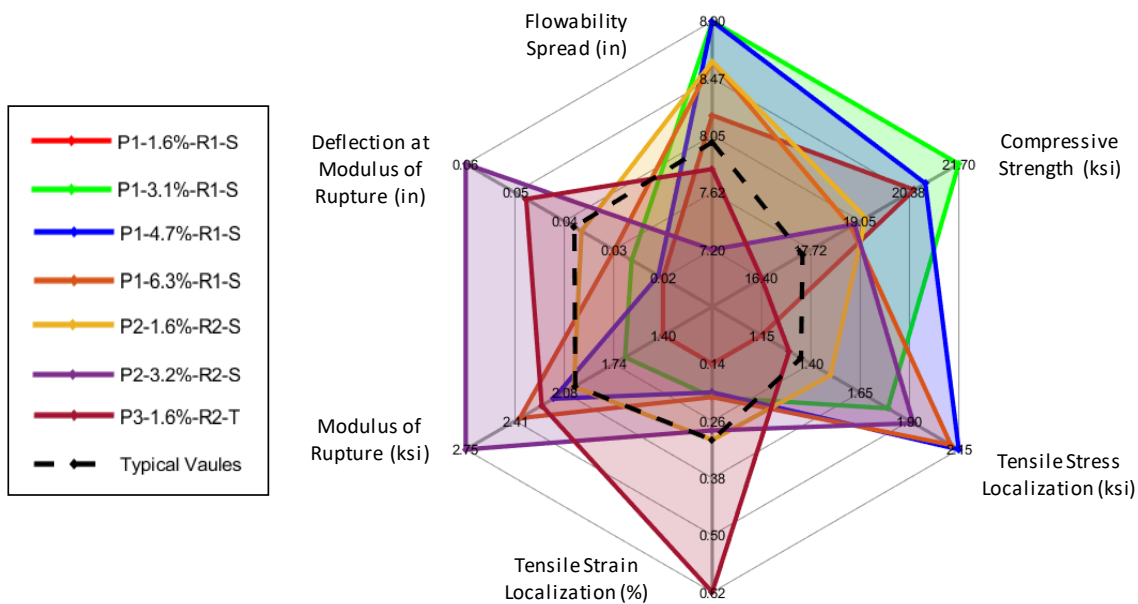
Figure 2-15. Visual summary of mechanical performance and synergism of Type I and II RSF UHPC using test results at 28-day age

3 TOWARDS SCALABLE ECONOMICAL UHPC: MATERIAL CHARACTERIZATION AND APPLICATION TO FULL-SCALE AXIAL COLUMNS

This chapter is a standalone paper that has been submitted to the Journal of Construction and Building Materials

Abstract

Ultra-high performance concrete (UHPC) has emerged as the future of concrete, with increasing popularity in bridge applications and high-rise buildings. However, the high cost of robust UHPC of proprietary nature and expensive constituents hinders mass production and expanding into full structural applications. This study provides the experimental research and validation to support new initiative in scalable economical UHPC of semi-proprietary nature that leverage local and sustainable materials, and explore the use of raw recycled tires fibers. The study provides first comprehensive material trials and mechanical characterization to assess effects of local sand, cement and fibers type. Next, a promising economical UHPC mixture is selected to fabricate and test five full-scale axial columns with varying reinforcement ratios, fiber ratio, and types of fibers. Overall, the result shows that incorporating local and sustainable components into proprietary mixtures does not compromise the mechanical properties of UHPC and successfully work for large structural applications.

Keywords: economical UHPC, local materials, mechanical characterization, recycled fibers, full-scale columns

3.1   Introduction

Ultra-high performance concrete (UHPC) is a rapidly growing advanced class of cementitious composite material capable of demonstrating superior mechanical and durability properties. UHPC is designed to have a low water-to-binder (and water-to-cement) ratio by utilizing bulk of dry components such as fine Portland cement, silica fume, ground quartz, fine aggregate sand, and a small volume of liquid components such as water and high-range water reducer (HRWR) admixtures. Typical commercial UHPC provides compressive strength of 140 MPa (~20 ksi) or more, which is about four times greater than normal strength concrete (NSC) [1]. In addition, steel fibers of typical dimensions of 0.2 mm × 13 mm are utilized in UHPC to bridge micro-cracks, improve ductility and durability, and provide sustained tensile strength of more than 5 MPa (~0.7 ksi) [2]. Because of the remarkable mechanical performance of UHPC, research continues to uncover the full potential of the material and utilize UHPC in large-scale applications. Accelerated bridge construction (ABC), whether in research or rapidly increasing actual implementations, has benefited from UHPC by improving connections on bridges [3-5], connecting field joints for prefabricated deck panels [6], and providing thin bonded overlays [7]. The exceptional performance of UHPC led to the rehabilitation of the Pulaski Skyway in New Jersey, which is one of the most extensively used UHPC in North America for a single project to date [8]. Figure 3-1 illustrate the rehabilitation of the Pulaski Skyway bridge precast deck panels with UHPC panels which represent the most common global application of UHPC nowadays. Regardless of the growing use, most robust UHPC products are still of proprietary nature, and with the need for steel

fibers being the most expensive component [9], large-scale production of UHPC for full structural components is still limited.

Mass production of UHPC and incorporation into full structural components and systems would be only possible with the advancement of cost-effective scalable UHPC mixtures in the market. In this introduction, we provide first an overview of previous efforts that looked into economic UHPC and the use of recycled fibers, then a brief literature review on one relevant structural application in axial columns, to provide the context and background of this study. The development of non-proprietary UHPC is increasingly explored as a viable solution to reduce the total cost of UHPC production. Several transportation agencies have developed design guidelines for non-proprietary UHPC in bridge applications [10-11]. El-Tawil et al. [11] utilized non-proprietary UHPC for joints of two precast bridge deck elements, where they used UHPC composed of ground granulated blast-furnace slag (GGBS) that reduces the amount of Portland cement and post-placement treatments, making the UHPC more cost-effective and greener. Abokifa and Moustafa [6, 12] investigated the application of non-proprietary UHPC with different aggregate gradations for accelerated bridge construction field joints. Amin et al. [13] examined the effect of recycled coarse aggregates and carbon nanofibers in UHPC by determining the mechanical properties. Despite the efforts to create an alternative solution for lowering the cost of UHPC by utilizing non-proprietary mixtures, the mechanical properties of non-proprietary UHPC, such as the compressive strength, tend to be inconsistent and relatively lower than the proprietary UHPC. More critically, most of the non-proprietary mixtures are not well scalable and experience significant reduction

in reliable mixing, workability, and mechanical properties when produced at scale [12]. In addition, most recent studies regarding non-proprietary UHPC still utilize high end manufactured steel fibers (MSF), which is a component that drives the high cost of UHPC.

A proposed solution to reduce the cost of fiber-reinforced concrete is replacing MSF with recycled fibers. Raw recycled steel fibers (RSF) are commonly derived from scrap vehicle tires in city landfills, typically piled for burning. However, these landfill tires can be processed to remove the wire fibers through different recycling methods, such as pyrolysis, shredding, and mechanical recycling [14]. Different studies have emerged to introduce RSF in fiber-reinforced concrete [15-17]. Samarakoon et al. [18] determined the mechanical performance of NSC with different RSF ratios (0.5% and 1%) using several reinforced concrete beams, and compared to beams with MSF at similar fiber ratios to show similar behavior in ductility and ultimate strength. Caggiano et al. [19] performed compressive and bending tests of NSC reinforced with hybrid fibers containing MSF and RSF of ratios 0, 0.75, 1.0, and 1.25%. The compressive strength showed an increase of 5-10% for hybrid steel fiber ratios up to 1% and a decrease of 5% for a 1.25% steel fiber ratio. These studies have shown evidence that RSF from tires can be a potential replacement for MSF but considered application in traditional fiber reinforced concrete and not UHPC.

With the success of RSF and promising results in NSC, applying RSF has opened possibilities for a more cost-effective, greener, and more sustainable UHPC. Limited studies have been conducted in the past few years investigating the effect of RSF in

UHPC. Abdolpour et al. [20] performed a mechanical characterization of RSF in UHPC using compressive and tensile tests. The results showed a 4% decrease in compressive strength while an improvement in tensile ductility for a fiber ratio greater than 1%. Yang et al. [21] compared UHPC with two types of RSF and three industrial MSF and showed that all fibers exhibited excellent mechanical properties; however, fibers with rubbers presence have relatively decreased compressive and tensile strength. Isa et al. [22] tested the flexural strength of several prisms with different fiber ratios containing recycled tire steel cords and recycled tire steel fibers. The study showed that impurities such as rubber residues and short recycled fibers significantly decrease flexural strength, and suggested that removing the impurities, longer fibers, and increased fiber ratio volume could improve flexural strength. While new studies incorporating RSF in UHPC are emerging and show lot of promise, such studies have been limited to small applications, and no research has yet utilized RSF in large-scale structural components.

One of the simplest structural applications of UHPC is axial columns in medium and high-rise buildings. As such, several studies start at UHPC columns when scalability and expansion into large-scale and structural systems is desired. Sugano et al. [23] studied the effect of pure axial loading in UHPC columns of dimensions 200 mm × 200 mm × 590 mm. The test results showed that UHPC columns with sufficient lateral reinforcements yield high axial load capacity. Similarly, Hosinieh et al. [24] performed several tests of six large-scale columns (250 mm × 250 mm × 1000 mm) with varying longitudinal and transverse detailing. In this study, a decrease in the spacing of the transverse reinforcement was shown to increase axial capacity with more defined post-peak

ductility. Another study was conducted by Shin et al. [25] to test nine UHPC square columns (220 mm × 220 mm × 900 mm) with different transverse reinforcement configurations and ratios and UHPC compressive strength. The study revealed that the use of hybrid micro-steel fibers helps with confinement of the UHPC columns, and a well-detailed configuration and closely spaced transverse reinforcement improves the post-peak ductility. A more recent study was performed by Aboukifa and Moustafa [26, 27] to further test the effect of varying longitudinal and transverse reinforcement and slenderness ratio for full-scale UHPC columns under concentric axial loading. The test results showed that decreasing the confinement reinforcement by half reduces the axial capacity by 12% and that the ACI-318 equations overestimated the axial load capacity for UHPC non-slender and slender columns on average by 13% and 9%, respectively. The study proposed a new strength reduction factor of 0.75, instead of 0.85, in the ACI 318 axial design equations for slenderness ratio less than 30. The main limitation with the mentioned studies is the use of fully proprietary and high-cost UHPC mixtures, so more work is needed for economical mixtures.

Based on the above summary, there are two main reasons that are likely hindering mass production or large-scale UHPC applications. First, the proprietary nature of UHPC is cost prohibitive and usually cause bidding issues for large or mega projects. Full non-proprietary UHPC mixtures can be an option; however, the mechanical performance and consistency will be far short from robust proprietary UHPC. The second reason is the high cost of steel fibers specifically, which drives the cost of the UHPC in magnitude for full-scale and larger applications and is not always needed in same way for all

applications. As such, the goal of this study is to propose a new economical type of UHPC that allows a combination of proprietary and non-proprietary UHPC components for scalable applications. Most of robust proprietary UHPC mixtures consists of special dry or wet premixes in combination with more standard components like sand, cement, and multi-purpose admixtures. Thus, separating the special blends and allowing users to mix such blends with locally sourced materials is what one commercial UHPC vendor (Cor-Tuf) has recently allowed and is leveraged in this study, for the first time, to demonstrate the extent of flexibility in the local materials specifications (e.g. fine sand size or gradation, cement type, etc.).

The specific objective of this study is two-fold: (1) introduce and validate the semi-proprietary concept of economical and scalable UHPC by investigating the effect of varying sand, cement, and fibers types on the mechanical properties of UHPC, and (2) experimentally test the scalability and performance of the economical UHPC in full-scale axial columns with varying fibers and steel reinforcement. The material variability study was conducted at our material and structures laboratories at the University of Nevada Reno (UNR) and presented in the next section. The details of the construction and large-scale testing of five 300 mm × 300 mm × 2750 mm columns at the University of California, Berkeley is presented afterwards. Finally, the paper provides concluding remarks drawn from both material and structural testing and validation.

3.2   Material Variability Study and Mechanical Characterization

To demonstrate the viability of semi-proprietary UHPC for a range of local materials, several material and mixing parameters were varied and tested using various mechanical characterization aspects. The first and main parameter is the fine aggregate (i.e. sand) type and gradation from different sources. The second parameter is cement type where commercial and local cement from typical construction and precast applications was considered. Other parameters included the fiber type (MSF and RSF), aggregate moisture (Oven dried and with natural moisture), curing condition (ambient or in control room), and mixer type (high shear and drum mixers with varying mixing energy and torque). As a result, 14 material batches were produced and hundreds of material samples were tested to characterize the UHPC flowability, compressive strength, modulus of elasticity (MOE), direct tensile strength, and flexural strength as presented in this section.

3.2.1 *Material Constituents and Variability*

Table 1 summarizes the details of the 14 batches and varying parameters completed in the material variability study, and Figure 3-2 shows the breakdown of the UHPC components. The UHPC-based commercial premix used for this study is provided by Cor-Tuf and was originally developed by the Army Corps of Engineers. The Cor-Tuf 25 (CT 25) powder is a proprietary blend that is primarily composed of quartz and silica fume. The CT25 powder is only a portion of the full UHPC mixture, and components like fine aggregates, cement, steel fibers, and admixtures are still required. Thus, it is on interest to investigate whether CT 25 is robust enough to blend with a range of local aggregates and cement. The UHPC mixtures include two HRWR and one corrosion inhibitor admixtures to enhance workability, improve concrete quality by reducing the

w/c ratio, and develop a favorable early strength. The water-binder ratio (*w/b*) is determined to be 0.17, lower than the recommended 0.2 [28].

A significant consideration for this study is the utilization of local aggregate and cement. Eight aggregate types were sourced from Nevada local quarries (Mix I & II), commercial stores (Mix III-IX), and a typical precast/prestressed plant in California (Mix X-XIV). Samples from each mix were sieved according to ASTM C136 specifications for coarse and fine aggregate [29] as illustrated in Figure 3-2. Aggregates from Nevada quarries and California precast sand were determined to be well-graded. However, most commercial aggregate samples were uniformly graded and dominated by two aggregate sizes with varying degrees of fineness. Note that some batch samples from Nevada and California aggregate were sieved to have a particular set of aggregate sizes. Most of the aggregate samples, except for Mix X, were dried using an industrial oven to ensure that no moisture was present during mixing so that it would not affect the w/b ratio. The cement type was also considered among variables and local sources and types are desired for economic UHPC. Cement can increase the cost (e.g., logistics and shipping) of UHPC and can be significant for large-scale applications. This study used Type I/II cement for Mix I-IX, XII, and XIV, while Type II/V was used for Mix X, XI, and XIII. The Type I/II cement was sourced from the local hardware store, and Con-Fab Precast provided the Type II/V cement.

Another important consideration herein is the use of raw RSF as an approach to reduce the UHPC cost. In this study, Mix VIII replaced the MSF with RSF that are both shown and compared in Figure 3-3. Because the RSF has varying densities due to different fiber

aspect ratios and impurities, the amount of the RSF was measured similarly to the weight of the MSF for a 2% volumetric ratio (6% by weight ratio). Instead of being density-based, the weight comparison was deliberately chosen to assess whether the same amount of RSF can perform as an alternative for MSF. The MSF was sourced from Tokusen and had specified dimensions of 0.200 mm ×13.0 mm [0.0079 in × 0.511 in] and tensile strength greater than 2,000 MPa [295 ksi]. The RSF had average dimensions of 0.28 mm ×16.0 mm [0.011 in × 0.62 in] and average tensile strength of 1,948 MPa [282.6 ksi]. The aspect ratio of MSF and RSF, calculated as length over diameter, was 65 and 60, respectively.

The mixing sequence is demonstrated in Figure 3-4. The dry components of the UHPC mix were first added into an IMER 360 Mortarman high-shear mixer with the steel fibers. After the dry components were homogenized, the chemical admixtures along with half of the total water amount were added. The remaining amount of water was included after two minutes. Although steel fibers, when added early, can generate clumping in the UHPC mixture [28], no clumping of fibers was observed. Additional variables of this study stems from UHPC mixing and production such as mixer type and curing regimen for material samples. A 5-ft^3 drum mixer was used for one of the batches instead of the high-shear mixer. Curing regimens such as ambient indoor temperature and humidity, and outdoor temperature in Reno, NV during the mixing times, and standard curing room were also considered when we looked at the compressive strength gain as discussed later. The range of temperatures recorded during this study is: (1) 23-27°C with 30% humidity

for ambient indoor curing, (2) 26-41°C with 12-15% humidity for fabrication yard outdoor curing, and (3) 23°C with 100% humidity for the standard curing room.

3.2.2   Flow Test Results

Flow tests were conducted according to ASTM C1437 and C230 with specific modifications from ASTM C1856 [30-32]. Fresh UHPC from the mixer was placed in the cone, and the cone was gradually lifted to let UHPC flow into the table. Figure 3-5 shows an example of UHPC in the flow table, including the average spread diameter for each mix. Two types of tests were performed for each batch. The first is a static flow test where the flow is recorded by taking the average spread diameter of the UHPC after two minutes or when the UHPC stops flowing, whichever occurs first. The second is a dynamic flow test which requires the application of 25 standard impacts in 15 seconds before lifting the cone and recording the average spread in two sides. Several guidelines and specifications, such as PCI and AASHTO, require flowability to range between 200-250 mm (8-10 in). Most batches met the recommended flowability (at least for the dynamic flow test) except for a few mixes. Mix I and II fell below the recommended flowability as the aggregate size was coarser than the typical fine aggregate. Using coarser aggregate makes the UHPC viscous and in turn, reduces the flowability as captured in standard flow tests.

3.2.3   Compression Test Results: Strength and Strength Gain

UHPC is known to have a superior compressive strength than NSC, which makes compression tests the most important mechanical test for evaluating UHPC. Moreover, the compressive strength gain and tracking early and late age strength is of interest since

UHPC is used for many accelerated construction applications. Compression tests were conducted in accordance to ASTM C39/C39M with a few modifications suggested from ASTM C1856 [33, 34]. Cylindrical samples were cast using 75 mm × 150 mm (3 in × 6 in mold) and were prepared by grinding both end surfaces to avoid any out-of-planeness that can affect the compressive strength. The samples were tested using a 2,000 kN [500 kips] Satec compressive loading machine. Figure 3-6 shows the preparation and final setup for the compression test. A loading rate of 1.0 MPa/sec [145 psi/sec] was used following ASTM C1856 specifications [32]. The compression test was used to determine the strength as well as the MOE following ASTM C469/C469M [33] (results shown in next subsection), and as such, a compressometer was used as illustrated in Figure 3-6. The average compressive strength at a specific age was obtained using at least three cylinder samples, and the compressive strength was obtained at age of 3, 7, 14, 28, 56, and 84 days.

Figure 3-7 shows the compressive strength gain for all the batches. In addition, the compressive strength result for all the batches was compared to Equation 1 proposed by Graybeal [35] for UHPC compressive strength gain. In this equation, f'_{ct} is the compressive strength at t days; f'_c is the compressive strength at 28 days; t is the time after casting; t_{start} is the initiating time of strength gain; a is a fitting parameter in days; and b is a dimensionless fitting parameter. The values used herein are as follows: the average compressive strength (f'_c) is 149 MPa (21.6 ksi), t_{start} is determined to be around 0.9 days, a is 3 days, and b is 0.6. As observed, most of the mixes were close by around 10% to the predicted compressive strength gain especially for the early ages and

28-days age. However, Equation 3-1 is only appropriate to estimate the compressive strength up to 28 days, which for late ages such as day 84, most of the mixtures show higher compressive and are underestimated by the equation. Nevertheless, the overall observation that any aggregate or cement type can still provide acceptable compressive strength of around 152 MPa (22 ksi) for 28 days, which exceeds the 120 MPa (17.4 ksi) set by the PCI [28] for instance.

$$f'_{ct} = f'_c [1 - e^{-\left(\frac{t - t_{start}}{a}\right)^b}]$$
(3-1)

A noticeable result was the underperformance of Mix VIII and IX, which had RSF and drum mixing involved, respectively. The slight decrease in the compressive strength of UHPC with RSF can be attributed to the weak confinement capabilities of the fibers and impurities present which affected the synergism between UHPC components. For the drum mixing, the UHPC components were observed to homogenize slower compared to a regular shear mixer. The lower mixing energy of the drum mixer resulted in a larger portion of unhydrated cement powder in the mixture affecting the compressive strength directly. The effect of the curing regimen was also studied. The results confirmed that the relatively higher outdoor summer temperature in Reno, NV when this study was performed, accelerated the hydration process of the samples, and in turn, led to higher compressive strength at early ages when compared to specimens of same batches cured indoor or in the standard curing room. Nonetheless, the compressive strength was shown to be similar at 28 days age for the different curing regimens, i.e., the results suggest that

heat curing can increase compressive strength at early age but does not provide additional strength at later ages.

3.2.4   Compression Test Results: Modulus of Elasticity

Figure 3-8 shows individual samples calculated MOE for all 14 different batches. The MOE was calculated using the best-fit linear approximation at 10-30% of the maximum peak stress [1]. The MOE ranges from 31-48 GPa (4,500-7,000 ksi) with a compressive strength of 138-172 MPa (20-25 ksi). The resulting MOE was compared to the recently published FHWA/AASHTO [36] prediction equation provided below (Equation 3-2). In Equation 3-2, E_c is the estimated MOE; K_1 is the adjustment factor for different types of UHPC; and f_c' is the recorded compressive strength. In this case, when we set K_1 to 1.0, the MOE was found to be overestimated. Thus, a best fit regression analysis was performed to estimate K_1, which was determined to be about 0.80. Therefore, a K_1 adjustment factor of 0.80 is proposed to use for the economical UHPC type of this study.

$$E_c = 2500K_1[f_c'^{\,0.33}] \quad (f_c' \ is \ in \ psi) \tag{2}$$

equation [38] with K_1 set to the standard value of 1.0 and the 0.8 value proposed herein

3.2.5   Direct Tension Test Results

Another important aspect of UHPC is the enhanced tensile strength and ductility with the help of the fibers. In this study, a direct tension test was performed using dog bone shaped specimens with test cross-sections of 25.4 mm ×12.7 mm (1.0 in × 0.5 in) and 25.4 mm ×25.4 mm (1.0 in × 1.0 in). An Instron machine with hydraulic wedge drips was used to test the dog bone samples. The test was conducted for days 7 and 28 and was only performed for mix I-VIII. Figure 3-9 shows the result of the direct tensile test where the

average tensile strength is shown to range from 11.4 to 19.4 MPa (1.65- 2.81 ksi). A noticeable trend is that finer aggregates have shown slightly higher tensile strength than samples with coarser aggregates. Nevertheless, the difference in tensile strength is not very significant to warrant a favorable aggregate size. Only when the standard MSF in mix VII was replaced by RSF in mix VIII, a 25.1% decrease in the tensile strength was observed.

3.2.6   *Flexural Test Results*

Although the direct tensile test can accurately measure the tensile strength, the method requires specialized equipment and practices that may not be available in most of typical material testing or quality control labs. In this case, a four-point bending test can be performed for UHPC as an alternative to estimate the need for direct tensile strength, which is the approach proposed by PCI. The flexural strength was determined based on ASTM C1609 and C1856 [32,37]. Since the MSF fiber length is 13 mm (0.51 in), the UHPC was placed in a prism with dimensions of 75 mm × 75 mm × 305 mm (3.0 in × 3.0 in × 12.0 in). The prisms were tested using an Instron machine, same as direct tension tests, with a 0.1 mm/min loading rate. Figure 3-10 shows the modulus of rupture of mix I-VIII for days 7 and 28 as obtained from the flexural tests. The modulus of rupture ranges from 11.5 to 46.9 MPa (1.66-6.80 ksi) for day 28. Notably, most of the mixes have modulus of rupture of 31-35 MPa (4.5-5.0 ksi) range at 28 days age. However, the modulus of rupture for RSF (mix VIII) significantly decreased by 65.3% when compared to its counter MSF mix (mix VII). The decrease in the modulus rupture for RSF can be attributed to the weaker tensile strength and lower aspect ratio of RSF. A lower aspect

ratio can cause fibers to slip easily, which can gravitate the cracking of UHPC and in turn, decrease the flexural strength.

3.3   Large-Scale Testing: Experimental Program Development

The second phase of this study focuses on the scalability and applicability of the economical semi-proprietary UHPC mixtures for structural applications, i.e., axial columns in this case. This section presents first an overview of the construction, companion materials properties, and the experimental testing program of the five full-scale UHPC columns. The tests results and discussions are provided in the following section.

3.3.1   Columns Design, UHPC Mixture, and Construction

Five full-scale columns were constructed at the fabrication yard of the University of Nevada, Reno (UNR) using one of the tested versions of the economical UHPC mixture as discussed later in this subsection. Table 2 shows the test matrix and details of each column with respect to different types of fiber, fiber ratios, and reinforcement detailing. The column reinforcement cages for this study were assembled and readily delivered to UNR by a commercial steel vendor. Strain gages were applied to longitudinal and transverse reinforcing bars at certain locations of the assembled cages as discussed later. All columns were chosen to have a dimension of 305 mm × 305 mm [12 in × 12 in] and a height of 2.74 m [9 ft]. During the construction phase, some minor construction errors were noted, and changes in the dimensions were accounted for. As shown in Figure 3-11, the formwork was constructed horizontally on a casting platform at UNR, and the

reinforcement cages were placed inside. Dobies were placed at the bottom of the reinforcement to allow a 20 mm [0.75 in] clear cover at all sides. Two big and four small rods with diameter of 25 mm [1 in] and 7.6 mm [0.30 in], respectively, were placed in the columns as illustrated in Figure 3-11 for lifting and handling as well as instrumentation during testing. With respect to the ends of the column, the big rods and small rods were inserted into the columns at distances of 305 mm [12 in] and 610 mm [24 in], respectively.

Figure 3-11 shows the reinforcement detailing of all five columns. The first column, specimen CT1, was designed using eight Φ16 mm [#5] longitudinal reinforcements with transverse reinforcements of Φ10 mm [#3] spaced at 76.2 mm [3 in]. The longitudinal and transverse reinforcement ratios were 1.72% and 0.61%, respectively. The reinforcement was detailed according to the ACI 318-19 provisions such that transverse reinforcement requirements satisfy both an s/d_b ratio of 4.8 and no unsupported longitudinal reinforcement of more than 150 mm [38]. In addition, CT1 was the basis of comparison for all column specimens, and differences within the results based on varying parameters are discussed in the next section. The remaining four columns were designed to have 12 Φ13 mm [#4] with transverse reinforcements of Φ10 mm [#3] spaced at 76.2 mm [3 in]. The s/d_b ratio of these columns was 6, and the inner longitudinal reinforcement based on the outside hoop is unsupported at 152 mm, which is around the threshold limit of ACI 318-19. Because of the non-ACI compliance of the columns, two columns were provided with an additional octagonal transverse reinforcement of Φ10 mm [#3] spaced at 76.2 mm [3 in] to ensure ACI compliance for the unsupported

longitudinal reinforcement. For columns CT2-CT5, longitudinal reinforcement ratio is 1.67%, and the transverse reinforcement ratio for the columns without and with additional transverse hoops are 0.61% and 1.22%, respectively. All reinforcement was Gr 60 [f_y = 420 MPa].

For the UHPC mixture used for the columns, Table 3 shows the final mixed proportions for each batch of UHPC. CT1, CT2, and CT3 had the same mix design of 2% MSF, while CT4 had the steel fiber reduced to a 1% fiber ratio, and CT5 utilized 2% RSF. For the columns, Mix VII from the material variability study was used based on the cost and availability of the supply. The UHPC was mixed and produced in many batches to fill the columns and construction took place in two different days in January and February 2022 at the fabrication yard of UNR. A total of 25 batches of two cubic feet were produced using the IMER 360 high-shear mixer. Before placing the UHPC in the columns, flow tests were performed as shown in Figure 3-12 for one of the batches. The average static flow was determined to be around 208 mm [8.2 in], which is acceptable according to the criteria set by ASTM C1856 [32]. The UHPC was poured from one side of the formwork to allow spreading in the horizontal direction and have fibers oriented in the columns longitudinal direction as shown in Figure 3-12b. The surfaces were disturbed using metal rods to avoid cold joints forming between each batch. After casting the UHPC in the formwork, the columns were covered in heat blankets to avoid heat escaping and reduce water freezing at night. The temperature during the winter in Reno during construction was noted to fluctuate between -5° to 10° C. After one month, the column formwork was removed, and three of the stripped columns are shown in Figure 3-12c. Whitewash paint

was applied to the columns to help better observe the cracks during testing. As shown in Figure 3-12d, the fabricated columns were loaded to a flatbed truck and transported to the University of California Berkeley PEER Laboratory for testing.

3.3.2   Companion Material Properties

Although UHPC mix VII has already been fully characterized as in the previous figure, this section provides the material properties from the actual UHPC batches used for fabricating the columns while also representing actual curing conditions of the columns. The companion UHPC samples were obtained for each column to test the compressive strength at early and late ages. Material samples of 15 UHPC cylinders per column with dimension of 75 mm × 150 mm [3 in × 6 in] were tested on days 3, 7, 14, 28, and 114 (test date). The samples were left outdoors next to the columns to represent actual curing conditions in the winter season, which differed from when the variability study was conducted in the summer, and track the compressive gain. The samples were prepared similarly as in phase one of this study, and the average compressive strength at a specific age was obtained using at least three cylinder samples. Note that the both CT1 and CT2 were produced ins same day from same batch cycles; thus, the UHPC samples obtained and tested from such batches represent the two columns.

Table 4 shows the summary results of the average compressive strength (f'_c), elastic modulus (E_{cyl}), and strain (ε) recorded at peak stress. The table shows that on days 7 and 14, the strength did not change significantly because extremely low temperatures of around -5° C were observed during that week difference which slowed down cement hydration [39]. The numbers previously reported in Section 3.2.3 for ambient temperature

curing showing acceptable compressive strength at similar ages can also render the low compressive strength recorded from the columns as isolated cases. For completeness, and in case needed for future modeling, Figure 3-13 shows the full stress-strain relationships of the different UHPC batches on day 28 and test days. The maximum compressive strength on day 28 was around 103 MPa [15ksi], which was relatively low compared to the reported strength in the variability study above and the literature in general [1], as full strength was yet to develop with the slow hydration and low temperatures. On the test day, the full compressive strength was almost gained where CT1/CT2 showed the lower bound strength of 136.6 MPa [19.8 ksi] and CT3 had the upper bound strength of 162.2 MPa [23.5 ksi]. The axial strain was also recorded at the peak stress, and the strain ranges typically from 0.4-0.5%. The MOE was calculated using the best-fit linear approximation at 10-30% of the maximum peak stress [1]. The MOE was observed to increase with the age of testing, and the average MOE at the test dates for the different columns batches was around 41.8-43.4 GPa [6,070-6,300 ksi].

The actual reinforcement properties were also determined using ASTM A370 tensile test procedure [40]. Longitudinal rebars of Φ13 [#4] and Φ16 [#5] and transverse rebars of Φ10 [#3], all of Gr 60, were utilized in all columns, and four coupons of 380 mm [15 in] length were tested from each rebar size using a displacement-controlled Instron machine and test results are provided in Table 5 for average yield strength, yield strain, ultimate strength, and ultimate strain.

3.3.3 Test Setup and Instrumentation

The columns were tested using the gigantic hydraulic universal testing machine at the UC Berkeley PEER laboratory, which has a capacity of 17,793 kN [4,000 kips] and can accommodate columns of up to 10.2 m [33.5 ft] in length. Steel plates were grouted at the floor and the bottom of the loading head to distribute uniform stress on the surface. Vertical brackets were placed at the bottom plate to hold the column in position and to prevent instability while testing. Figure 3-14 shows the complete setup for one of the columns sitting under the press machine. Some of the columns were noticed to be tilting when placed between the leveling plates indicating that the top and bottom ends were uneven or unparallel, which required some adjustments that led to some loading eccentricity. The columns were tested under a supposedly concentric axial loading with a loading rate of 4.45 kN/sec [1 kip/sec]. Each column test took around 20-30 minutes to reach the maximum force. The test was terminated when the force dropped around 50% of the peak force.

The columns were instrumented using string potentiometers, displacement transducers, reinforcement strain gages, and select columns with concrete gauges. The instruments were placed to measure the global and local response of the column subject to the concentric axial loading imposed. Figure 3-14 illustrates the displacement instrumentation, i.e. six linear variable differential transducers (LVDTs), attached to the big and small rods at the north and south sides, and the string potentiometers that were attached to the plates at the west and east sides. The average axial strain was calculated from the displacement measurements based on the average length change (ΔL) over the

initial test length, L_o. All columns reinforcement were heavily instrumented with strain gages at several critical sections with a total of 20 to 28 strain gages used in each column.

3.4   Large-Scale Testing: Results and Discussions

This section provides the experimental results from the full-scale columns tests in terms of the global behavior, i.e. observed damage, axial load-strain relationships, and axial stiffness, as well as the local behavior in terms of reinforcement strains. The section also provides a dedicated discussion of the effects of the tested parameters.

3.4.1   Observed Damages

The damage patterns during and after each test were observed. During testing, minor cracks were observed from the top of the column, which was expected since the surface was uneven and experienced some stress concentrations. Surface cracks had developed mainly on the bottom and top of the columns before failure, but no significant damage was observed in any of the columns until failure. When the column reached its peak capacity, a loud noise was heard indicating the compressive failure of the UHPC and reinforcement rupture. Longitudinal rebar buckling and tie ruptures were observed and caused local sections to bulge; thus, concrete cover spalling occurred at these locations. However, the steel fibers helped keep the columns integrity and avoid severe spalling, i.e. lessened the typical explosive nature in HSC or NSC by bridging the spalled cover and the core. Figure 3-15 shows the damaged state of the columns at the end of each test. The spalled concrete cover was still intact for all the columns except for CT5, where large

UHPC portions fell at the top. The spalled cover was manually removed later to better observe the reinforcement damage and characterize the columns failure mode.

Specimen CT1 was observed to have a failure concentration at the bottom with permanent global buckling. The specimen did not exhibit as much damage as expected since the column was adequately confined. The observed behavior was different for specimens CT2 and CT5, as local buckling combined with transverse tie rupturing caused damage at the top portion of the columns. Note that these two columns were underdesigned with less confinement than specimen CT1; thus, local buckling was not a surprise. Although both specimens reached similar axial capacity, the top south cover section of CT5 (which had RSF) exploded and exposed the longitudinal and transverse reinforcement. Localized cracking expanded on the south section because of the buckling and tie rupturing combined with the low resistance from the recycled fibers, which eventually caused major spalling of the concrete cover. The damage state for specimens CT3 and CT4 with the comparative 2% and 1% MSF ratios was observed. Because of the decrease in fiber ratio, the damage state for CT4 was significant relative to CT3. It was also noted that adding the octagonal reinforcements helped avoid local rebar buckling compared to CT2 and CT5, but could not prevent buckling across multiple hoops and ties rupture was still the failure mode for CT3 and CT4.

3.4.2 *Axial load-strain relationships and stiffness*

The axial load was measured using a load cell connected to the big press machine. Six LVDTs and two string potentiometers were used to measure axial shortening, and in turn, relate to the original length to calculate the average axial strain within different portions

of the column. Some LVDTs and string potentiometers were knocked down as the failure point was approached, and in such cases, recorded data were excluded from the average axial load strain. Figure 3-16 show the average axial load-strain relationship for all the columns. As noticed in the response, the strain on the north and south sides differed significantly throughout the loading, indicating eccentricity in the column. The difference between the strain at 50% of the peak loading was calculated to understand how eccentricity played a significant role in the strain variation at specific sections in the column. The accidental eccentricity in the columns was attributed to the uneven and unparallel construction of the top and bottom surfaces, causing one side to experience more compression. The eccentricity was more pronounced in the north-south direction for most of the columns, except for CT3 that showed eccentricity in the west-east direction as evidenced from the final damage.

Since eccentricity caused a variation in the measured shortening at the two opposite sides, the average of the axial load-strain relationships to reduce or eliminate the effect of eccentricity. Figure 3-16f compares the obtained average axial load-strain relationships for all five columns. All columns had similar behavior with almost a linear response up to about 80% of the load capacity followed by an increased nonlinear behavior, and a plateau in some cases, as the load capacity is achieved. A sudden drop in the load was then recorded, which indicated failure of the column and evidenced with spalling of the concrete cover, buckling of the longitudinal reinforcement, and rupture of tie reinforcement.

To further compare the five columns with less dependency on the UHPC compressive strength that varied among the columns, a normalized axial load was calculated using $P_{norm} = P_{max}/(f_c' \times A_g)$. Figure 3-17 shows the normalized axial load-strain relationship with the detailed necessary calculations summarized in Table 6 along with the corresponding differences among the columns. Specimen CT1 obtained the highest normalized axial loading of 0.71, as expected, with a difference of 6-26% compared to other columns. A significant drop in the normalized axial load was observed for specimens CT2 and CT5, which yielded almost the same magnitude of 0.56 and 0.54, respectively. The results were expected as the s/d_b of these columns does not satisfy the provisions set by ACI 318-19, such that the longitudinal reinforcement was more susceptible to a pre-mature buckling. Slightly higher results were calculated in specimens CT3 and CT4 compared to CT2 and CT5, which obtained a normalized axial load of around 0.67 and 0.61, respectively. The addition of the extra octagonal hoops helped increase the maximum normalized axial load.

The axial stiffness of the columns based on the experimental average load-displacement relationship was determined and used to backcalculate the MOE of the UHPC in the columns. If comparable MOE values are shown from the UHPC columns and cylinders, then the column axial stiffness estimation directly from the cylinders MOE can be confirmed and verified. The axial stiffness based on the tangential modulus (K_t) was obtained from the best-fit linear approximation from 10% to 30% of the peak strength to be consistent with what we do for the UHPC cylinders. Equation 3-3 show how the UHPC MOE is estimated from the experimental columns stiffness. In Equation 3-3, K is

the axial column stiffness; E is UHPC MOE, A is column cross-sectional area, E_s is the MOE of steel, and A_s is the area of longitudinal reinforcing steel. In this case, E_s is estimated to be around 2×10^5 MPa [29,000 ksi], typical for the steel reinforcements used. Table 7 shows the column axial stiffness and the backcalculated MOE from UHPC columns. Note that the axial stiffness yielded an average value of 2,108 kN/mm [12,036 k/in] for the tested columns.

$$K = \frac{(E \cdot A)_{total}}{L} \; ; \; (E \cdot A)_{total} = E_{UHPC} \cdot (A_g - A_s) + E_s \cdot A_s \qquad (3)$$

Using the derived column axial stiffness, the average MOE from all the UHPC columns was determined to be ~36,226 MPa [~5,254 ksi] as shown in Table 7. The MOE from all columns except CT3 was noticeably similar, but when compared with cylinders, the MOE of columns are shown to be on average 85% of the corresponding cylinders MOE values. The difference can be attributed to the column size effect and nature of measurement methods at both scales, but a similar trend was previously reported by Aboukifa and Moustafa [12]. This observation indicates that an adjustment of the UHPC cylinders MOE with a 0.85 is necessary for axial stiffness calculations.

3.4.3 Reinforcement Strains

All columns used reinforcement strain gages at different sections along column height in select longitudinal reinforcement and transverse reinforcement. Few strain gages were damaged during the casting of the UHPC, so no strain measurements were recorded at those gages. The longitudinal gages (6 to 8) were placed at three sections in the middle of the column and 230 mm [9 in] below and above the center. Similarly, 14 to 20 strain

gages were placed at the transverse reinforcements at the height center hoops and positioned around 230 mm [9 in], 460 mm [18 in], and 685 mm [27 in] above and below. Table 8 summarizes the maximum strain recorded at different sections along the column height in the instrumented longitudinal rebars. All longitudinal reinforcement yielded in compression. However, comparing the strain recorded in different sides show a variation that can explain the eccentricity effects and eventually the observed rebar buckling (see Figure 3-15). Figure 3-18 shows the axial load versus longitudinal reinforcement strain for all column specimens recorded at -230 mm [-9 in] from the center. The yield strain value (red line) crosses the different rebar strain to a wide gap that indicates not all longitudinal rebars yielded at same axial load value.

Similarly, the transverse reinforcement strain was measured at different column sections. Unlike the strains in longitudinal reinforcement, the transverse reinforcement strain in tension, providing confinement in the columns. Based on the maximum strains recorded, none of the instrumented transverse reinforcement reached yielding. However, the no yielding of transverse reinforcement does not entirely reflect in other sections as hoop ruptures were observed elsewhere. In addition, the strains were slightly higher on specific sections, indicating a high concentration of local stress around the area as it is close to the location of the damaged portion in the column. Figure 3-19 shows the transverse reinforcement strain close to the column section where the failure occurred. The gap between the strain recorded at the opposite sides of the same transverse reinforcement clearly shows local behavior as the reinforcement experienced different strain engagements at specific axial loading. The behavior showed that specific longitudinal

reinforcements pushed the transverse reinforcement more aggressively than other longitudinal reinforcements.

3.4.4   Effect of tie configuration, fiber ratio, and types of fibers

The effect of different tie configurations, fiber ratios, and types of fibers used was investigated to further assess the performance of the utilized economical UHPC in full-scale columns. The reinforcement ratios and hoop/tie configuration were varied in CT1-CT3 to evaluate whether ACI detailing reinforcement can be relaxed in UHPC columns to further reduce overall costs and carbon footprint. Looking at the damage state of the columns, CT1 showed lesser cracks and spalling relative to CT2 and CT3. Major spalling was noticed on the upper section of CT2 as local buckling occurred, which was not seen in columns CT2 and CT3. By changing only the size of the longitudinal reinforcement and keeping the longitudinal reinforcement ratio close, column CT1 with #5 longitudinal reinforcement reached higher axial load capacity than CT2 and CT3 with #4 longitudinal reinforcement by 26.8% and 6.1%, respectively. Since the difference in the longitudinal reinforcement ratio is negligible and the transverse reinforcement ratio is identical for CT1 and CT2, the decrease in axial load capacity in CT2 can be attributed mainly to unsupported longitudinal reinforcement not confined properly according to ACI 318-19 [27]. The need for additional confinement for CT2 was further validated when extra octagonal hoops (increased ρ_t from 0.61% to 1.22%) were added in CT3, which raised the normalized axial load relative to CT2 by 19.5% but still fell short by 5.7% relative to CT1. In addition, the strain output for the transverse reinforcement (not fully shown for brevity but illustrated in Figure 3-19) shows good engagement, especially with the

octagonal transverse, emphasizing the importance of confinement for UHPC columns. Thus, the results and discussion here suggest that proper detailing in light of existing ACI 318 provisions to provide well-confinement benefits the UHPC columns significantly.

The result of reducing the fiber ratio for economical UHPC was tested by varying the fiber volume ratio of 1% versus 2% for specimens CT4 and CT3, respectively, while keeping the reinforcement identical. The effect of reducing the fiber ratio can be directly observed in the damage state in CT4 where major cracks and spalling were seen at the top and bottom of the column compared to CT3, that had localized cracks only at the bottom section. In addition, a reduction of fiber ratio by 1% of the total volume led to a decrease in the maximum normalized axial load by 9.5%. Reducing the fiber ratio volume also increased the strain in the reinforcement in some sections as the confinement effect of the fibers decreased. The result also agrees with the UHPC cylinders tested in pure axial compression for CT4, as it shows a decrease in compressive strength by around 3.7% relative to the UHPC samples from CT3. The results thus further validate that fibers help bridge microcracks and overall enhance UHPC confinement and achieve higher axial capacity.

Since one of the objectives of this study is to potentially reduce the cost of UHPC by incorporating recycled materials, the effects of RSF in the full-scale columns were examined. Column CT5 was constructed using the same reinforcement detailing in CT2 but cast with RSF UHPC. The characteristics of the RSF were visualized better after testing both specimens CT2 and CT5, which was manifested in significant spalling and cracks, especially at the column top. The substantial damage was caused by the

combination of more pronounced local buckling of the longitudinal rebars and the weaker confinement of the RSF. Meanwhile, the tested UHPC cylinders already showed that RSF slightly reduced the strength by 4.9% compared to using MSF, which mapped to a decrease in the axial capacity of columns. Such reduction can be attributed to the overall weaker properties of the RSF and the impurities in the fibers like rubber crumbs [26]. Nevertheless, the difference in the normalized axial load for both columns was almost negligible, indicating that the RSF can be still an alternative source for full-scale columns subjected to axial compression.

3.5   Conclusions

This study aimed at introducing and validating the concept of semi-proprietary economical and scalable UHPC that can combine a proprietary blend, i.e., smaller portion of the constituents that brings robustness and advanced material technologies, with local sand, cement, admixtures, and steel fibers of users choice, which form the larger portion of the constituents and drives cost down to brings economy and sustainability. First, a detailed material variability study was conducted to investigate the effect of varying sand, cement, and fibers (manufactured versus recycled tires fibers) types as well as aggregate gradation on the mechanical properties of UHPC. Next, five full-scale columns were fabricated using the successfully validated economic UHPC mixture and designed with different steel and fiber reinforcement. The columns were tested under concentric axial loading at the UC Berkeley PEER Laboratory. Based on both parts of this study, the following conclusions and recommendations can be drawn:

- Overall, using a wide range of local materials (sand of varying gradation settings, cement, and admixtures) with a commercial powder of proprietary blend of supplementary constituents is verified to successfully produce a scalable economical UHPC with compressive strength that can reach and exceed 150 MPa [~22 ksi] under ambient curing conditions. The corresponding tensile and flexural strength are also determined to be acceptable in light of emerging UHPC construction specifications with a slight reduction observed only for UHPC with recycled steel tires wires/fibers.

- The economical UHPC mixture is demonstrated to be a viable candidate for axial columns as one potential large-scale application of future UHPC structures. Moreover, the overall response of columns with both high-end manufactured fibers and recycled steel fibers should a small difference, which renders the recycled fibers as promising candidate for ultra economical UHPC and motivates future research to properly investigate the full potential of using raw and processed/sorted recycled steel fibers.

- While accounting for various ambient curing conditions between the material variability study and columns fabrication, the economical UHPC mixture shows robustness and maintain an average compressive strength in the range of 130-162 MPa [20-23 ksi] along with modulus of elasticity in the range of 41.8-43.4 GPa [6,070-6,300 ksi].

- Spalling, tie rupturing, and buckling of the reinforcement are common damage states observed in axial UHPC columns failure. Comparatively, properly detailed columns in light of ACI 318 provisions showed lesser damage and higher axial capacity by up

to 26.8% compared to those with less confinement and improperly supported longitudinal reinforcement. In fact, adding the extra octagonal hoops for the non-ACI compliant columns increased the axial load capacity by about 19.5%.

- The columns with less than 2% fiber ratio and recycled fibers exhibited more spalling and damage overall, confirming the effect of fibers in slowing crack propagation at failure and its effectiveness in improving the axial response of UHPC columns. This is demonstrated when decreasing the fiber ratio from 2% to 1% by volume lowered the axial capacity by 9.5%. However, using recycled steel fibers as an alternative to manufactures fibers showed only a negligible effect on the axial capacity as suggested by the comparable normalized capacity.

- The modulus of elasticity of UHPC as estimated from cylinders tests in accordance with the relevant ASTM standard is recommended to be adjusted by a factor of 0.85 to use for estimating axial stiffness of UHPC columns. This recommendation is drawn based on direct comparisons of companion cylinders and columns results.

3.6   Acknowledgments

3.7   References

[1] Graybeal, B. A. (2006). Material property characterization of ultra-high performance concrete. FHWA final report, https://www.fhwa.dot.gov/publications/research/infrastructure/structures/11038/.

[2] Graybeal, B. A. (2011). Ultra-high performance concrete (No. FHWA-HRT-11-038)

[3] Aboukifa, M., Moustafa, M. A., & Saiidi, M. S. (2021). Seismic response of precast bridge columns with composite non-proprietary UHPC filled ducts ABC connections. Composite Structures, 274, 114376.

[4] Tazarv, M., & Saiidi, M. S. (2015). UHPC-filled duct connections for accelerated bridge construction of RC columns in high seismic zones. Engineering Structures, 99, 413–422.

[5] Shafieifar, M., Farzad, M., &; Azizinamini, A. (2018). New connection detail to connect precast column to cap beam using ultra-high-performance concrete in accelerated bridge construction applications. Transportation Research Record: Journal of the Transportation Research Board, 2672(41), 207–220.

[6] Abokifa, M., & Moustafa, M. A. (2021). Full-scale testing of non-proprietary ultra-high performance concrete for deck bulb tee longitudinal field joints. Engineering Structures, 243, 112696.

[7] Dean, N. & Stevens, C. & Hastings, J., (2019) "Accelerated Bridge Construction Methods for Bridge 1-438 Replacement", International Interactive Symposium on Ultra-High Performance Concrete 2(1).

[8] Foden, A. J. & McDonagh, M. D., (2016) "Benefits of Ultra-High Performance Concrete for the Rehabilitation of the Pulaski Skyway", International Interactive Symposium on Ultra-High Performance Concrete 1(1).

[9] Shafei, B., & Karim, R. (2022). Non-proprietary ultra-high performance concrete mix design for ABC Applications. Accelerated Bridge Construction. https://abc-utc.fiu.edu/research-projects/isu-research-projects/non-proprietary-ultra-high-performance-concrete-mix-design-for-abc-applications/

[10] Berry, M., Snidarich, R., & Wood, C. (2017). Development of non-proprietary ultra-High-performance concrete (No. FHWA/MT-17-010/8237-001). Montana. Dept. of Transportation. Research Programs.

[11] El-Tawil, S., Alkaysi, M., Naaman, A. E., Hansen, W., & Liu, Z. (2016). Development, characterization, and applications of a non-proprietary ultra-high performance concrete for highway bridges (No. RC-1637). Michigan. Dept. of Transportation.

[12] Abokifa, M., & Moustafa, M. A. (2021). Mechanical characterization and material variability effects of emerging non-proprietary UHPC mixes for accelerated bridge construction field joints. Construction and Building Materials, 308, 125064.

[13] Amin, M., Hakeem, I. Y., Zeyad, A. M., Tayeh, B. A., Maglad, A. M., & Agwa, I. S. (2022). Influence of recycled aggregates and carbon nanofibres on properties of ultra-high-performance concrete under elevated temperatures. Case Studies in Construction Materials, 16.

[14] Liew, K. M., & Akbar, A. (2020). The recent progress of recycled steel fiber reinforced concrete. Construction and Building Materials, 232, 117232.

[15] Aghaee, K., & Yazdi, M. A. (2014). Waste steel wires modified structural lightweight concrete. Materials Research, 17(4), 958–966.

[16] Centonze, G., Leone, M., & Aiello, M. A. (2012). Steel fibers from waste tires as reinforcement in concrete: A mechanical characterization. Construction and Building Materials, 36, 46–57.

[17] Aiello, M. A., Leuzzi, F., Centonze, G., & Maffezzoli, A. (2009). Use of steel fibres recovered from waste tyres as reinforcement in concrete: Pull-out behaviour, compressive and flexural strength. Waste Management, 29(6), 1960–1970.

[18] Samarakoon, S. M. S., Ruben, P., Wie Pedersen, J., & Evangelista, L. (2019). Mechanical performance of concrete made of steel fibers from tire waste. Case Studies in Construction Materials, 11.

[19] Caggiano, A., Folino, P., Lima, C., Martinelli, E., & Pepe, M. (2017). On the mechanical response of hybrid fiber reinforced concrete with recycled and industrial steel fibers. Construction and Building Materials, 147, 286–295.

[20] Abdolpour, H., Niewiadomski, P., & Sadowski, Ł. (2021). Recycling of steel fibres and spent equilibrium catalyst in ultra-high performance concrete: Literature review, Research Gaps, and future development. Construction and Building Materials, 309, 125147.

[21] Yang, J., Peng, G.-F., Shui, G.-S., & Zhang, G. (2019). Mechanical properties and anti-spalling behavior of ultra-high performance concrete with recycled and industrial steel fibers. Materials, 12(5), 783.

[22] Isa, M. N., Pilakoutas, K., Guadagnini, M., & Angelakopoulos, H. (2020). Mechanical performance of affordable and eco-efficient ultra-high performance concrete (UHPC) containing recycled tyre steel fibres. Construction and Building Materials, 255, 119272.

[23] Sugano, S., Kimura, H., & Shirai, K. (2007). Study of new RC structures using ultra-high-strength fiber-reinforced concrete (UFC). Journal of Advanced Concrete Technology, 5(2), 133–147.

[24] Hosinieh, M. M., Aoude, H., Cook, W. D., & Mitchell, D. (2015). Behavior of ultra-high performance fiber reinforced concrete columns under pure axial loading. Engineering Structures, 99, 388–401.

[25] Shin, H.-O., Min, K.-H., & Mitchell, D. (2017). Confinement of ultra-high-performance fiber reinforced concrete columns. Composite Structures, 176, 124–142.

[26] Aboukifa, M., & Moustafa, M. A. (2022). Reinforcement detailing effects on axial behavior of full-scale UHPC columns. Journal of Building Engineering, 49, 104064.

[27] Aboukifa, M., & Moustafa, M. A. (2022). Structural and buckling behavior of full-scale slender UHPC columns. Engineering Structures, 255, 113928.

[28] "Guidelines for the Use of Ultra-High-Performance Concrete (UHPC) in Precast and Prestressed Concrete." 2022, https://doi.org/10.15554/tr-9-22.

[29] "Standard Test Method for Sieve Analysis of Fine and Coarse Aggregates." ASTM International - Standards Worldwide, https://www.astm.org/standards/c136.

[30] "Standard Test Method for Flow of Hydraulic Cement Mortar." ASTM International - Standards Worldwide, https://www.astm.org/c1437-20.html

[31] "Standard Specification for Flow Table for Use in Tests of Hydraulic Cement." ASTM International - Standards Worldwide, https://www.astm.org/c0230_c0230m-20.html

[32] "Standard Practice for Fabricating and Testing Specimens of Ultra-High Performance Concrete." ASTM International - Standards Worldwide, https://www.astm.org/standards/c1856.htm.

[33] "Standard Test Method for Static Modulus of Elasticity and Poisson's Ratio of Concrete in Compression." ASTM International - Standards Worldwide, https://www.astm.org/c0469_c0469m-22.html

[34] "Standard Test Method for Compressive Strength of Cylindrical Concrete Specimens." ASTM International - Standards Worldwide, https://www.astm.org/c0039_c0039m-21.html

[35] Russell, H. G., & Graybeal, B. A. (2013). Ultra-high performance concrete: A state-of-the-art report for the bridge community. (Inc. Henry G. Russell, Ed.; FHWA-HRT-13-060).

[36] Graybeal, B. A., & El-Helou, R. (2023). Structural design with ultra-high performance concrete (United States. Department of Transportation. Federal

Highway Administration. Office of Infrastructure Research and Development, Ed.; FHWA-HRT-23-077).

[37] "Standard Test Method for Flexural Performance of Fiber-Reinforced Concrete (Using Beam With Third-Point Loading)." ASTM International - Standards Worldwide, https://www.astm.org/c1609_c1609m-12.html

[38] Building Code Requirements for Structural Concrete (ACI 318-19): An ACI Standard: Commentary on Building Code Requirements for Structural Concrete (ACI 318R-19), an ACI Report. American Concrete Institute, 2019.

[39] Ibrahim, M., & Moustafa, M. (2022). Robust methods for UHPC early-strength determination and quality control for Accelerated Bridge Construction.

[40] ASTM International, (2017) "Standard Test Methods and Definitions for Mechanical Testing of Steel Products." A370-17a, West Conshohocken, PA.

Table 3-1 − Variability of different UHPC batches used in the study

Batch ID	Aggregate Type	Sieved Type	Moisture Presence	Cement Type	Steel Fiber	Mixer Type	Curing Regimen*
Mix I	Nevada Sand	Well-graded	Oven/Dry	Type I/II	MSF	High Shear	Ambient
Mix II	Nevada Coarse	Uniform	Oven/Dry	Type I/II	MSF	High Shear	Ambient
Mix III	Playground sand	Uniform	Oven/Dry	Type I/II	MSF	High Shear	Ambient
Mix IV	Coarse Sand	Uniform	Oven/Dry	Type I/II	MSF	High Shear	Ambient
Mix V	Fine Sand	Uniform	Oven/Dry	Type I/II	MSF	High Shear	Ambient
Mix VI	Superfine Sand	Uniform	Oven/Dry	Type I/II	MSF	High Shear	Ambient
Mix VII	Fine Sand	Partial Uniform	Oven/Dry	Type I/II	MSF	High Shear	Ambient
Mix VIII	Fine Sand	Partial Uniform	Oven/Dry	Type I/II	RSF	High Shear	Ambient
Mix IX	Fine Sand	Partial Uniform	Oven/Dry	Type I/II	MSF	Drum	Ambient
Mix X	Local precast Sand	Well-graded	Wet	Type II/V	MSF	High Shear	OT & CR
Mix XI	Precast Local Sand	Well-graded	Oven/Dry	Type II/V	MSF	High Shear	OT & CR
Mix XII	Precast Local Sand	Well-graded	Oven/Dry	Type I/II	MSF	High Shear	OT & CR
Mix XIII	Precast Local Sand	Uniform	Oven/Dry	Type II/V	MSF	High Shear	OT & CR
Mix XIV	Precast Local Sand	Uniform	Oven/Dry	Type I/II	MSF	High Shear	OT & CR

* Ambient/OT: Fabrication Yard Outdoor Temperature in Reno, NV at time of mixing; CR: Curing Room

Table 3-2 – UHPC columns test matrix and reinforcement detailing

Specimen ID	SF type and ρ_v [%]	Long. Rft.	ρ_l [%]	Trans. Rft.	ρ_t [%]	ACI compliant?
CT1	2% MSF	8 #5	1.72	#3 at 3"	0.61	Yes
CT2	2% MSF	12 #4	1.67	#3 at 3"	0.61	No
CT3	2% MSF	12 #4	1.67	#3 at 3" (w/ #3 octagonal)	1.22	Yes
CT4	1% MSF	12 #4	1.67	#3 at 3" (w/ #3 octagonal)	1.22	Yes
CT5	2% RSF	12 #4	1.67	#3 at 3"	0.61	No

Table 3-3 – UHPC mixture composition for different columns in kg/m^3 [lb/ft^3]

Specimen ID	CT25 powder	Sand	Cement	Admixtures	Water	SF
CT1, CT2, CT3, CT5 (2% MSF or RSF)	640.7 [40.0]	800.9 [50.0]	752.9 [47.0]	77.5 [5.0]	160.2 [10.0]	157.2 [9.8]
CT4 (1% MSF)s	640.7 [40.0]	825.0 [51.5]	752.9 [47.0]	77.5 [5.0]	160.2 [10.0]	78.6 [4.9]

Table 3-4 – Mechanical properties of companion UHPC material samples tested at different ages

Age: 3 days			Age: 7 days			Age: 14 days			Age: 28 days			Age: Test Day		
σ, MPa [ksi]	ε, %	E_{cyl}, MPa [ksi]	σ, MPa [ksi]	ε [%]	E_{cyl}, MPa [ksi]	σ, MPa [ksi]	ε [%]	E_{cyl}, MPa [ksi]	σ, MPa [ksi]	ε [%]	E_{cyl}, MPa [ksi]	σ, MPa [ksi]	ε [%]	E_{cyl}, MPa [ksi]
Samples from CT1 and CT2														
44.8 [6.5]	0.53	17991 [2609]	69.4 [10.1]	0.51	25215 [3657]	77.2 [11.2]	0.38	30898 [4481]	104.9 [15.2]	0.52	34688 [5031]	136.1 [19.8]	0.43	41845 [6069]
Samples from CT3														
50.8 [7.4]	0.45	22589 [3276]	71.2 [10.3]	0.42	26973 [3912]	86.8 [12.6]	0.43	33945 [4923]	109.2 [15.8]	0.47	34353 [4982]	157.0 [22.8]	0.49	43376 [6291]
Samples from CT4														
45.7 [6.6]	0.46	19445 [2820]	67.6 [9.8]	0.47	26258 [3808]	93.9 [13.6]	0.44	36228 [5254]	107.2 [15.5]	0.47	33683 [4885]	151.2 [21.9]	0.48	42626 [6182]
Samples from CT5														
44.4 [6.4]	0.44	20084 [2913]	70.7 [10.3]	0.4	25830 [3746]	76.9 [11.2]	0.35	31686 [4596]	103.4 [15.0]	0.51	33876 [4913]	148.3 [21.5]	0.44	43395 [6294]

Table 3-5 Actual tensile properties of reinforcement bars used in all the columns

Rebar Size metric [US]	Yield Strength MPa [ksi]	Yield strain ε_y (%)	Ultimate Strength MPa [ksi]	Ultimate strain ε_{ult} (%)
Φ10 [#3]	504.5 [73.2]	0.33 %	711.1 [103.1]	17.5%
Φ13 [#4]	483.3 [70.1]	0.37 %	690.2 [100.1]	14.7%
Φ16 [#5]	490.8 [71.2]	0.39 %	659.3 [95.6]	17.9%

Table 3-6 – Comparison of the normalized maximum axial loading for each column specimen.

Mechanical Properties	Columns Specimens ID				
	CT1	**CT2**	**CT3**	**CT4**	**CT5**
f'_c MPa [ksi]	136.17 [19.75]	136.17 [19.75]	157.06 [22.78]	151.20 [21.93]	148.24 [21.50]
$p_{max,}$ kN [kips]	9,503 [2,136]	7,222 [1,624]	10,302 [2,316]	9,317 [2,095]	7,753 [1,743]
A_g , mm^2 [in^2]	98,387 [152.5]	94,839 [147.0]	98,129 [152.1]	10,1871 [157.9]	96,451 [149.5]
$p_{max} / (f'_c \times A_g)$	0.71	0.56	0.67	0.61	0.54
$\Delta_{CTn/CT1}$ (%)	-	-21.1	-5.7	-14.7	-23.5
$\Delta_{CTn/CT2}$ (%)	26.8	-	19.5	8.2	-3.0
$\Delta_{CTn/CT3}$ (%)	6.1	-16.3	-	-9.5	-18.8
$\Delta_{CTn/CT4}$ (%)	17.2	-7.6	10.5	-	-10.3
$\Delta_{CTn/CT5}$ (%)	30.6	3.0	23.1	11.5	-

Table 3-7 – Experimental axial stiffness and estimation of MOE from columns versus cylinders

Column ID	UHPC Variation	$K_{avg,}$ kN/mm [kip/in]	EA_{avg} kN [kips]	E_{col} MPa [ksi]	Mean E_{col} MPa [ksi]	E_{cyl} MPa [ksi]	E_{col}/E_{cyl}
CT-1		2,221 [12,683]	3,894,003 [875,411]	36,329 [5,269]			
CT-2	2% MSF	2,242 [12,799]	3,872,969 [870,682]	37,578 [5,450]	35,137 [5,096]	42,355 [6,143]	0.83
CT-3		2,000 [11,419]	3,400,944 [764,566]	31,504 [4,569]			
CT-4	1% MSF	1,932 [11,033]	4,122,350 [926,746]	37,419 [5,427]	37,419 [5,427]	42,626 [6,182]	0.88
CT-5	2% RFS	2,145 [12,250]	3,793,097 [852,726]	36,123 [5,239]	36,123 [5,239]	43,395 [6,294]	0.83
				Average:	36,226 [5,254]	42,792 [6,206]	**0.85**

Table 3-8 – Maximum longitudinal reinforcement strain recorded at different sections of the column

Section mm [in]	CT1		CT2		CT3				CT4				CT5	
	NE	SW	NW	SE	N	W	NE	SW	W	S	NE	SW	NW	SE
229 [9]	-0.79	-0.23	-1.00	-	-0.35	-0.77	-0.69	-0.42	-0.55	-0.72	-0.40	-0.48	-0.63	-0.38
0	-0.39	-0.53	-1.00	-	-	-	-	-	-	-	-	-	-0.49	-0.35
-229 [-9]	-0.76	-0.25	-0.88	-0.14	-0.51	-0.63	-0.24	-0.49	-0.23	-0.88	-0.16	-0.56	-0.33	-0.52

Figure 3-1. Most common application of UHPC in ABC: example from rehabilitation of Pulaski Skyway in New Jersey: (a) precast deck panels before furnishing UHPC; (b) casting of UHPC in the field joints [8]
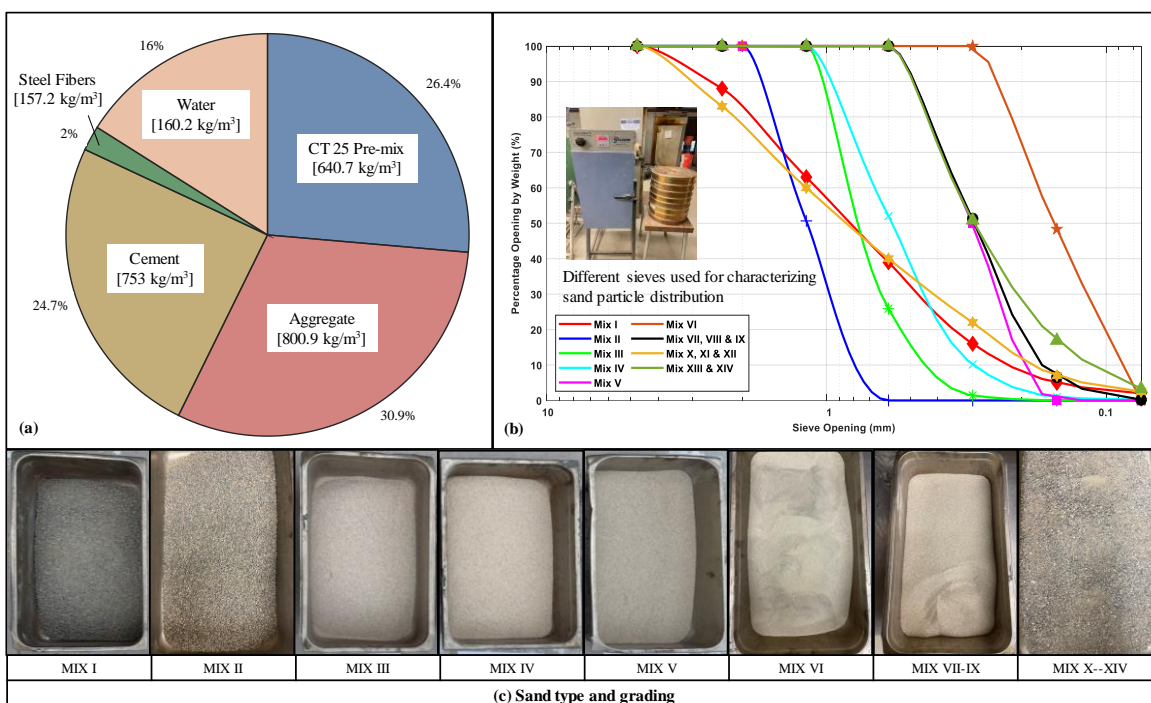
Figure 3-2. (a) UHPC mix constituents and breakdown, (b) sand sieve analysis, and (c) different used sand

Figure 3-3. Comparative appearance between the MSF and RSF used in this study

Figure 3-4. UHPC material batch sequencing using a high-shear mixer
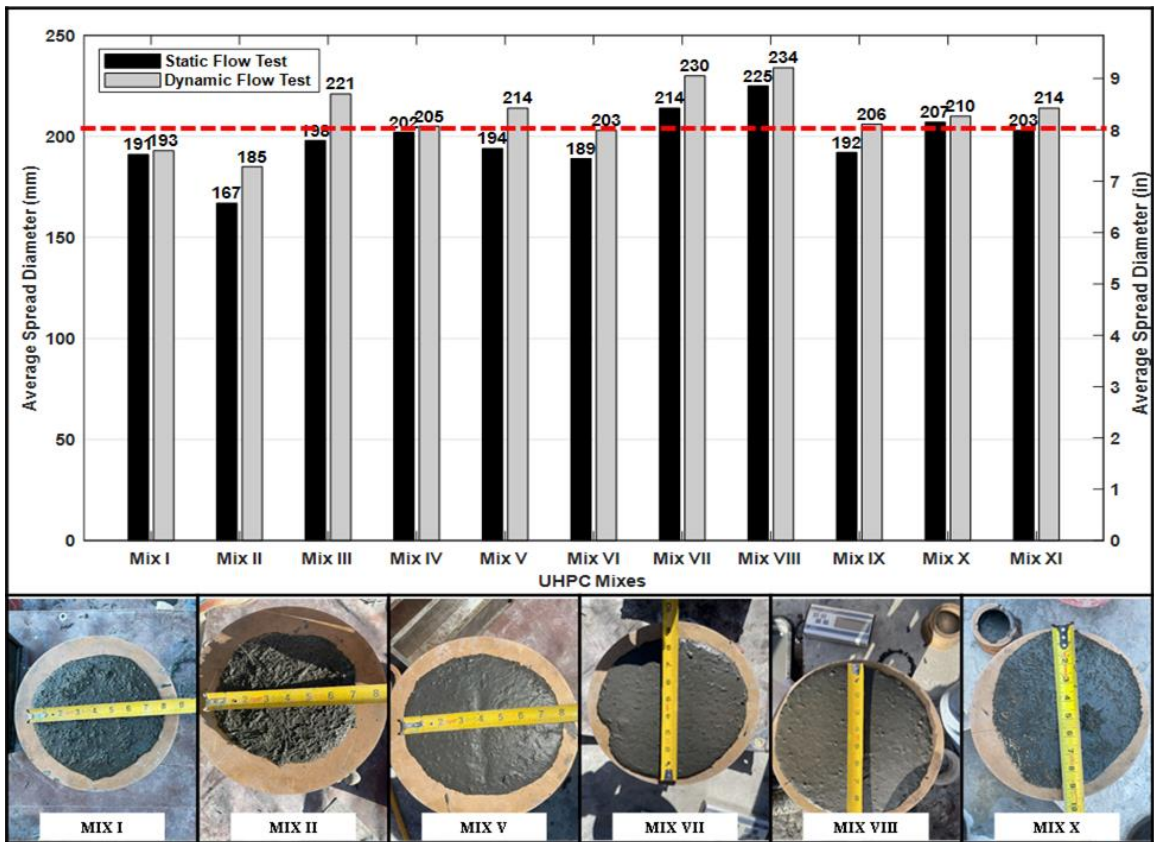
Figure 3-5. Flow test results for Mix I-XI and photographs from selected batches
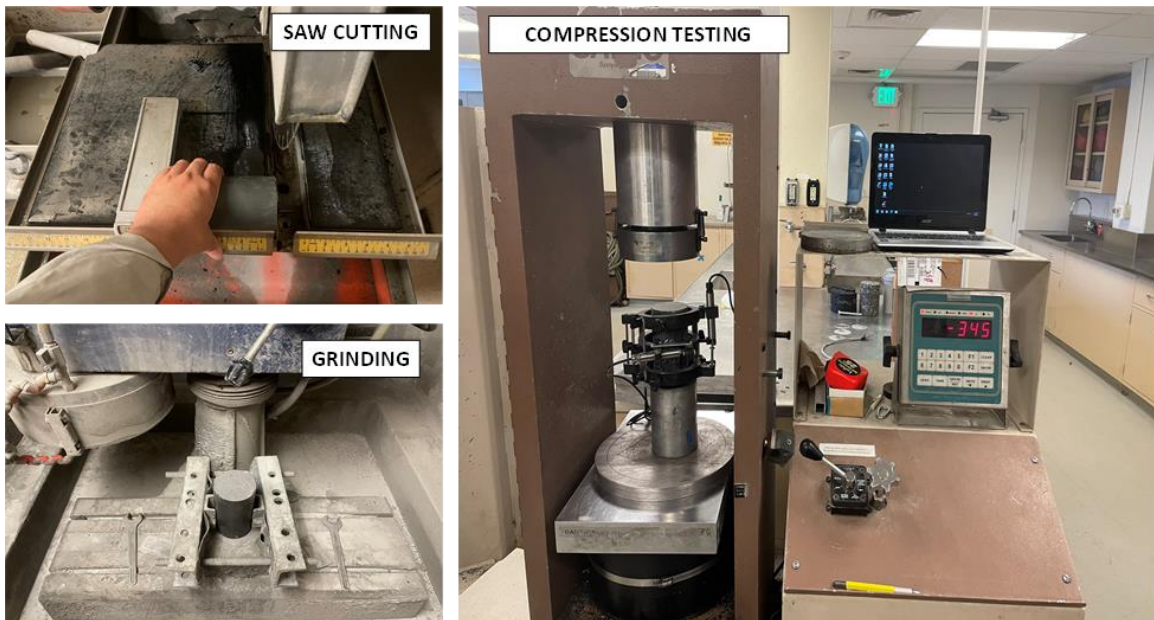
Figure 3-6. UHPC preparation and test setup for compression testing
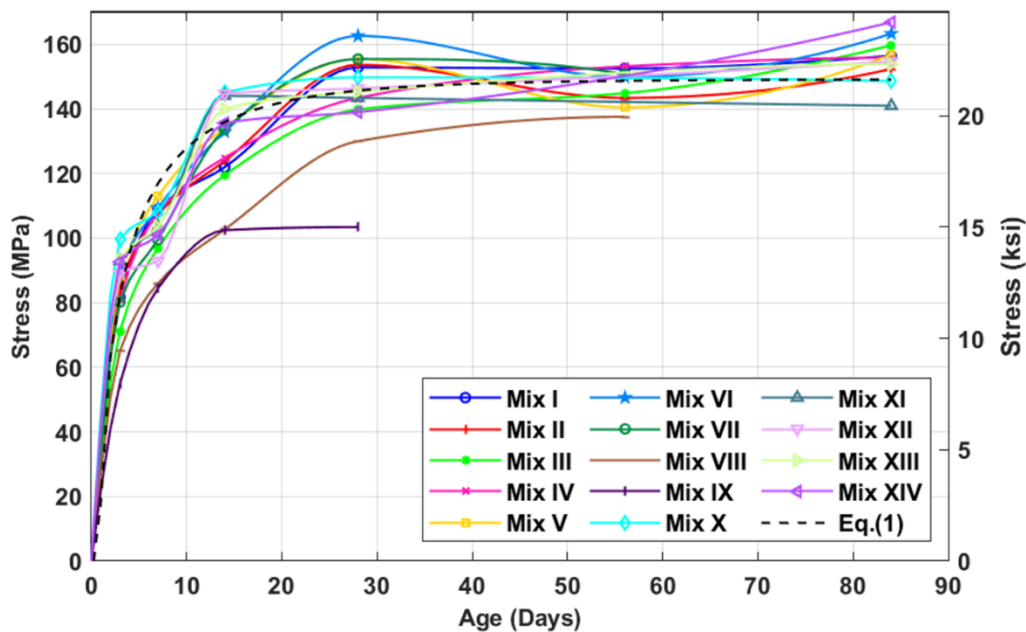
Figure 3-7. Compressive strength gain for all tested UHPC batches as compared to analytical prediction
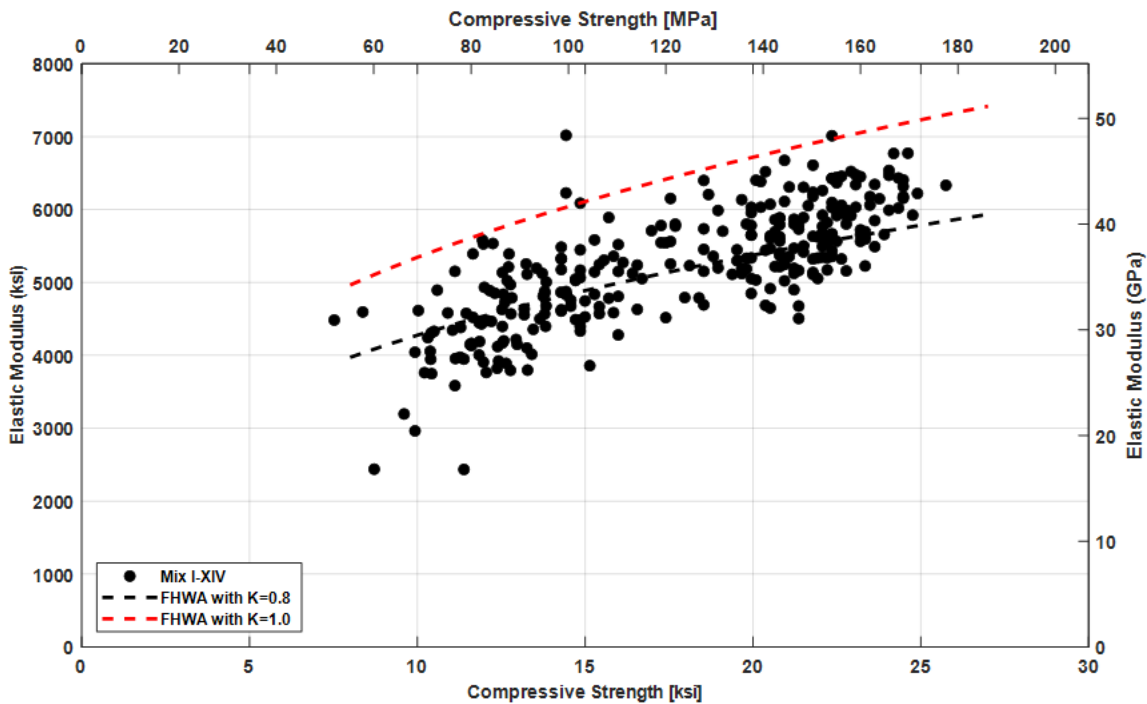
Figure 3-8. Summary of all cylinders MOE versus strength and comparison against the FHWA prediction
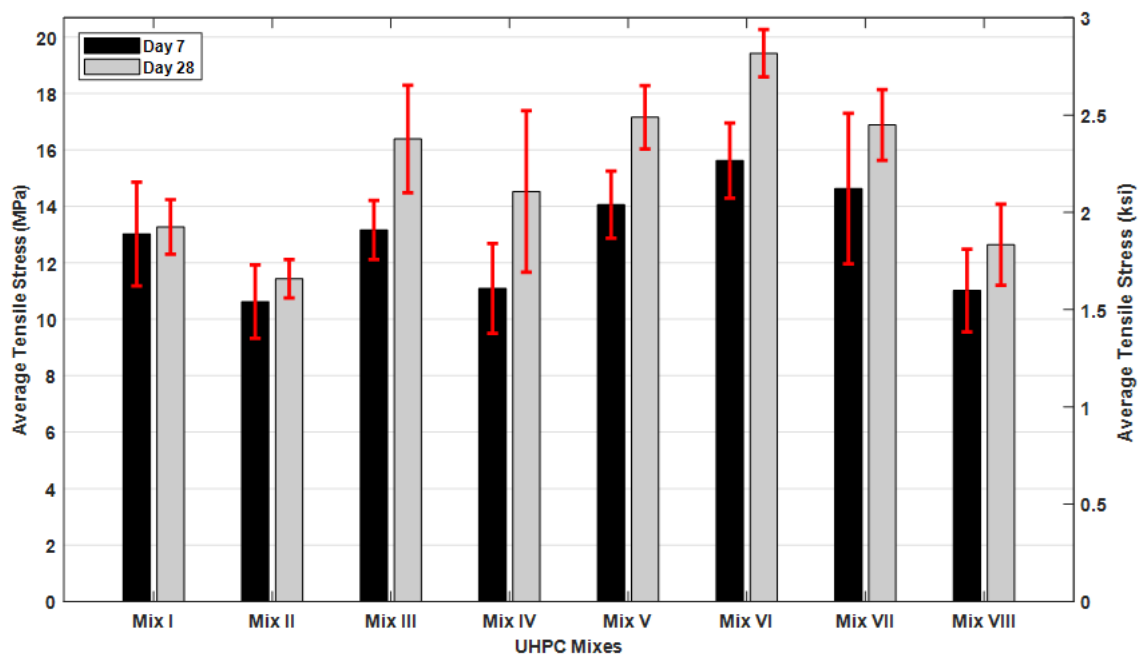
Figure 3-9. Average direct tensile strength for days 7 and 28
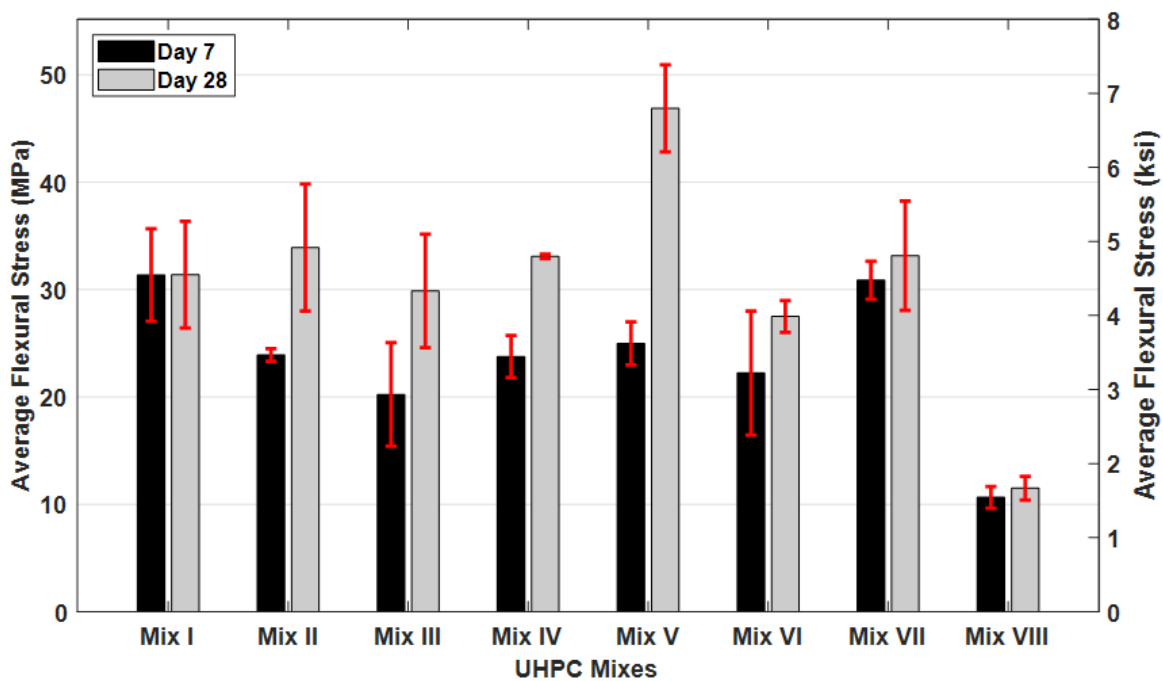
Figure 3-10. Average flexural strength for days 7 and 28
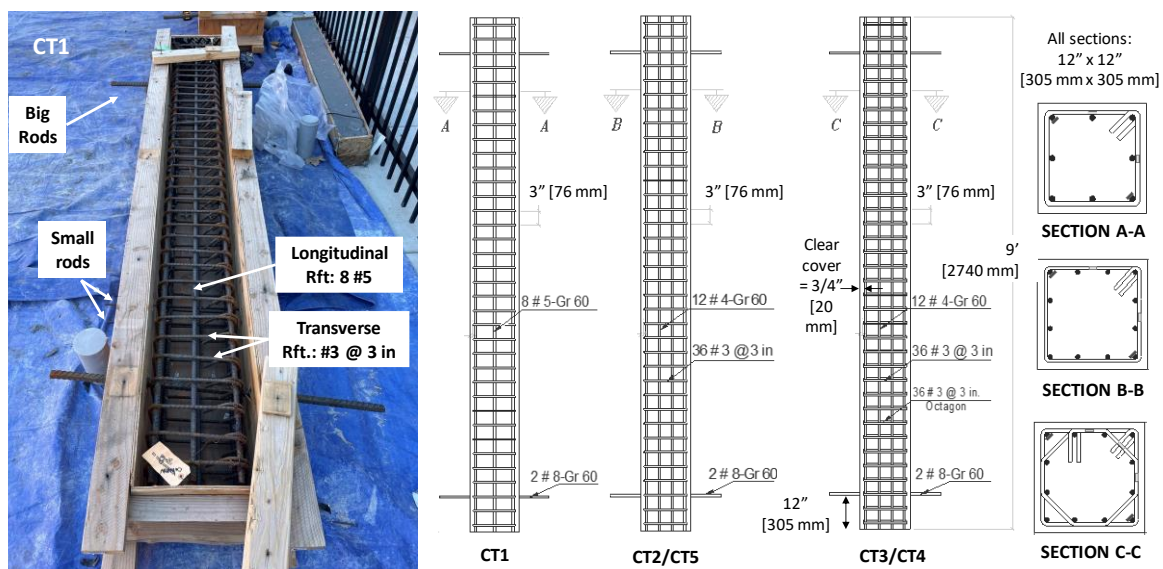
Figure 3-11. Typical formwork and construction setting shown for column CT1 (left), and details of the reinforcement profile and cross-sections of the five full-scale UHPC columns

Figure 3-12. Photographs from columns construction: (a) flow test of one of one of the batches, (b) pouring UHPC into one of the columns, (c) completed columns with a coat of whitewash paint, and (d) loading the columns to a flatbed truck to be transported to the UC
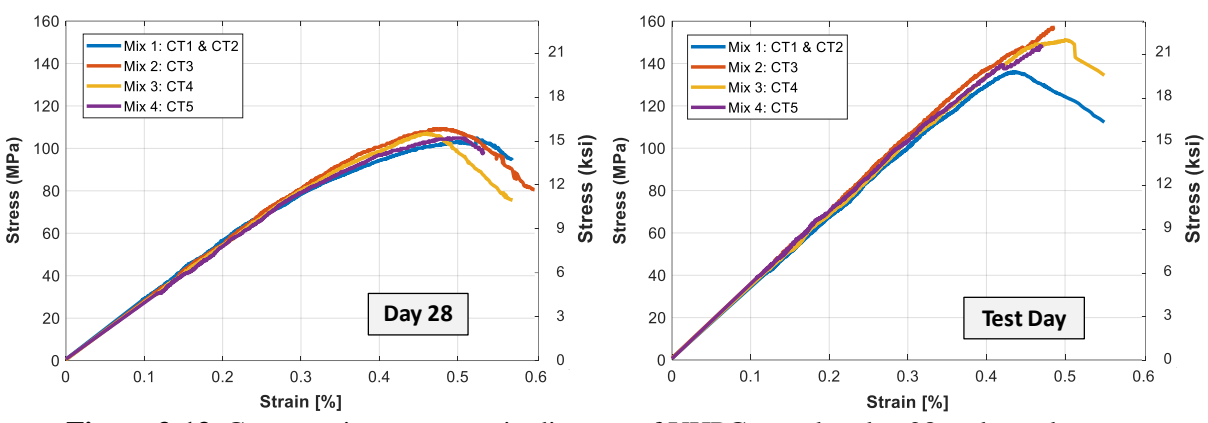
Figure 3-13. Compressive stress-strain diagram of UHPC tested at day 28 and test date
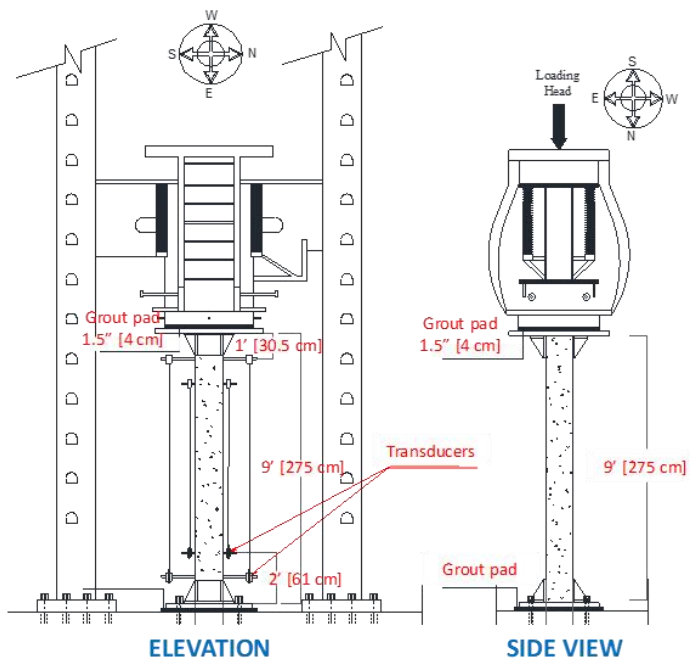
Figure 3-14. Typical axial UHPC column test setup at UC Berkeley PEER lab

Figure 3-15. Damage patterns for all five UHPC columns after axial failure
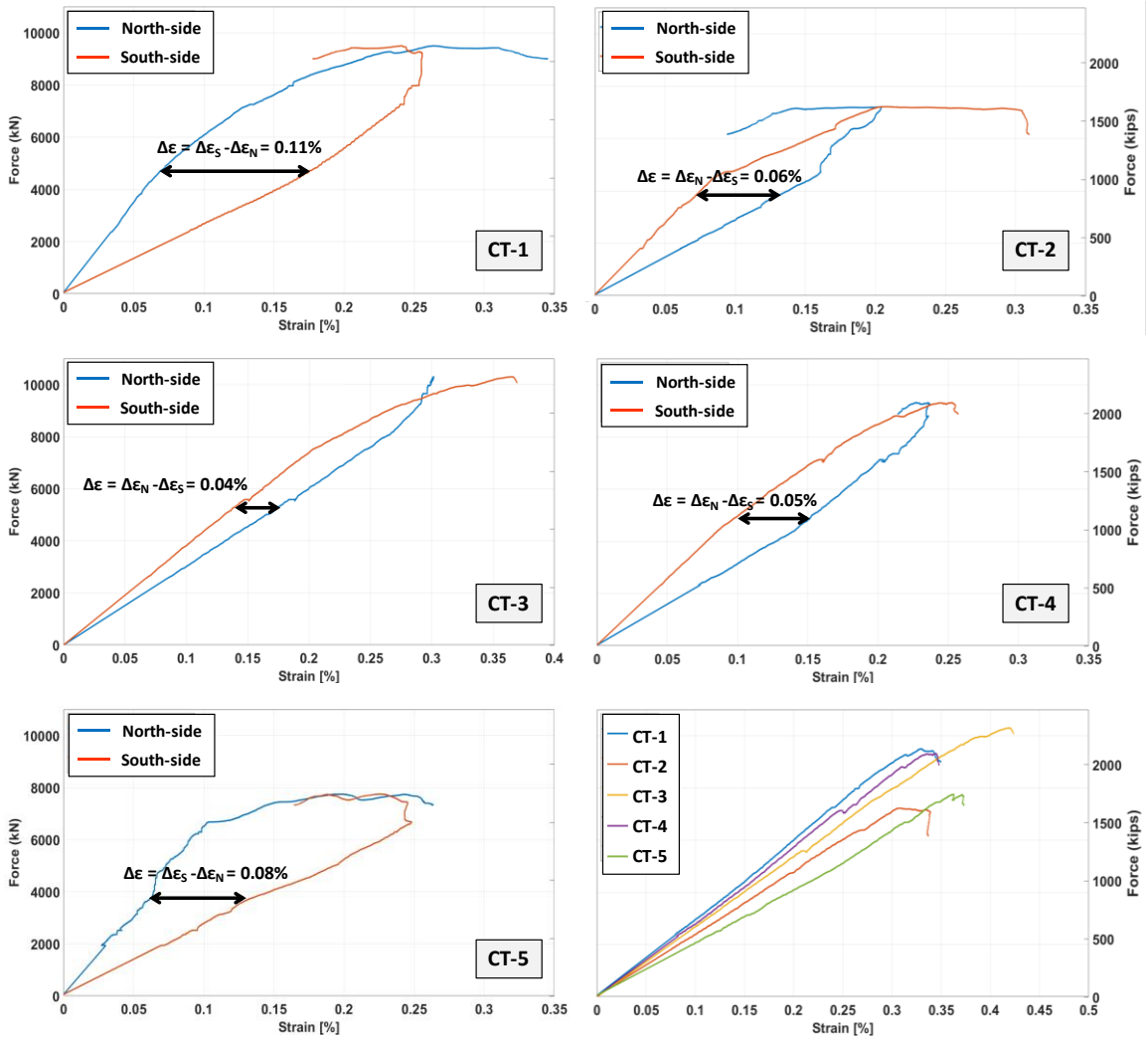
Figure 3-16. Eccentricity and average axial-load strain relationship for columns CT1-CT5
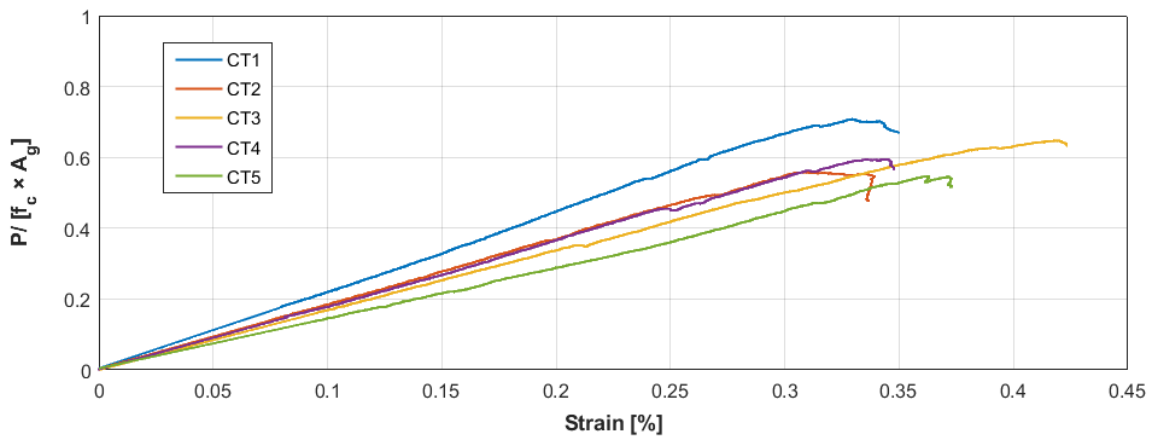
Figure 3-17. Comparative normalized axial-load strain relationship of all UHPC columns
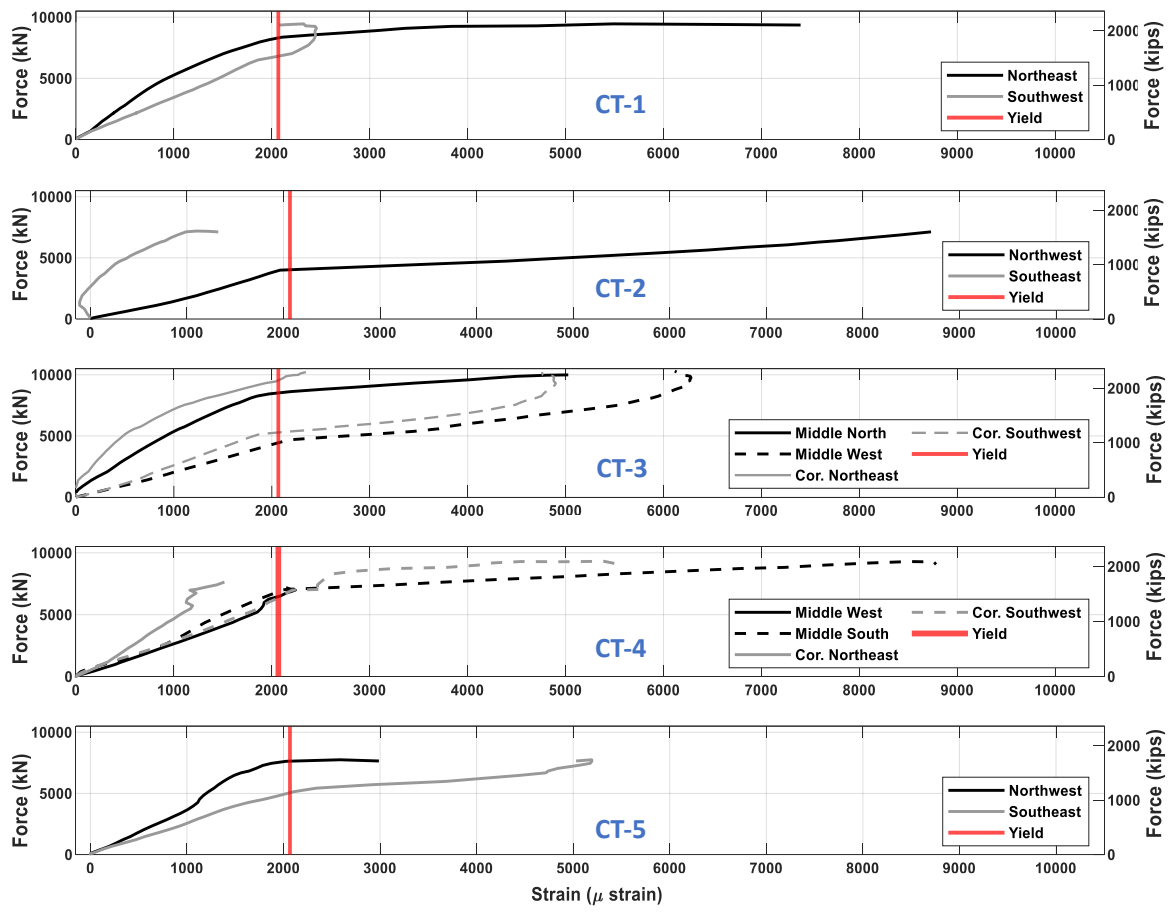
Figure 3-18. Axial load-strain relationship for longitudinal rebars recorded at 229 mm [9 in] below center
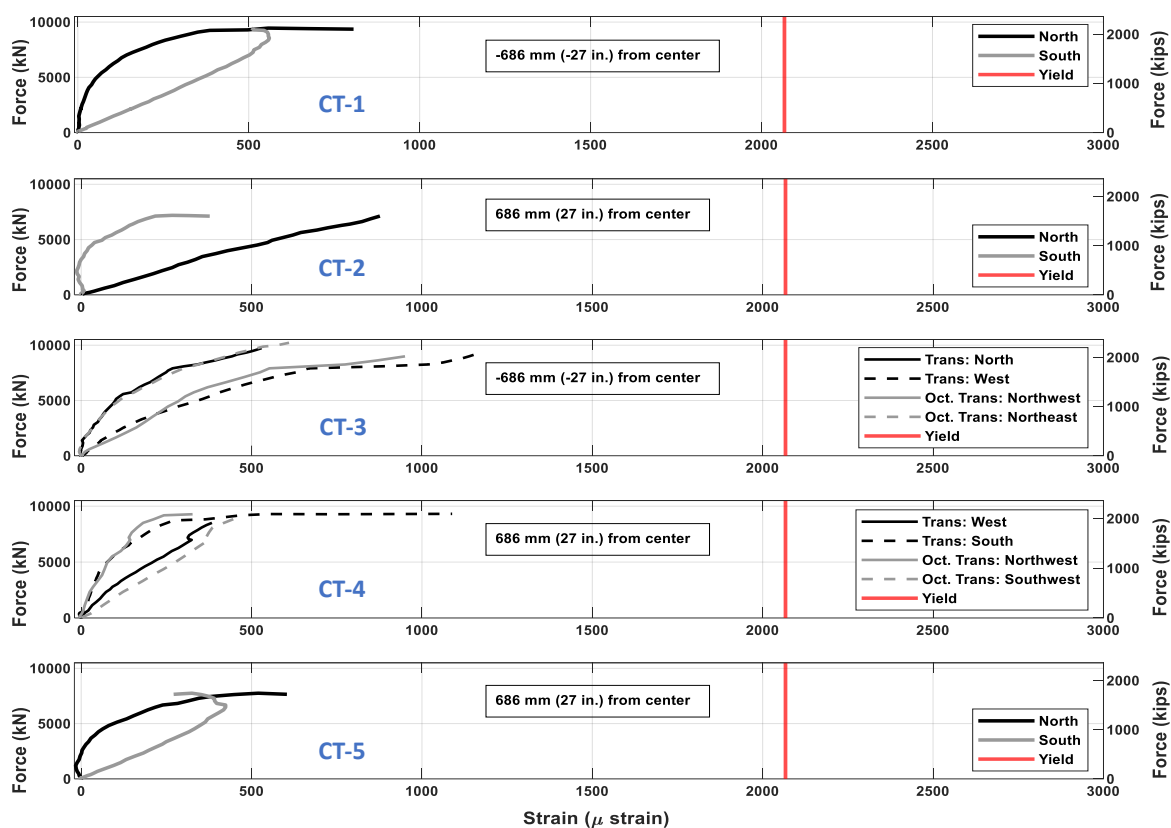
Figure 3-19. Axial-load strain relationship for transverse reinforcement recorded near the failure sections

4   UPCYCLING OF RECYCLED TIRES WIRES AT SCALE: APPLICATION TO FULL PRECAST ECONOMIC ULTRA-HIGH PERFORMANCE CONCRETE BRIDGE COLUMNS

This chapter is a standalone paper that has already been submitted to the Journal of Cleaner Production

Abstract

Ultra-high performance concrete (UHPC) has become increasingly popular for bridge construction because of its superior mechanical performance. However, the large-scale implementation of UHPC has yet to be fully realized because of some barriers like the material high cost that is attributed mainly to the steel fibers that are key constituents of UHPC. While emerging economic UHPC mixtures use local and sustainable materials, this study leverage and expand on such UHPC mixtures by exploring, for the first time, a major large application of the upcycling of chopped wires and fibers from recycled tires when incorporated into full structural precast UHPC applications. The objective of the paper is to assess and compare the structural performance of eco-UHPC full precast bridge columns with both recycled steel fibers (RSF) and manufactured steel fibers (MSF). Two sets of identical 1/3-scale UHPC bridge columns, designed with pocket or duct connections, were cast at a precast plant, and assembled with four conventional reinforced concrete footings. The specimens were tested under combined axial and quasi-static cyclic lateral force at the University of Nevada, Reno. Overall results show that UHPC RSF columns generate sufficient energy dissipation, more than 10% drift ratio, and ductility greater than 6.7; all desired design qualities that render the use of RSF from

recycled tires for UHPC bridge columns as major successful application. The RSF columns reasonably compared to the high-end columns with MSF in terms of mechanical characteristics, which further validates the use of RSF for structural UHPC columns.

Keywords: Economical UHPC, upcycling, recycled steel fibers, precast columns, structural behavior

4.1   Introduction

Ultra-high performance concrete (UHPC) continues to emerge as the next generation of advanced concrete materials because of its enhanced mechanical performance and superior durability [1-3]. Recent developments and improvements in UHPC performance have inspired the use of the material for bridge applications such as overlays [4-5], field deck joints [6], and full girders [6]. Although UHPC is gaining attraction, as evidenced by the uprising use in bridge applications, mass production for structural purposes is yet a challenge because of the relatively high cost associated with the material in general, and some of the vital UHPC constituents like steel fibers in particular. Many efforts have been made toward developing economical UHPC [8] and using recycled materials as alternatives to some UHPC components [9-11]. Steel fibers, a key component of UHPC, drive the cost of UHPC [12] and can contribute significantly to the carbon footprint on top of the cementitious component of UHPC. To address this issue, recycled steel fibers (RSF) can be considered an alternative component for high-end manufactured steel fibers (MSF), which aims to reduce the costs and carbon footprint of UHPC. Using chopped steel wires and fibers from recycled tires as a clean source of RSF is an ideal upcycling

application that add value to a major waste source like the millions of used tires that go to landfills every year. As such, and with the increased interest in UHPC bridge applications, incorporating RSF can be a viable solution to achieve a cleaner, economical, and sustainable UHPC use for future bridge designs.

Limited studies have investigated the use of RSF in UHPC, mainly focusing on basic material characterization or mechanical performance for small-scale applications. In most studies, the compressive strength of UHPC with RSF from tires was slightly decreased due to the presence of rubber impurities covering the fibers [13-14]. However, the reduced compressive strength was observed from several experiments conducted typically for small cylinder samples, whose effects can be expected to be negligible for full-scale structural components. RSF, with a higher length and diameter ratio, shows better flexural performance as it provides anchorage for macro cracks [14]. Similarly, the authors also conducted mechanical characterization of UHPC with RSF and showed that a lower aspect ratio of RSF can significantly reduce the flexural performance of UHPC [15]. With the agreement of using raw RSF with a higher aspect ratio, this type of RSF can preferably be used for structural systems with high flexural demands, such as seismic bridge columns. However, careful assessment should be done with RSF of high aspect ratio, as it can negatively affect workability, and fiber segregation can occur [13]. Even though existing experimental works on RSF are limited in the literature, the promising preliminary results of UHPC with RSF motivates this study to expand to structural applications such as in bridge columns because of its reasonable compressive and flexural performance.

The potential of UHPC with RSF for bridge applications can be demonstrated in precast components for accelerated bridge construction (ABC). In ABC, a bridge can be rapidly constructed using prefabricated components through specialized connection detailing. The benefits of ABC include reduced construction and closure time, lowered cost and resources, and decreased workforce and shoring requirements; all aspects of the larger cleaner production applications in the construction industry. Over the past decade, studies have been developed to understand the behavior of ABC columns with different detailing configurations. Two standard column connections, pocket and duct connections, have been commonly used in ABC applications. In a pocket connection, a full "pocket" with a diameter greater than the column is intentionally placed at the footing or girder, where a full precast column is inserted. Conversely, a duct connection is designed to have multiple ducts in the adjoining member patterned directly from the longitudinal reinforcement extending out of the column. Figure 4-1 shows a simplified ABC bridge subassembly utilizing a pocket and duct connection.

Previous studies have investigated pocket and duct connections for ABC bridges [16-18], and recently, the National Cooperative Highway Research Program (NCHRP) has sponsored the development of seismic specifications of ABC applications [19]. However, the development of these existing reports was validated with experimental programs that related only to conventional concrete types, i.e. normal strength concrete (NSC), and UHPC applications in all previous works have been limited only for the use in the connections as joint filling material. Furthermore, no previous studies have considered using full UHPC columns that are fully precast and suited for ABC applications.

Moreover, no experimental work has yet investigated UHPC with RSF in large-scale applications, specifically for bridge design. Existing ABC studies did not conduct any experimental works that used sustainable and cleaner materials for larger economical and environment-friendly applications at scale like in bridge structures. In addition, there are no attempts in existing literature to perform and experimentally demonstrate large-scale mixing of UHPC with RSF.

Based on above, this study fills several important knowledge gaps by experimentally assessing the structural performance of UHPC with RSF from recycled tires for full precast columns in ABC applications. Specifically, the objectives of this study are to: (1) perform large-scale mixing of UHPC with RSF using current precast practices and fabricate full structural columns, (2) assemble and test four large-scale bridge columns, two sets with RSF and MSF with different ABC footings connections, under combined axial and quasi-static cyclic loading with increasing drift ratio, and (3) comparatively assess the structural response of the tested UHPC columns with RSF and MSF in terms of the global and local behavior to validate the use of raw RSF from recycled tires for the proposed precast bridge columns application. The paper presents first the experimental program development in details with focus on the UHPC precast mixing and fabrication and the bridge columns production phase. Next, the tests results are presented discussed in terms of damage visualization, hysteretic behavior, failure mode, total energy dissipation, curvature analysis, and strain profile assessment.

4.2   Experimental Program Development

This study considers two sets of precast UHPC bridge column specimens with different ABC connections, and each set consists of two identical specimens that vary only in the type of steel fibers used in the UHPC columns, i.e. RSF and MSF. All columns used a commercially available UHPC that can be economically sourced using local sand and cement typically available in precast plants. This section presents the details of the test specimens, the construction details, material characterization of the produced UHPC, instrumentation, and test setup.

4.2.1   Test Matrix and Specimen Detailing

Two pairs of identical UHPC columns with different ABC column-to-footing connections and detailing were considered for this study to fabricate using two UHPC mixtures that use both raw RSF from recycled tires as well as high-end MSF. The sets will allow for comparing and assessing the structural response of UHPC columns with RSF against MSF when implemented for either type of ABC connections. Currently, no existing design guidelines provide the detailing of UHPC columns. In addition, the columns were not designed based on a prototype bridge; however, the dimensions were drawn from typical specimens previously tested for seismic applications at the University of Nevada Reno [20]. The two common ABC connections used herein are pocket and grouted duct connections, which were both designed following the proposed AASHTO seismic specifications for ABC column connections [19]. The diameter of the columns was 16 in (41 cm) and had a height of 62 in. (157 cm). A loading head with a dimension of 20 in $\times$ 20 in $\times$ 20 in (50.8 cm $\times$ 50.8 cm $\times$ 50.8 cm) was designed at the column's top end to attach the actuator for applying the intended vertical and lateral loading protocol.

Table 4-1 summarizes the connection and detailing of the columns. The specimen ID follows the specimen number, connection type, and fiber type used in UHPC. For example, SP1-P-RSF represents specimen 1 with pocket connection and UHPC column with RSF. Two pairs of ABC columns were designed to fully understand the effect of using RSF (each pair contains UHPC with both RSF and MSF for comparison). The first pair used a pocket connection with 10 #6 longitudinal reinforcement and transverse reinforcement of #3 spiral at 3 in (7.6 cm) pitch. The longitudinal and transverse reinforcement ratio for the columns was 2.19% and 1.04%, respectively. Similarly, the grouted duct connections columns were designed to have same longitudinal reinforcement; however, the spacing of the transverse reinforcement was reduced to 1.5 in (3.8 cm), i.e. longitudinal and transverse reinforcement ratios of 2.19% and 2.08%, respectively, to provide another comparison case for columns with different confinement levels.

An embedment length for the pocket and duct connection was determined using equations (4-1) and (4-2), respectively, which were proposed in the NCHRP design specification [19]. The code versions of the equations that depend on the f_c' of the concrete were not considered for determining the embedment length as the UHPC has high compressive strength [19]. In this equation, D_{cm} is the column diameter, d_{bl} is the diameter of the longitudinal reinforcement bar, f_{ye} is the expected yield stress of the reinforcement bar, and f_g' is the compressive strength of the grout. The calculated embedment length was approximately 16.0 in (41 cm), and 11.0 in (28 cm) for pocket and duct connection, respectively, based on the assumption that d_{bl} is 0.75 in (1.9 cm),

f_{ye} is 60 ksi (414 MPa), and f'_g is 8 ksi (55 MPa). However, the embedment length was increased to 24 in (61 cm) for both connections, to ensure that no rebar and duct pullout would occur and allow for developing the plastic hinge fully within the column. Figure 4-2 shows the reinforcement detailing of the UHPC columns with both pocket and duct connections.

$$l_e \geq D_{cm}, 24d_{bl} \tag{4-1}$$

$$l_e = \frac{0.68d_{bl}f_{ye}}{\sqrt{f'_g}} \tag{4-2}$$

The footing was designed as capacity-protected members to ensure it would not yield whenever the column develop a full plastic hinge mechanism at high lateral drift ratio. Figure 4-3 shows the two different footings reinforcement details, which at the center accommodate the embedment requirements for the different ABC connections. The footing had a plan dimension of 6 ft × 6 ft (183 cm × 183 cm) and had a depth of 28 in (71 cm). Helical corrugated galvanized steel pipes of 0.06 in (1.5 cm) thickness and diameters of ∅ 20.0 in (51 cm) and ∅ 2.5 in. (6.3 cm) were used for the pocket and duct connections, respectively. The pocket pipe or ducts are placed around the embedment to create a bond with grouting material (which is UHPC with MSF in this study) and to provide a path for the principal stress generated from the column. The footing cage used reinforcement of #8 rebar with four different bend configurations. For pocket connections, a smaller 90°-bend configuration was placed to accommodate the pocket and help the connection remain uninhibited for ease of column placement. Also, an additional eight #8 diagonal reinforcement and #3 spiral hoops were placed around the

pocket as recommended in [19]. A total of 40 #3 reinforcement stirrups were placed around the footing to provide additional stability and shear resistance. Four anchors were placed in two opposite sides along the footings side to provide lifting points for handling during testing setup.

4.2.2 *Large-Scale UHPC Production and Specimens Construction and Assembly*

All UHPC columns with both steel fibers types were fabricated following typical precast practices at the ConFab California, LLC precast plant. Figures 4-4a and 4-4b show the assembly of the column reinforcement cages and placement in the formwork. After placing the columns cage, the UHPC was mixed the following day using a typical truck mixer for day-to-day precast activities. It is noted that this is the first time economic UHPC is mixed and furnished at this scale for a research project. The economic nature of the utilized UHPC mixture stems from the flexibility a commercial UHPC powder allows to mix with any local sand and cement, which is ideal for larger precast applications as proposed herein. Table 4-2 shows the summary of the UHPC mix design. UHPC components are a combination of the commercial premix and local precast sand and cement. Another unique aspect of this study is the use of raw RSF, as obtained from a recycled tires processing vendor, which exhibited an average aspect ratio of 93 (as opposed to 65 for high-end MSF). It is noted that side preliminary studies were conducted at our lab at UNR using a high-shear mixer to test whether a 2% by volume RSF works. The result of 2% by volume showed fiber segregation; thus, the fiber content was adjusted to 1.6% by volume, which showed less segregation. The moisture content of the sand used in the mixtures was determined on the day of the mixing, and the water

content in the mix was adjusted accordingly. The initial batch of the UHPC with MSF was produced and cast into first set of columns on March 23, 2023, while the UHPC with RSF was mixed and cast into the second columns set in the following week.

All the dry components except the fibers were initially placed into the truck mixer (Fig. 4-4c), and the admixtures were delayed for about five minutes. As the mixture became more fluid and viscous, the fibers were placed manually from the truck top gate/opening, as illustrated in Fig. 4-4d. The blended materials in the truck were mixed for another five minutes, and the first batch of UHPC was then furnished through the truck's chute and cast into the columns head, as shown in Fig. 4-4e.

There was no noticeable fiber clumping for the UHPC with MSF; however, fiber clumping was observed in the case of UHPC with RSF. Nonetheless, since the loading head has no reinforcement in the middle, the UHPC flowed easily into the column without the fiber getting caught. Curing blankets (Fig. 4-4f) were placed around the column to maintain warm ambient temperatures for uniform curing. The footings on the other side were fabricated and cast at Jensen Precast in Sparks, Nevada. Figures 4-4g and 4-4i show the casting of the pocket and duct footings. Unlike the columns, all footings were made using NSC. Once the concrete cured and hardened after a few days, the formwork of the columns and footings was stripped (Fig. 4-4j). The columns and footings were cured for about four additional weeks then they were transported using a flatbed truck and delivered at UNR Earthquake Engineering Fabrication Yard (Fig. 4-4k and 4-4l). For the full specimens assembly, the UHPC columns were lifted using a high-

capacity forklift and aligned with the footings connections. Additional batches of UHPC with MSF were mixed on-site at UNR fabrication yard to use as the grouting material for all the columns. For the columns with pocket connection, the grouting UHPC was applied once the column was positioned inside the pocket. However, for the other type, the ducts were filled first with UHPC, then the columns were slowly lowered into the connection as illustrated in Fig. 4-4m.

4.2.3   Material Properties

To characterize the UHPC used in all parts of the specimens, material samples were obtained following the ASTM C1856 standards [21]. Before placing UHPC in the columns, a static flowability test was performed by obtaining fresh UHPC from the truck mixer [22, 23]. The UHPC was placed in a cylindrical cone, lifted, and waited for around two minutes to measure the average spread diameter. The average spread diameter of the UHPC used for SP2-P-MSF and SP4-D-MSF was 8.9 in (23 cm), while that for SP1-P-RSF and SP3-D-RSF was 7.8 in (20 cm). The batch with RSF was observed to have fiber clumping, as shown in Fig. 4-4n. However, as mentioned earlier, even though fiber clumping was evident in the flowability test, the flowability was not an issue when UHPC RSF was poured directly into the columns. The compressive strength was determined using 3 in × 6 in (7.5 cm × 15 cm) cylindrical specimens that were carefully prepared by grinding the top and bottom ends (Fig. 4-4o) to avoid any eccentricity effects that can reduce the compressive strength. A 500-kip Satec compressive machine was used to test at least three samples from each set at day 28 and the test day, and the strain was measured using a digital compressometer. The results shows a higher compressive

strength of 22.1 ksi (152 MPa) for SP2-P-MSF and SP4-D-MSF, while SP1-P-RSF and SP3-D-RSF showed a slightly lower compressive strength of 20.1 ksi (139 MPa).The compressive strength of the UHPC used for all connections and NSC of the footings was also determined. Table 3 summarizes the results of all UHPC compressive tests for completeness (strength, strain at peak, and modulus of elasticity). The NSC used in the footings showed a strength of about 6.2 ksi (42.8 MPa) at the test days.

To further characterize the utilized UHPC, direct tension and four-point bending tests were also performed to obtain the tensile strength and modulus of rupture. Dog bone specimens of 1.0 in × 1.0 in (2.5 cm × 2.5 cm) cross-sections were tested in an Instron machine with hydraulic grips using a displacement-controlled loading rate that started with 0.005 in/min (0.012 cm/min) and was increased to 0.08 in/min (0.2 cm/min) once the maximum load dropped by around 10%. The strain was measured using a laser extensometer with laser tags attached to the specimens. The four-point bending test used same Instron machine where the load was applied by a two-point fixture to prism specimens of 3.0 in × 3.0 in × 12.0 in (75 mm × 75 mm × 305 mm) dimensions, and a laser tag was placed at the mid-point to measure the deflection. The loading rate was kept around 0.1 in/min (0.25 cm/min) throughout the test. The results from the direct tension and flexure tests are also summarized in Table 3 (tensile strength, strain localization, modulus of rupture, and deflection at modulus of rupture). Unlike the samples from the column, the UHPC in the connection and footing were not tested for direct tension and four-point bending tests.

All columns and footings were reinforced with A706 [24] Grade 60 bars, and the reinforcement properties were determined using tensile tests and the reinforcement properties, including the yield, ultimate strength, and elongation at the peak strength, are summarized in Table 4.

4.2.4 Test Setup and Instrumentation Plan

The test specimens were carefully instrumented to capture the global and local behavior of all the UHPC columns. Instrumentation included strain gages that were applied to the rebars before UHPC casting along with various displacement measuring instruments. All specimens were tested under combined axial and lateral cyclic loading at the Earthquake Engineering Laboratory (EEL) at UNR. Figure 4-5 shows the schematic test setup along with the locations of instrumented sections of the columns. Each specimen was grouted to the strong floor of the laboratory using a 1.5-in (3.8-cm) grout pad for leveling purposes. Six Dywidag bars were placed and tensioned evenly around the footing to fix the specimen to the strong floor. A 110-kip servo-hydraulic actuator was mounted to a steel plate reacting against the reaction wall, and was used to apply the displacement-controlled quasi-static cyclic loading. A spreader beam and two hollow core jacks were placed on top of the column to provide the axial load during the tests. Each core jack was placed with high-strength axial rods that extended through the footing, reacting against the strong floor. On the day of the testing, these rods were tensioned to provide a total of 80-kip (356-kN) axial load that remained constant during the tests.

A total of 38 channels were used to collect instrumentation data throughout the test. Four string potentiometers were placed at four corners of the loading head to record the

displacement history and confirm that the intended actuator displacement was achieved. Eight displacement transducers were placed at four sections above the footing interface, 6.0 in (15 cm) apart, to calculate the local curvature of the column. Twenty-four strain gauges were placed at four sections within the expected plastic hinge zone (Figure 4-5). Four strain gauges in the critical longitudinal reinforcement and two at the opposite sides of the transverse spiral reinforcement were placed at each section. For the duct connection columns, the strain gauges were aligned approximately with the location of the transducers. However, the strain gauges of the pocket columns were shifted 6.0 in (15 cm) below the footing interface to measure the strain activity at the connection. A full overview of the actual achieved test setup is shown in Figure 4-6.

4.2.5   *Loading Protocol*

As mentioned before, all columns were tested under combined axial and lateral cyclic loading. A total of 80 kips (356 kN) of axial load was applied and maintained throughout the tests. This axial load corresponds to a 2% axial load index (ALI), which is the ratio of the total axial load and the product of the average compressive strength of UHPC (estimated as 20 ksi) and gross cross-section area of the column. A lower ALI was deliberately chosen, assuming that the total axial load demand does not change if column material was changed from NSC to UHPC in actual bridge applications. An 80 kips axial load with a NSC compressive strength of 5 ksi (35 MPa) constitutes an 8% ALI, which is typical in bridge structures. For the lateral loading, the actuator was attached to the column at the loading head to provide a displacement-controlled cyclic loading using a FEMA 461 loading protocol as in previous similar tests conducted at UNR [25]. Figure

4-7 shows the complete cyclic loading protocol as function in drift ratio; the ratio of lateral displacement in the loading head to the effective column height. Each run was set to reach a particular drift and complete two cycles. Up to the 3% drift ratio, the loading rate was set to 1 in/min (2.5 cm/min). Afterwards, the rate was increased to 5 in/min (13 cm/min). Before completing each cycle, the test was paused at half a cycle before completion to inspect and observe the damage progression in the column.

4.3   Results and Discussions

This section provides the means to assess and validate the use of RSF for large structural UHPC applications by carefully comparing the local and global behavior of two sets of UHPC columns with MSF and RSF. The response and global behavior is presented in terms of the visual damage, force drift relationships, and columns energy dissipation and stiffness degradation with testing. Moreover, the local behavior is evaluated in terms of the reinforcement strains and moment-curvature relationships.

4.3.1   *Damage progression and failure mode.*

Each of the tested columns damaged state was progressively tracked each run by briefly halting the test half cycle from finishing and carrying out a visual inspection. To facilitate the crack tracking and damage progression, all columns were painted with a whitewash. The cracks were marked with different colors to differentiate and assess their progression for each run. Since the cyclic motion was directed in the east-west direction, most of the damage was recorded in this direction. Overall, most damage was observed in the plastic hinge zone of the column, and no damage was seen in the footing or around the

connection. Checkpoints for damage assessment and comparisons included status at yielding, maximum lateral force, and after failure.

Minor flexural cracks were developed in the initial runs up to yielding. Crack formations were minimal as the drift ratio achieved was relatively low, and the columns were still essentially elastic. When the columns reached the yielding point, defined as the first yielding of the longitudinal reinforcement, the difference in the total flexural crack formed between UHPC columns with RSF and MSF was already significant. Figure 4-8 shows the visual damage of the specimens at yielding. In the case of pocket connections, larger flexural cracks were observed in SP1-P-RSF compared to SP2-P-MSF. This is expected since the higher-end MSF have a better fiber performance due to the lower aspect ratio, which holds micro-cracks formation longer than in case of RSF. Similar observations were also noted for SP3-D-RSF versus SP4-D-MSF.

After the column yielded, damage within the plastic hinge zone continued progressing until distinct flexural cracks were observed when maximum lateral force was achieved. Figure 4-9 shows the damage state of the plastic hinge zone when the column reached its maximum lateral force. Although multiple flexural cracks were noted in the initial testing, crack localization was observed as specimens approached failure. In tensile testing of UHPC, when UHPC goes tensile hardening, crack localization can be considered at the maximum force [26]. This is also similar observation from previous experimental tests on prestressed UHPC girder under flexural loading where a localized crack formed at midspan [27]. In the pocket connections, SP1-P-RSF and SP2-P-MSF showed crack localization along the west direction, approximately 7.0 in above the

column interface. The duct connection columns, however, had a different case as crack localization only appeared for SP3-D-RSF, and no additional cracks were noted for SP4-D-MSF with the better fibers. Although RSF and MSF were expected to provide additional confinement, particularly on the clear cover, minor spalling on SP1-P-RSF was still observed close to the footing interface as the column started to experience significant compression, causing the concrete cover to crush. However, no spalling was observed with SP2-P-MSF.

Damage continued progressing at higher drifts while the lateral force remained almost constant. Dominated by a localized crack, the columns began to hinge at this section, and the damage became more severe and concentrated. The columns were considered failed, and ultimate drift capacity was noted, when longitudinal reinforcement ruptured, which was indicated by a loud popping sound during the test and properly identified later from the force drop in the data. After the first rupture, when the loading was reversed and column was pushed in the other direction, more longitudinal reinforcements ruptured, and the test was stopped for safety purposes after at least three longitudinal reinforcements failed. Figure 4-10 shows the final damage state of the plastic hinge zone of all columns after the final run.

As can be noted in the figure 4-10, the plastic hinge damage state differed for each column specimen. The documented failure modes of the SP1-P-RSF column were major spalling, rupturing of the longitudinal reinforcement due to local buckling, and tie rupturing at a considerable section in the plastic hinge zone. The case was different for SP2-P-MSF, with minor spalling and rupturing of the longitudinal reinforcement at the

localized crack. However, the recorded damages of SP1-P-RSF and SP2-P-MSF were reached at different ultimate drift ratios, where the SP2-P-MSF had an 8.23% drift ratio at Run 10, and the SP1-P-RSF column had a higher drift of 12.33% at Run 12. The major spalling in SP1-P-RSF can be attributed to the local buckling in the longitudinal reinforcement and tie rupture, causing a major portion of the clear cover to expand. However, these spalled covers were partially attached through the fiber and were manually removed to have a better view of the damage in the reinforcement. Even though the RSF in SP1-P-RSF provided good confinement throughout the test, the spalling behavior was still similar to typical NSC columns with no fibers when higher drift ratios progressed. On the contrary, the localized crack in SP2-P-MSF caused the reinforcement to experience high local strain, causing the longitudinal reinforcing bars to rupture earlier, achieving a relatively lower ultimate drift ratio. Unlike SP1-P-MSF, SP2-P-RSF only had a minor spalling, which was attributed to the good confinement effect of MSF and no tie ruptures were observed in that column.

In the case of SP3-D-RSF and SP4-D-MSF, the columns failure mode was dominated by the tensile rupture of the longitudinal reinforcements at the footing interface. When both columns started reaching failure, the extent of the damage in the plastic hinge zone was significantly reduced. In addition, shear cracks developed in the column base aligned with the longitudinal reinforcement. These observations revealed that high strain concentration at the footing interface was occurring, causing the column to having an almost rocking behavior. The effect of strain localization at the interface influenced the

reinforcing bars strain values and caused the ultimate drift to be relatively lower, with 10.49% at Run 11 for SP3-D-RSF versus 7.96% at Run 10 for SP4-D-MSF.

4.3.2 Force-Drift Ratio

The lateral force-drift relationship was recorded to understand the columns overall performance and assess their yielding, energy dissipation, and ductility. The lateral force was measured using a load cell located at the actuator. The lateral displacement was recorded, using the average of the four string potentiometers attached at the corners of the loading head, and related to the columns effective height of 72 in (183 cm) to obtain the drift ratio. For sign convention, a positive drift ratio indicates the pulling of the column toward the east direction, while a negative drift ratio indicates the pushing of the column toward the west direction. Figure 4-11 shows the cumulative force-drift hysteresis of the four UHPC columns.

Regardless of the connection type, the force-drift relationship of all the UHPC columns showed stable and wide hysteretic loops, indicating good energy dissipation. However, the force-drift behavior of columns with RSF showed wider hysteretic loops than columns with MSF. Hysteretic loops before failure were fairly symmetrical until the longitudinal reinforcing bars ruptured. These ruptures were reflected in the sudden drops in the lateral force shown in the force-drift relationships. The backbone of the force-drift hysteresis was traced, creating both a positive and negative envelope, and presented in Figure 4-12. Moreover, the key response values as obtained from the average force-drift ratio relationships envelop are summarized in Table 5.

Overall, the UHPC columns with RSF achieved higher drift capacity while the columns with MSF showed a slightly higher force capacity. At the first yielding of longitudinal reinforcement, the drift ratio was about 1.0% and the lateral force ranged from 25-30 kips (110-137 kN) among the four columns. SP1-P-RSF exhibited a maximum lateral force of 38.9 kips (173 kN), which is 12.5 % lower than the 44.1 kips (196 kN) capacity of SP2-P-MSF. A 6.3% difference in the maximum lateral force was also observed between SP3-D-RSF and SP4-D-MSF, which recorded around 38.3 kips (170 kN) and 40.8 kips (181 kN), respectively. The ultimate drift ratio of the column was determined as the corresponding value when the maximum recorded lateral force dropped by around 20%. The ultimate drift ratio of SP1-P-RSF was determined to be ~10.9%, while SP2-P-MSF only had ~7.6% drift, i.e. 35% lower than SP1-P-RSF. A similar case was observed with the duct connection where SP3-D-RSF and SP4-D-MSF had ~10.3% and ~7.0% drift ratios, respectively, and the difference was calculated to be around 38.4%. Another way of looking at the same data is also provided in Figure 4-13 which shows the estimated elastoplastic curve of the four UHPC columns based on the average positive and negative envelope.

Referring to Figure 4-13, the elastoplastic curve was determined by projecting a linear line passing through the yield displacement. Then, the effective displacement yield was estimated by equalizing the area above and below the plastic region. The columns' displacement ductility (μ_d) was calculated by determining the ratio between the recorded ultimate displacement and the estimated effective displacement yield. The four columns showed displacement ductility of 5.85-7.36, which well exceeds the ductility demand of 5

required for typical seismic bridges as per the California Seismic Design Criteria for instance [28]. In general, the ductility of the column with RSF was relatively higher than that with UHPC MSF, regardless of the ABC connection type. The displacement ductility of SP1-P-MSF is determined to be 7.36, which is 22.8% higher than the 5.85 ductility of SP2-P-RSF. Despite the longitudinal reinforcement rupture at the footing interface, the displacement ductility of the duct connection columns was determined to be 6.66 and 6.14 for SP3-D-RSF and SP4-D-MSF, respectively.

4.3.3   Column Energy Dissipation

The total energy dissipation of the UHPC columns was determined by calculating the area enclosed in the hysteretic loops. Figure 4-14 compares the cumulative total energy dissipation of UHPC columns pairs with RSF and MSF for each of the ABC connection types. Since the columns with RSF reached a relatively higher drift ratio than those with MSF, the cumulative dissipated energy of RSF columns was also found to be higher. However, the dissipated energy of UHPC with MSF was relatively higher through Run 1-10. At yielding in the 1% drift ratio, the SP2-P-MSF column had 45% higher total energy dissipation than SP1-P-RSF. Similarly, SP4-D-MSF showed a 19.8% higher energy dissipation than SP3-D-RSF. It is also noted that as the drift ratio increased in each run, the difference in energy dissipation became smaller.

4.3.4   Column Stiffness

The column stiffness degradation was tracked after each test run. The stiffness was estimated by performing a best-fit linear approximation from 10-30% of the maximum lateral force at the first cycle of each run. Figure 4-15 shows the column stiffness

degradation versus the drift ratio. All UHPC columns lost about 50% of the stiffness when the column reached yielding around 1% drift ratio. It is noted that the very first estimated stiffness value for any of the four columns does not represent the virgin initial stiffness of the columns because the columns are already cracked once the actuator start first load application. Nonetheless, the close to the virgin stiffness from the 0.25% runs is reported to be 68.6 kip/in (12 kN/mm) and 80.9 kip/in (14.2 kN/mm) for SP1-P-RSF and SP2-P-MSF, respectively, and 45.1 kip/in (7.9 kN/mm) and 79 kip/in (13.8 kN/mm) for SP3-D-RSF and SP4-D-MSF, respectively.

Upon initial observation, Figure 4-15 suggests that UHPC columns with RSF experienced faster stiffness degradation than MSF columns. The rapid stiffness degradation of RSF columns can be attributed to the difference in the fiber dispersion of the UHPC with MSF and RSF. To get a better sense of the varying fiber dispersion uniformity in the two different fibers types, Figure 4-16 shows spalled parts from the UHPC columns with MSF and RSF which fell off the plastic hinge zone. Initial observations show that MSF are relatively better distributed within the UHPC matrix than RSF that also show a lower fiber count in some sections. This was expected in case of RSF since fiber segregation was observed to some extent during casting. The low fiber dispersion of RSF in some sections of the column caused the UHPC to develop more micro-cracks rapidly, and attributed to the significant reduction in the column stiffness. The higher aspect ratio of RSF still helped bridge macro-cracks and providing stiffness in the column which was more effective and demonstrated in SP3-D-RSF.

4.3.5 *Reinforcement Strains*

The reinforcement strain values and profiles were measured using strain gauges attached to the surface of selected longitudinal and transverse rebars as shown before. Each longitudinal reinforcement in the pocket connection had four strain gauges spaced at 6 in (15.2 cm) and ranging from 6 in (15.2 cm) below the footing to 12 in (30.5 cm) above the footing interface. Similar layout was applied for the duct connection columns with one difference that the location of all the strain gauges was shifted 6 in (15.2 cm) up to start at the interface level. It is noted that some strain gauges were damaged at higher runs and no reliable data was recorded in such cases. Figure 4-17 shows the strain profile of the four UHPC columns in one of the instrumented longitudinal reinforcements. Initial observation shows that the column reinforcement remained elastic up to Run 4 (1% drift ratio) except for SP4-D-MSF where the reinforcement yielded at Run 3 at 0.75% drift ratio. Regarding pocket connection columns, SP1-P-RSF exhibited a distributed strain at post yielding around the plastic hinge zone. The strain is reflected in the observed damage at the location where most of the rebars fractured due to buckling. However, for SP2-P-MSF, the strain recorded at 6 in (15.2 cm) was relatively higher than other strains, which was expected since this is where the localized crack and ruptured rebars were observed.

Regarding the strain in the duct connection columns, high strain readings were observed close to the interface. After the 1% drift ratio runs, high strain was recorded at the interface and at 6 in (15.2 cm) above the interface of SP3-D-RSF. However, exact strain readings were not conclusive after 3% drifts when strain gauges were damaged.

Nonetheless, the strain was already more than 2% when the drift ratio was around 2%. A similar case was observed with the SP4-D-MSF. A high strain reading of more than 3% was recorded only at the interface when the drift ratio was at 2%. Regardless of the type of fiber, strain localization was evident at the interface for UHPC duct columns. This can be an issue since high strain at the interface can cause the reinforcement to rupture rapidly, especially if the reinforcing bars are not ductile or if the bridge is subjected to dynamic loading, such as an earthquake.

The strain was also recorded at the transverse reinforcement and results from instrumented bars are shown in Figure 4-18. The strain gauges were placed at similar locations as the longitudinal reinforcement, but none of the strain gauges recorded any yielding. Meanwhile, the observed rupture of ties in columns like SP1-P-MSF occurred in ties that were not instrumented.

4.3.6   *Moment Curvature*

The curvature profile of the columns was estimated using LVDT measurements within four segments of the plastic hinge zone. The locations of the four segments were 6, 12, 18, and 24 in (15.2, 30.5, 45.7, and 61.0 cm) above the column interface. Figure 4-19 shows the curvature profile of the four UHPC columns. High curvature was observed at the region close to the footing interface and was generally reduced further away from the interface. For the pocket connection columns, the higher curvature was primarily observed at 6 in and 12 in (15.2 cm and 30.5 cm) above the footing connection, which agrees with the observed significant spalling and rebar rupture at such location. In addition, highest curvature was recorded at 12 in (30.5 cm) of SP2-P-RSF as the crack

localization occurred around this region. On the contrary, duct connection columns showed highest curvature at 6 in (15.2 cm) above the interface, which reflects the minor damage observed at the plastic hinge zone and the tensile rebar rapture at the interface.

The moment-curvature behavior was determined at the similar location where curvature was calculated. The moment was determined as the product of the measured lateral force and the distance between the loading head center and instrumentation plane. The moment-curvature relationship was then estimated by calculating the average positive and negative backbone from the moment-curvature hysteresis. Only the moment-curvature behavior obtained within the first segment at 6 in (15.2 cm) above the footing was of interest. For brevity, only the comparative average moment-curvature relationships of the different fiber types are shown in Figure 4-20 for the for two column pairs with different connection types.

For the pocket connection columns, the estimated maximum bending moment for SP1-P-RSF and SP2-P-MSF was 2,578 kip-in and 2,836 kip-in (291 kN-m and 320 kN-m), respectively. The maximum bending moment of SP2-P-MSF was 9.5% higher than SP1-P-RSF. However, the ultimate curvature of SP2-P-MSF (~0.0051 rad/in (0.2 rad/m)) was significantly lower than SP1-P-RSF (~0.0107 rad/in (0.42 rad/m)). The low curvature of SP2-P-MSF can be attributed to MSF bridging micro-cracks. As MSF minimizes the crack formation around the plastic hinge zone, a single crack localization was developing with first instrumented segment. The fibers started to debond and pull out, causing the localized crack to widen. At this stage, the column was observed to show a rocking behavior, causing high strain in the reinforcement and sooner reinforcement rupture

earlier, and in turn, leading to lower drift capacity. However, this case differed for SP1-P-RSF, where RSF allowed UHPC to develop micro-cracks while holding the macro-cracks in place. Since RSF allowed micro-cracks to develop, a typical plastic hinge mechanism was formed with damage extended over larger portion of the column, and allowing a better strain distribution in the reinforcement. This caused the column to achieve higher curvature and drift capacities.

For ABC duct columns, the maximum bending moment capacity of SP3-D-RSF and SP4-D-MSF was very comparable with obtained values of 2,515 kip-in and 2,676 kip-in (284 kN-m and 302 kN-m), respectively. Moreover, the curvature capacity of SP3-D-RSF and SP4-D-MSF was found to be 0.0139 rad/in and 0.01 rad/in (0.55 rad/m and 0.39 rad/m), respectively, which is about 32% difference. The UHPC column with RSF recorded higher curvature than the MSF column, which same observation as in pocket connection columns. Although the difference in curvature can be attributed to the fibers, the curvature of duct columns can be additionally attributed to the high strain concentration of the reinforcing bar at the footing interface. For SP3-D-RSF, the damage was not as severe when compared with SP1-P-RSF, even though both columns had RSF. In addition, no distinct crack localization was observed for SP4-D-MSF compared to SP2-P-MSF. Similarly, when the column reached a higher drift ratio, it was also observed to have a rocking behavior, and no significant damage was observed above the interface. Thus, the high curvature recorded within first instrumented segment was dictated by the high strain in the reinforcement at the interface, which helped achieve adequate ductility.

4.4   Conclusions

This study presents the feasibility of economical UHPC with RSF for precast bridge columns with different ABC connections. The structural response of two UHPC columns pairs with pocket and duct connections was compared for using RSF versus MSF. The columns were fabricated, for the first time in a research study, in a precast plant and UHPC was produced using truck mixer. The columns were connected to conventional concrete footings and the assembled specimens were tested under combined axial and lateral cyclic loading. Overall, the UHPC columns with RSF are demonstrated to be promising clean and sustainable solution for bridge columns with sufficient ductility that meets current design codes and comparable strength to higher end UHPC columns with MSF. This overall validation of RSF use is supported by the following conclusions that are drawn from the experimental testing:

- Economical UHPC columns can be successfully produced using current precast practices and equipment while using local and sustainable components such as RSF derived from landfill tires. Typical concrete truck mixers can be effective for mixing and furnishing UHPC with both MSF and RSF. The scalable produced UHPC features a compressive strength of more than 20 ksi (138 MPa), a tensile strength of more than 1.6 ksi (11 MPa), and a modulus of rupture of more than 2 ksi (14 MPa). Only a minor limitation of using RSF is fibers clumping and segregation risks in the fresh UHPC, which did not have adverse effects in the tested columns but yet needs future investigation of further RSF sorting and processing.

- The typical mode of failure for full precast UHPC columns with pocket connection is shown to be major spalling and longitudinal reinforcement rupture due to buckling in case of using RSF, and a lesser damage extent with distinct crack localization when using MSF. On the other hand, tensile reinforcement rupturing at the column/footing interface is the mode of failure when ABC duct connections are used for UHPC columns.

- Generally, UHPC columns can achieve good energy dissipation as suggested by the force-drift hysteretic behavior. However, UHPC columns with RSF are shown to have a more favorable drift capacity and only less than 20% decrease in lateral force capacity when compared to UHPC columns with high end MSF. Moreover, the estimated displacement ductility for all the tested UHPC columns meets current seismic design code provisions, which provide an ultimate validation for the UHPC columns with RSF that is proposed in this study as a potential major upcycling application of landfill tires.

- The stiffness of UHPC columns with RSF is found to be less than the columns with MSF, which is attributed to the less favorable fiber dispersion of RSF leading to lower fiber count in some sections that in turn, host more cracks and adversely reduce the stiffness.

- UHPC columns with pocket connections exhibit more evenly distributed strain profiles within the plastic hinge zones, unlike the very high strain concentration that is observed at the column/footing interface when grouted duct connections are used. Similar trends are shown using curvature data. As such, pockets connections are

recommended to consider for UHPC columns. However, future work is suggested to explore methods of improving the behavior of grouted duct UHPC columns and mitigating the high strain concentration at the interface such as reinforcement bar debonding within the interface region.

4.5   Credit authorship contribution statement

Allan Joseph Romero: Methodology, Formal analysis, Writing-original draft, Visualization. *Mohamed A. Moustafa:* Conceptualization, Writing - review & editing, Supervision, Project administration, Funding acquisition.

4.6   Acknowledgment

This project was supported in part by the US Department of Transportation Accelerated Bridge Construction-University Transportation Center (ABC-UTC). The authors are grateful for the support of PCI West, ConFab California, LLC, and Jensen Precast for their generous donations for specimens fabrication. The authors also acknowledge the in-kind support of Cor-Tuf and Sika for donating UHPC materials for the columns.

4.7   References

[1] Shafieifar, M., Farzad, M., & Azizinamini, A. (2017). Experimental and Numerical Study on Mechanical Properties of Ultra High-Performance Concrete (UHPC). Construction and Building Materials, 156, 402–411. https://doi.org/10.1016/j.conbuildmat.2017.08.170

[2] Cimesa, M., & Moustafa, M. A. (2022). Experimental Characterization and Analytical Assessment of Compressive Behavior Of Carbon Nanofibers Enhanced UHPC. Case Studies in Construction Materials, 17, e01487. https://doi.org/10.1016/j.cscm.2022.e01487

[3] Voss, M. S., Riding, K. A., Alrashidi, R. S., Ferraro, C. C., & Hamilton, H. R. (2022). Comparison Between Direct Tension, Four-Point Flexure, and Simplified Double-Punch Tests for UHPC Tensile Behavior. Journal of Materials in Civil Engineering, 34(9), 04022229. https://doi.org/10.1061/(ASCE)MT.1943-5533.0004371

[4] Newtson, C. M., Weldon, B. D., Al-Basha, A. J., Manning, M. P., Toledo, W. K., & Davila, L. D. (2018). Bridge deck overlays using ultra-high performance concrete (New Mexico State University & Transportation Consortium of South-Central States (Tran-SET) University Transportation Center for Region 6, Eds.; 17CNMS01). https://rosap.ntl.bts.gov/view/dot/62797

[5] United States. Department of Transportation. Federal Highway Administration. Office of Research, Development, and Technology. (n.d.). Technote: Ultra-high performance concrete (UHPC) overlays: an example of lifecycle cost analysis. https://doi.org/10.21949/1521955

[6] Abokifa, M., & Moustafa, M. A. (2021). Experimental behavior of precast bridge deck systems with non-proprietary UHPC transverse field joints. Materials, 14(22), 6964. https://doi.org/10.3390/ma14226964

[7] Morcous, G., & Tadros, M. K. (2023). Ultra-high-performance concrete (Uhpc) bridge decked i-beam: Design, production, and testing. Third International Interactive Symposium on Ultra-High Performance Concrete. Third International Interactive Symposium on Ultra-High Performance Concrete. https://doi.org/10.21838/uhpc.16640

[8] Alsalman, A., Dang, C. N., Martí-Vargas, J. R., & Micah Hale, W. (2020). Mixture-proportioning of economical UHPC mixtures. Journal of Building Engineering, 27, 100970. https://doi.org/10.1016/j.jobe.2019.100970

[9] Leng, Y., Rui, Y., Zhonghe, S., Dingqiang, F., Jinnan, W., Yonghuan, Y., Qiqing, L., & Xiang, H. (2023). Development of an environmental Ultra-High Performance Concrete (Uhpc) incorporating carbonated recycled coarse aggregate. Construction and Building Materials, 362, 129657. https://doi.org/10.1016/j.conbuildmat.2022.129657

[10] Choi, D., Hong, K., Ochirbud, M., Meiramov, D., & Sukontaskuul, P. (2023). Mechanical Properties of Ultra-High Performance Concrete (UHPC) and Ultra-High Performance Fiber-Reinforced Concrete (UHPFRC) with Recycled Sand. International Journal of Concrete Structures and Materials, 17(1), 67. https://doi.org/10.1186/s40069-023-00631-2

[11] Khan, M. I., Fares, G., Abbas, Y. M., & Alqahtani, F. K. (2024). Eco-innovative UHPC—Enhancing sustainability, workability, and ductility with recycled glass

cullet powder and plastic bottle hybrid fibers. Materials, 17(2), 393. https://doi.org/10.3390/ma17020393

[12] Graybeal, B. A. (2013). Development of non-proprietary ultra-high performance concrete for use in the highway bridge sector: Techbrief (United States. Federal Highway Administration, Ed.; FHWA-HRT-13-100). https://rosap.ntl.bts.gov/view/dot/34789

[13] Abdolpour, H., Niewiadomski, P., & Sadowski, Ł. (2021). Recycling of steel fibres and spent equilibrium catalyst in ultra-high performance concrete: Literature review, research gaps, and future development. Construction and Building Materials, 309, 125147. https://doi.org/10.1016/j.conbuildmat.2021.125147

[14] Isa, M. N., Pilakoutas, K., Guadagnini, M., & Angelakopoulos, H. (2020). Mechanical performance of affordable and eco-efficient ultra-high performance concrete (Uhpc) containing recycled tyre steel fibres. Construction and Building Materials, 255, 119272. https://doi.org/10.1016/j.conbuildmat.2020.119272

[15] Romero, A. J., & Moustafa, M. A. (2023). Material characterization of UHPC with recycled fibers and wires for future large-scale structural applications. Third International Interactive Symposium on Ultra-High Performance Concrete. Third International Interactive Symposium on Ultra-High Performance Concrete. https://doi.org/10.21838/uhpc.16719

[16] Mohebbi, A., Saiidi, M. S., & Itani, A. M. (2017). Development and seismic evaluation of pier systems w/pocket connections, CFRP tendons, and ECC/UHPC

columns (University of Nevada, Ed.; CCEER 17-02). https://rosap.ntl.bts.gov/view/dot/41829

[17] Tazarv, M., Shrestha, G., & Saiidi, M. S. (2021). State-of-the-art review and design of grouted duct connections for precast bridge columns. Structures, 30, 895–909. https://doi.org/10.1016/j.istruc.2020.12.091

[18] Haber, Z. B. (2013). Precast Column-Footing Connections for Accelerated Bridge Construction in Seismic Zones (Order No. 3566256). Available from Dissertations & Theses @ University of Nevada Reno; ProQuest One Academic. (1416356419).

[19] Saiidi, M. S., Mehraein, M., Shrestha, G., Jordan, E., Itani, A., Tazarv, M., Sanders, D., Murphy, T. P., Reno, M. L., & Pohll, M. N. (2020). Proposed AASHTO seismic specifications for ABC column connections. Transportation Research Board. https://doi.org/10.17226/25803

[20] Alian Amiri, S. M. (2020). Performance of Reinforced Concrete Bridge Columns with Various Reinforcement Details Subject to Long-Duration Earthquakes (Order No. 28261332). Available from Dissertations & Theses @ University of Nevada Reno; ProQuest One Academic; Publicly Available Content Database. (2480231575).

[21] "Standard practice for fabricating and testing specimens of Ultra-High Performance Concrete." ASTM International - Standards Worldwide, https://www.astm.org/c1856_c1856m-17.html

[22] "Standard Test Method for Flow of Hydraulic Cement Mortar." ASTM International - Standards Worldwide, https://www.astm.org/c1437-20.html

[23] "Standard Specification for Flow Table for Use in Tests of Hydraulic Cement." ASTM International - Standards Worldwide, https://www.astm.org/c0230_c0230m-20.html

[24] "Standard Specification for Deformed and Plain Low-alloy Steel Bars for Concrete Reinforcement." ASTM International - Standards Worldwide, https://www.astm.org/a0706_a0706m-22.html

[25] "Interim Testing Protocols for Determining the Seismic Performance Characteristics of Structural and Nonstructural Components " (2007). Federal Emergency Management Agency (FEMA). FEMA 461.

[26] Haber, Z. B., De la Varga, I., Graybeal, B. A., Nakashoji, B., & El-Helou, R. (2018). Properties and Behavior of UHPC-Class Materials (FHWA-HRT-18-036). https://rosap.ntl.bts.gov/view/dot/37528

[27] El-Helou, R. G., & Graybeal, B. A. (2022). Flexural Behavior and Design of Ultra High-Performance Concrete Beams. Journal of Structural Engineering, 148(4), 04022013. https://doi.org/10.1061/(ASCE)ST.1943-541X.0003246

[28] "Seismic Design Criteria Version 2.0" (2019). California Department of Transportation (Caltrans). https://dot.ca.gov/programs/engineering-services/manuals/seismic-design-criteria

Table 4-1 – Specimen detailing of the four UHPC columns

Specimen ID	Test Matrix						
	ABC Connection	Column	Connection	Long. Rft.	ρ_l [%]	Transverse Rft.	ρ_t [%]
SP1-P-RSP	Pocket	UHPC w/ RSF	UHPC w/ MSF	10 #6	2.19	#3 spiral at 3" pitch	1.04
SP2-P-MSF	Pocket	UHPC w/ MSF	UHPC w/ MSF	10 #6	2.19	#3 spiral at 3" pitch	1.04
SP3-D-RSP	Grouted duct	UHPC w/ RSF	UHPC w/ MSF	10 #6	2.19	#3 spiral at 1.5" pitch	2.08
SP4-D-MSF	Grouted duct	UHPC w/ MSF	UHPC w/ MSF	10 #6	2.19	#3 spiral at 1.5" pitch	2.08

Table 4-2 – UHPC mix design, per ft^3 (m^3), for two mixtures with different fibers types

Specimens ID	Cor-Tuf premix (CT 25), lb (kg)	Fine Sand, lb (kg)	Type II/V Cement, lb (kg)	Fibers, lb (kg)	HRWRA, lb (kg)	Water, lb (kg)
SP1-P-RSF & SP3-D-RSF	40.0 (641)	52.9 (847)	48.5 (777)	9.8 (157)	6.6 (106)	7.85 (126)
SP2-P-MSF & SP4-D-MSF	40.0 (641)	53.4 (855)	48.5 (777)	4.9 (79)	6.6 (106)	7.26 (116)

Table 4-3 – Mechanical properties of UHPC material samples tested at different ages

Mechanical Properties	Age	SP 1 & SP3	SP 2 & SP4	Pocket	Duct
Compressive Strength, ksi [MPa]	Day 28	20.3 [139.9]	16.8 [115.8]	15.2 [104.8]	12.8 [88.3]
	Test Date	22.1 [152.3]	20.1 [138.6]	17.4 [120.0]	17.1 [117.9]
E_{cyl}, ksi [GPa]	Day 28	5,094 [35.1]	4,696 [32.3]	5,237 [36.1]	5,462 [37.7]
	Test Date	5,050 [34.8]	5,090 [35.1]	5,467 [37.7]	6,409 [44.2]
ε_{cyl} [%]	Day 28	0.52	0.46	0.36	0.26
	Test Date	0.55	0.55	0.42	0.32
Tensile Strength, ksi [MPa]	Day 28	1.71 [11.8]	1.29 [8.9]	n/a	n/a
	Test Date	1.68 [11.6]	2.03 [14.0]		
ε_{loc} [%]	Day 28	0.32	0.62		
	Test Date	0.41	0.97		
Modulus of Rupture, ksi [MPa]	Day 28	4.83 [33.6]	1.94 [13.4]		
	Test Date	4.09 [28.2]	2.00 [13.8]		
δ_{mod}, in [mm]	Day 28	0.061 [1.55]	0.049 [1.24]		
	Test Date	0.075 [1.91]	0.051 [1.30]		

Table 4-4 – Reinforcement steel tensile properties

Rebar Size	Grade	Yield, psi [MPa]	Ultimate, psi [MPa]	Elongation at Maximum Force
#3	A706/ A615 Gr 60	71,340 [492]	101,622 [701]	n/a
#6	A706/ A615 Gr 60	64,198 [443]	95,542 [659]	14 %
#8	A706/ A615 Gr 60	70,800 [488]	99,400 [685]	7 %

Table 4-5 – Key response results for all tested columns as obtained from average envelop relationships

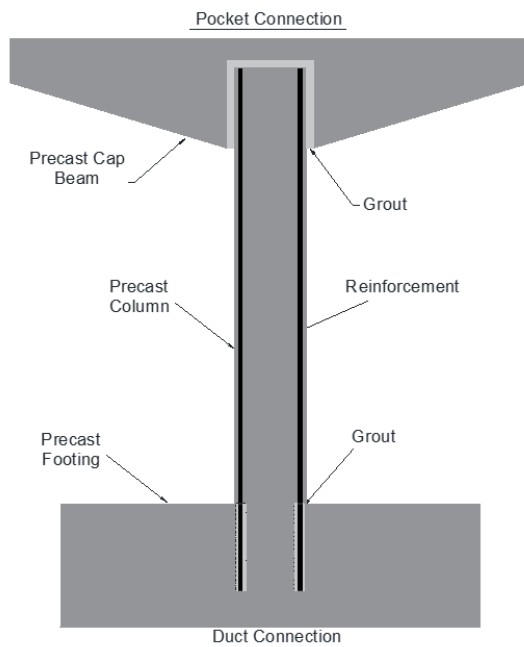| Column ID	Yield Point		Peak Point		Ultimate Point	
	Drift Ratio (%)	Force, kips (kN)	Drift Ratio (%)	Force, kips (kN)	Drift Ratio (%)	Force, kips (kN)
SP1-P-RSF	0.99	25.3 (113)	7.75	38.9 (173)	10.89	31.2 (139)
SP2-P-MSF	1.00	30.7 (137)	2.96	44.1 (196)	7.61	35.2 (157)
SP3-D-RSF	1.12	26.8 (119)	8.28	38.3 (170)	10.27	30.7 (137)
SP4-D-MSF	0.73	24.8 (110)	4.84	40.8 (181)	6.96	32.7 (145)

Figure 4-1. Schematic illustration of two different ABC bridge column connections: pocket connection (shown at the top) and grouted duct connection (shown at the bottom)
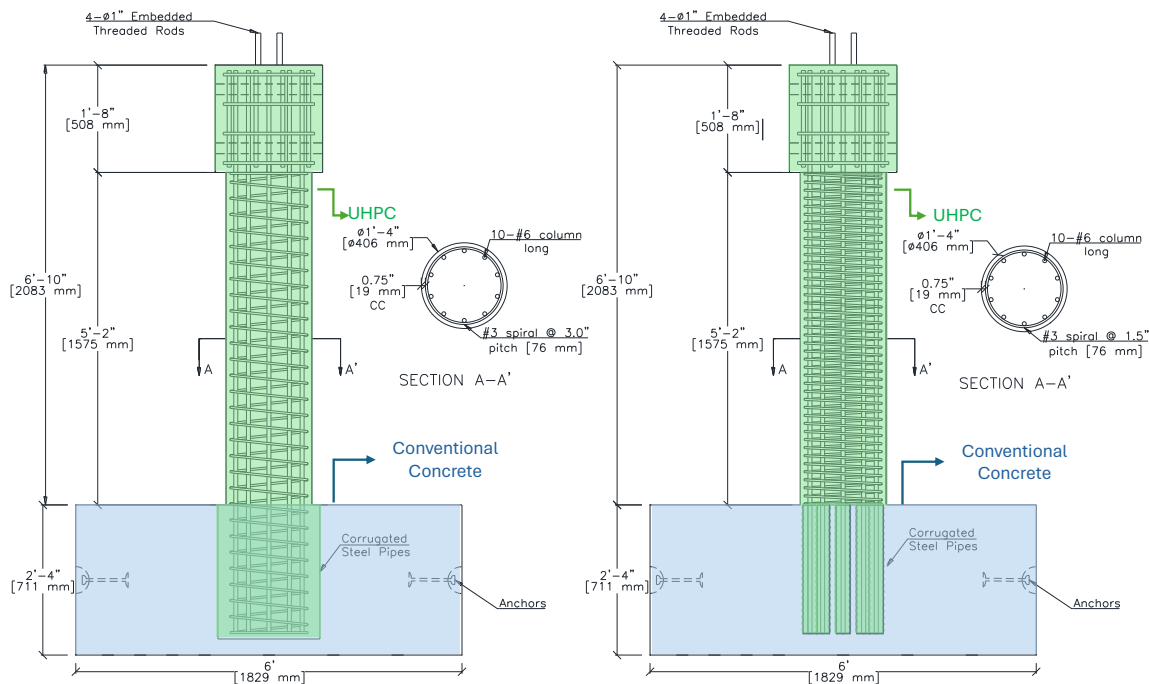

Figure 4-2. Reinforcement details of UHPC columns with pocket (left) and duct (right) connections
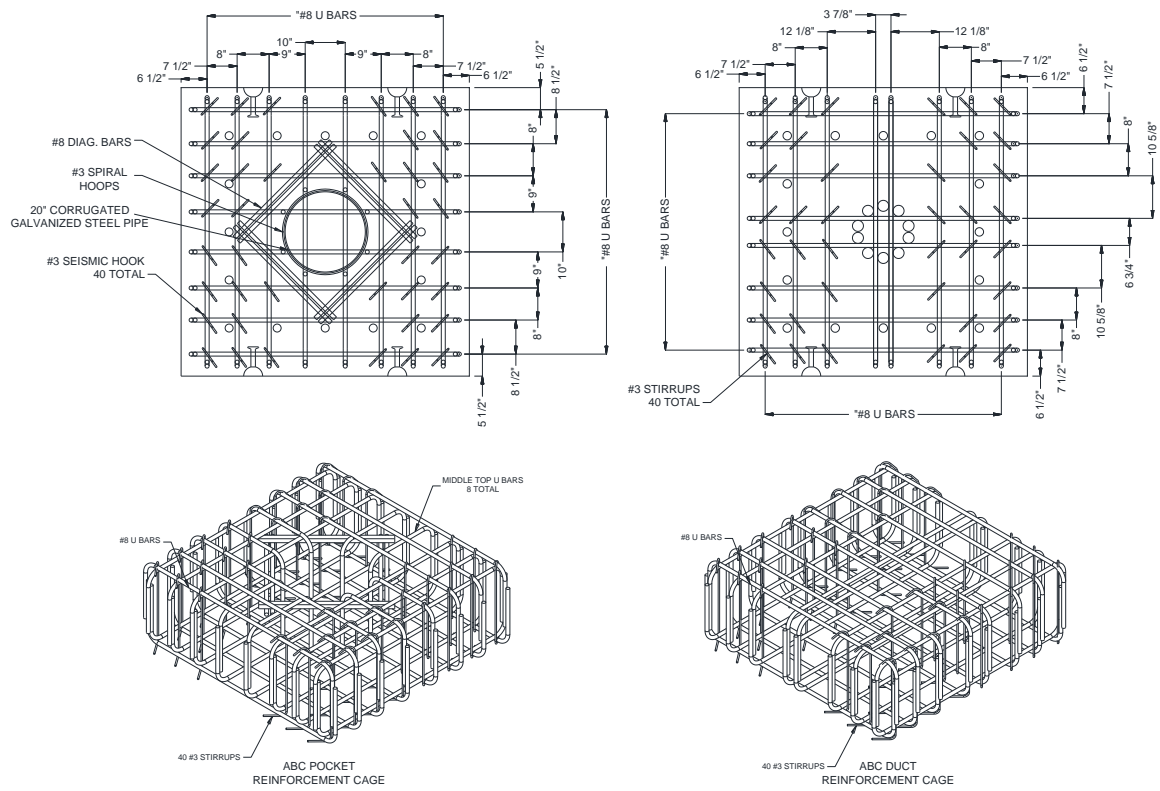
Figure 4-3. Reinforcement details of the NSC footings for both ABC connection types

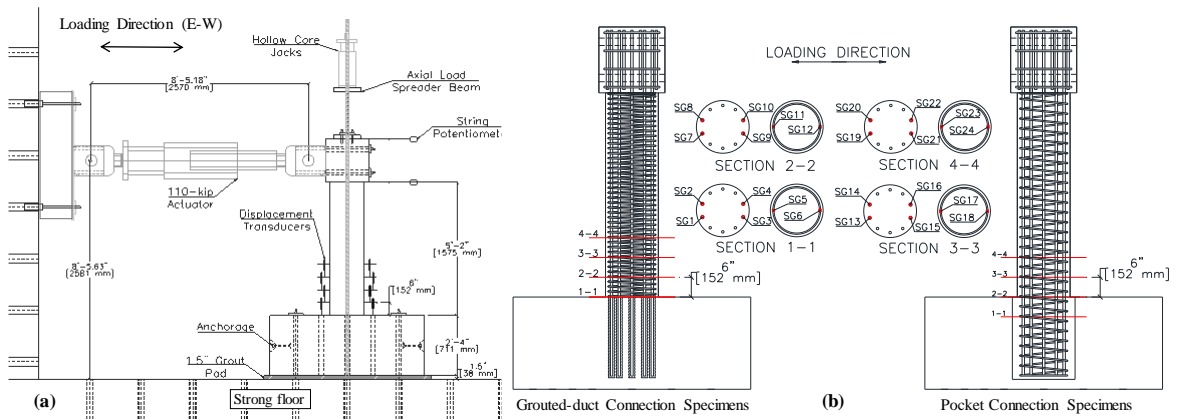**Figure 4-4**. Catalog of photographs documenting the various construction phases of the test specimens

Figure 4-5. Schematic illustration of the instrumentation plan and the overall testing setup

Figure 4-6. Overall test setup of UHPC columns under combined axial and lateral loading
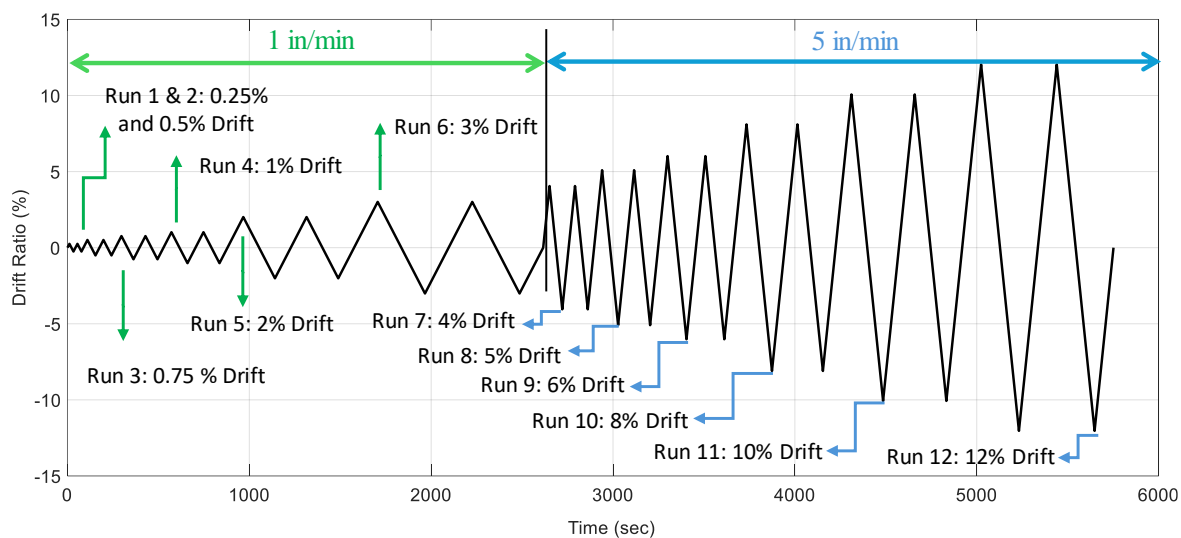
Figure 4-7. Quasi-static cyclic protocol for UHPC columns
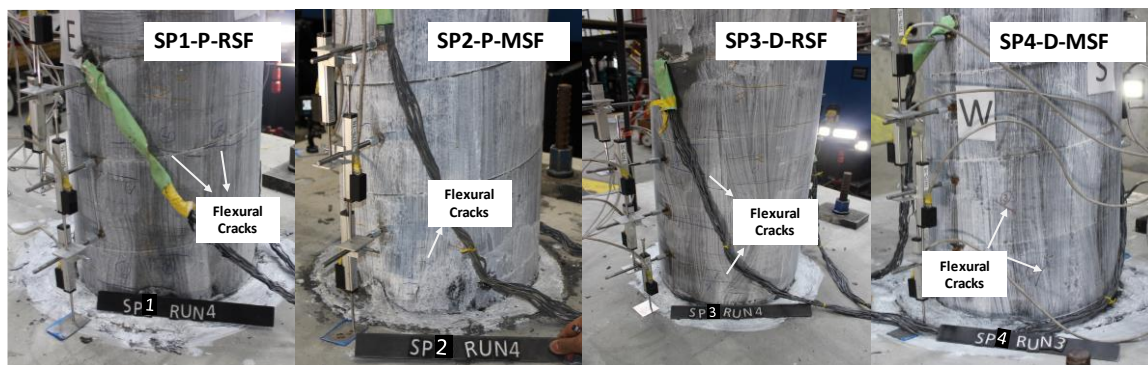
Figure 4-8. Damage progression of UHPC columns at yielding
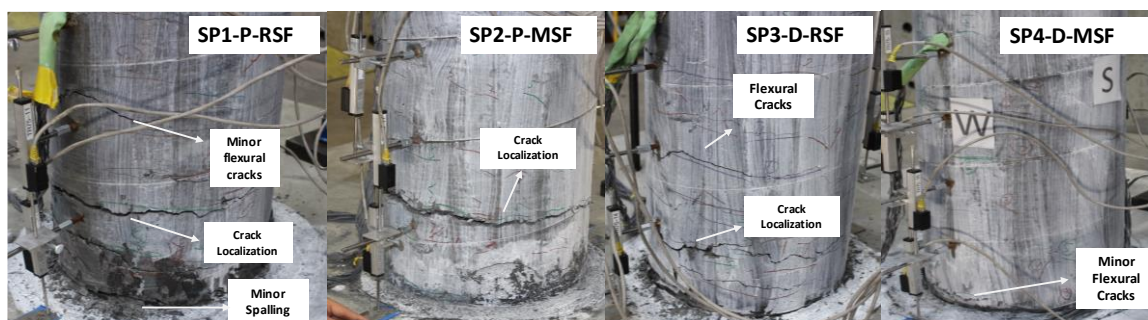
Figure 4-9. Major flexural cracks and some spalling at maximum lateral force obtained for each column
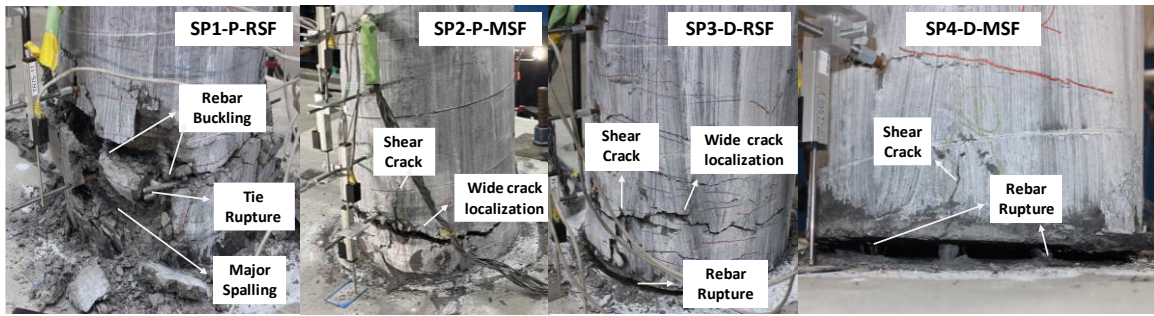
Figure 4-10. Damage state of the plastic hinge zone at failure
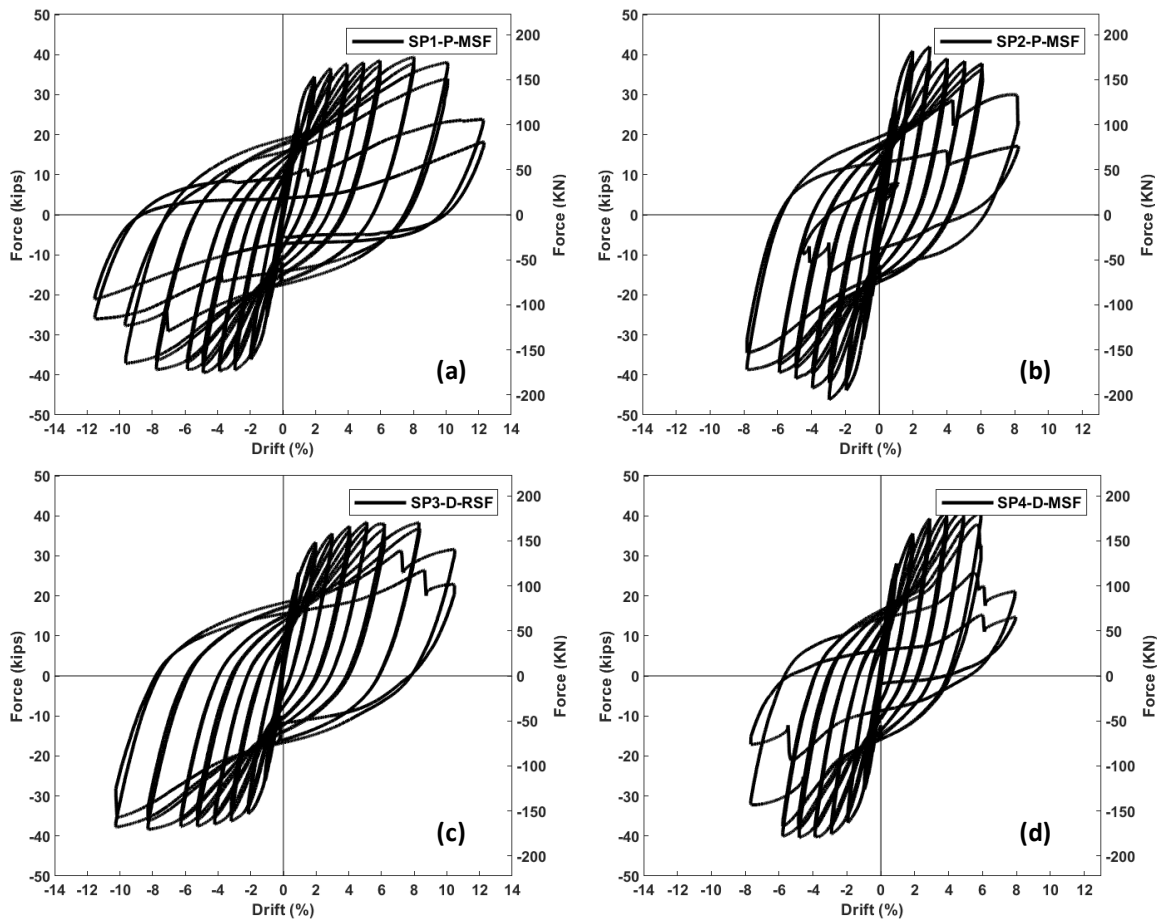
Figure 4-11. Force-drift hysteresis relationships of the four tested UHPC columns
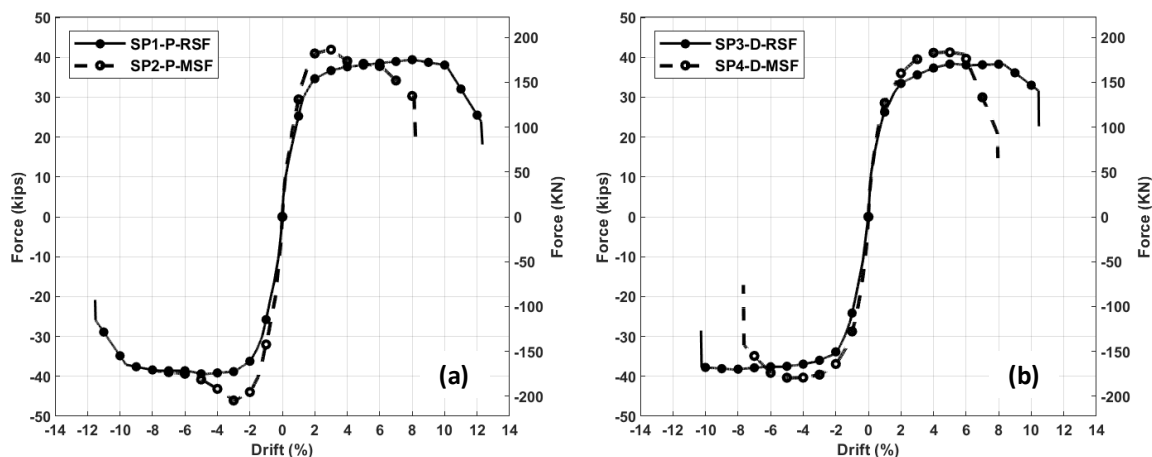
Figure 4-12. Comparison of the force-drift backbone envelope curve.
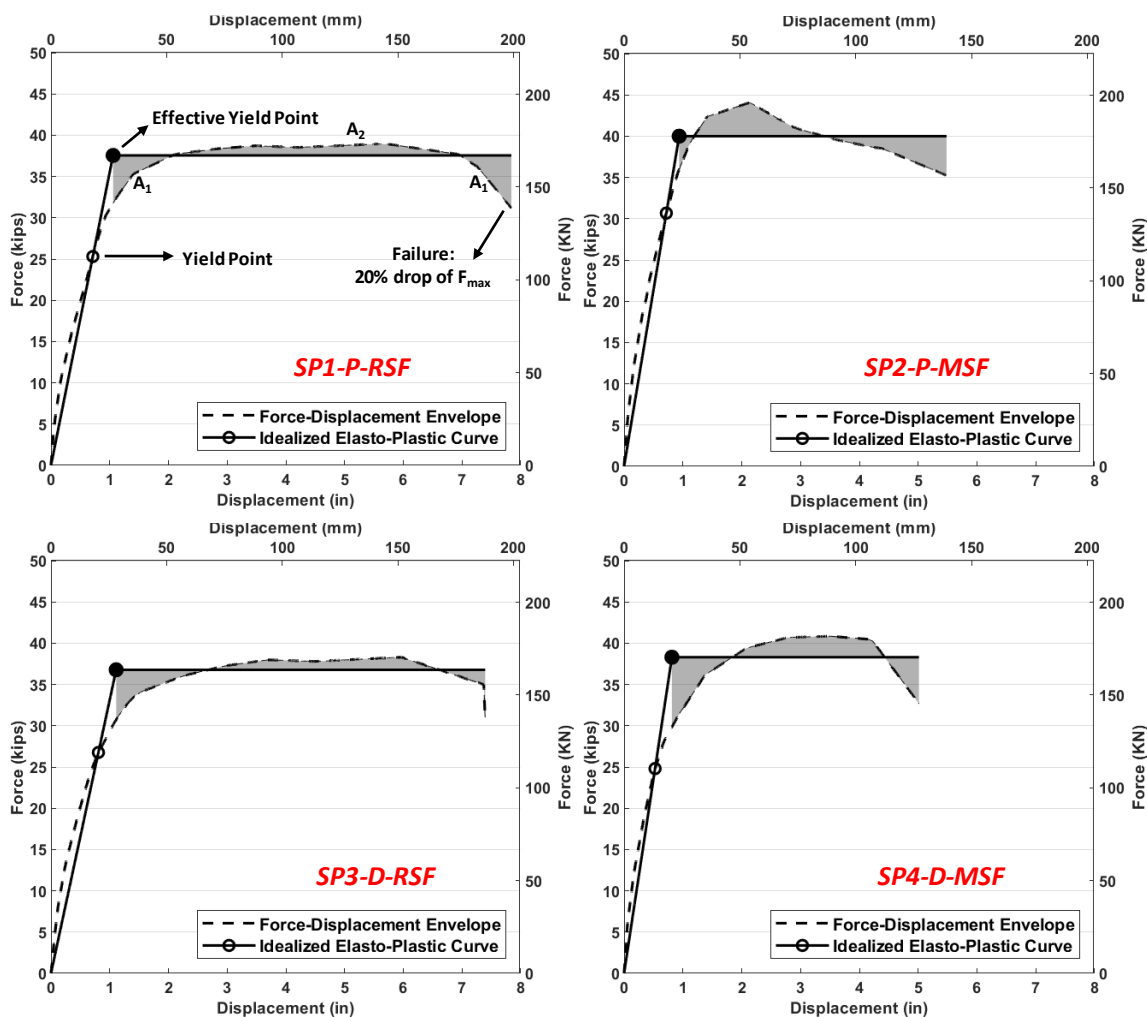
Figure 4-13. Idealized elastoplastic curve based on the average force-drift envelope.
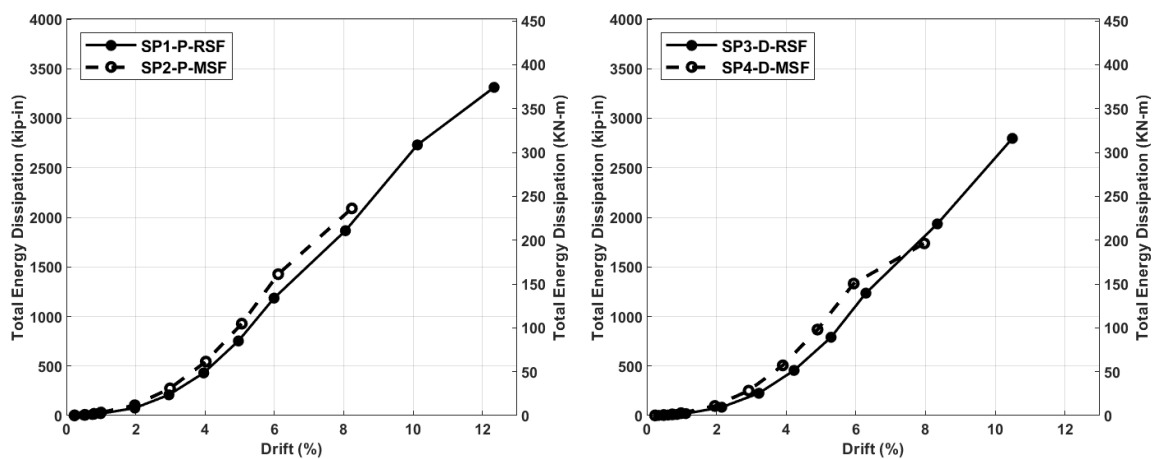
Figure 4-14. Comparison of total energy dissipation of ABC columns using UHPC RSF and MSF
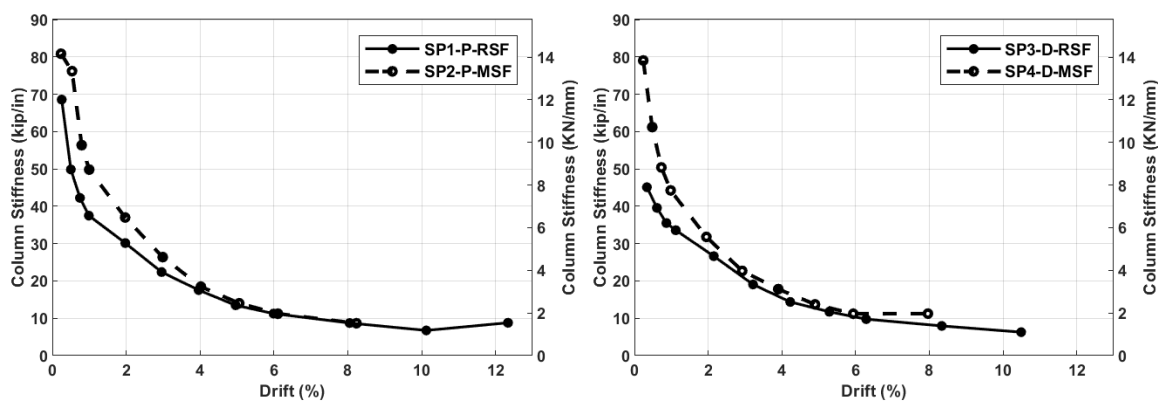
Figure 4-15. Column stiffness degradation of UHPC columns
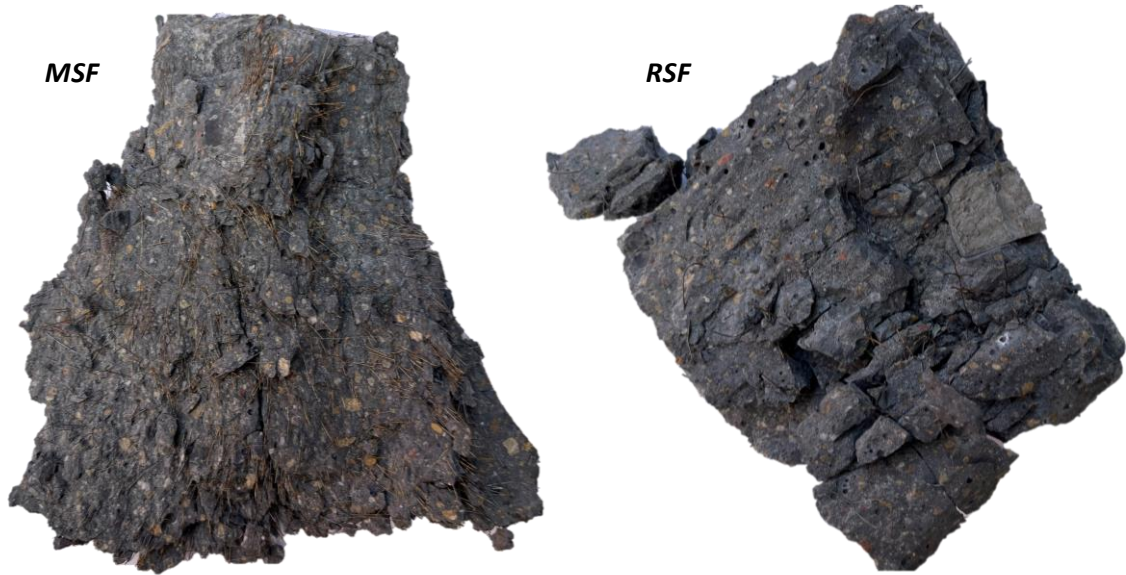
Figure 4-16. Views of spalled UHPC parts from the plastic hinge zone of columns with different fibers
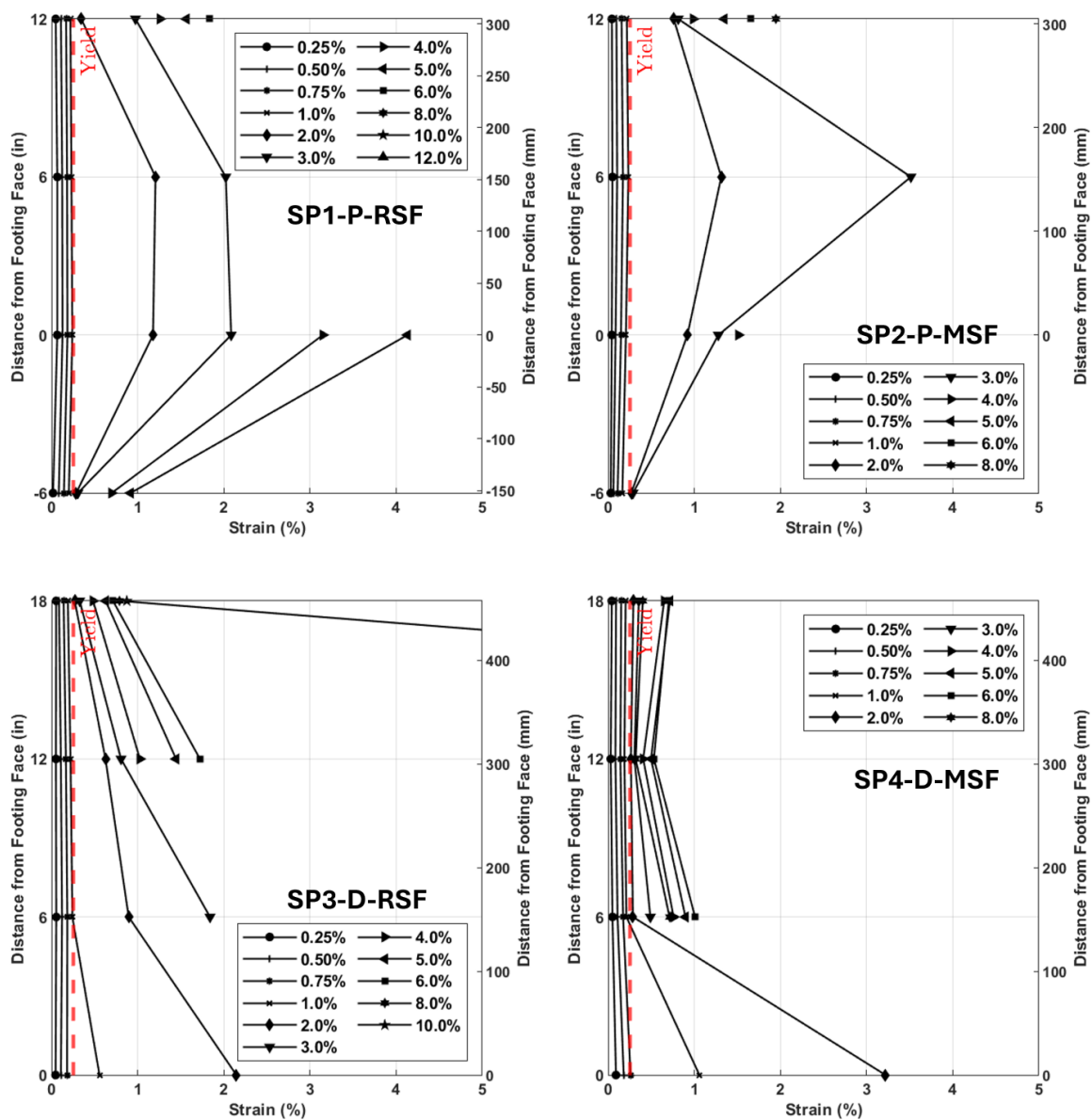
Figure 4-17. Strain gauge reading of the longitudinal reinforcement
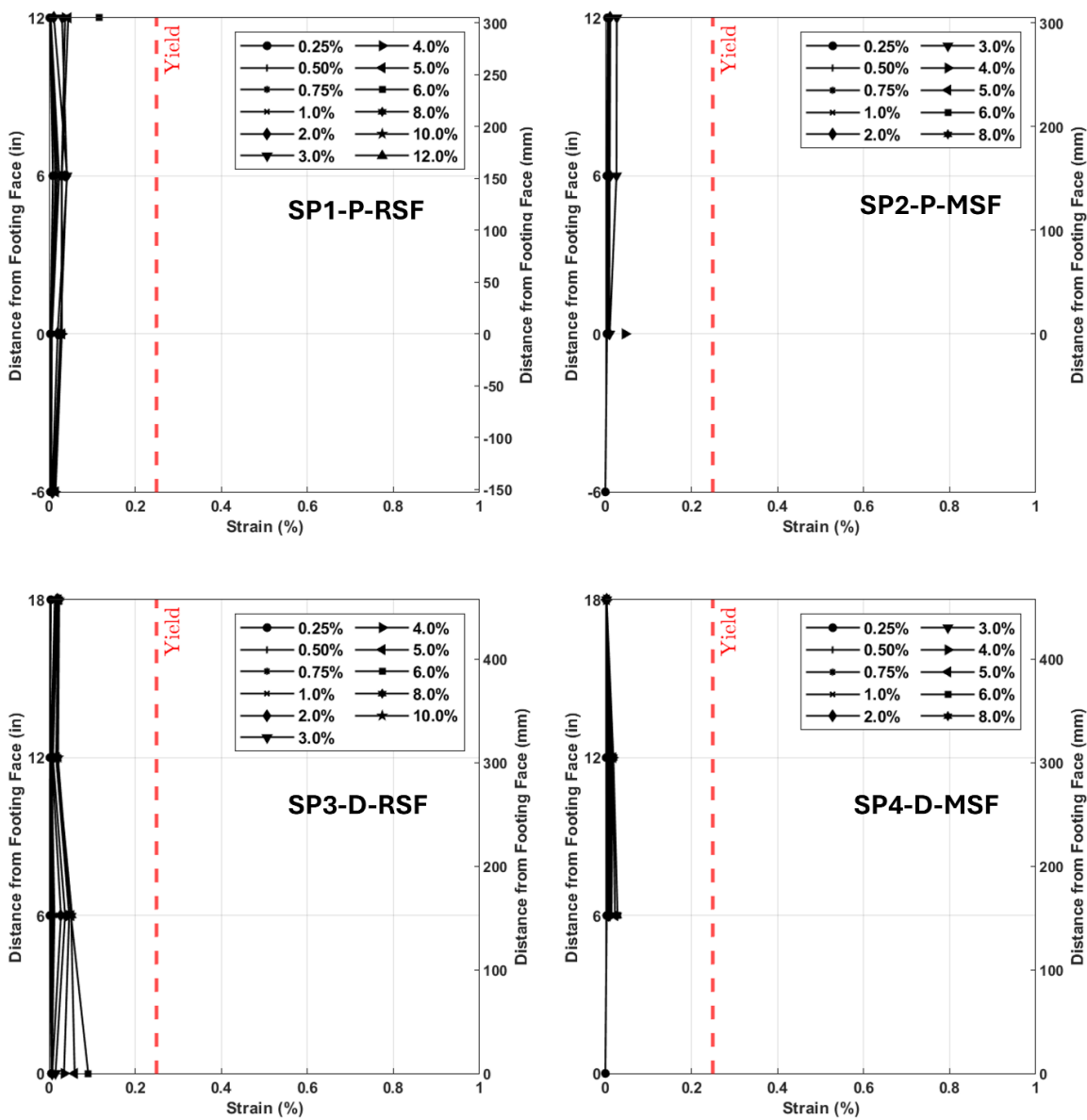
Figure 4-18. Strain gauge reading of the transverse reinforcement
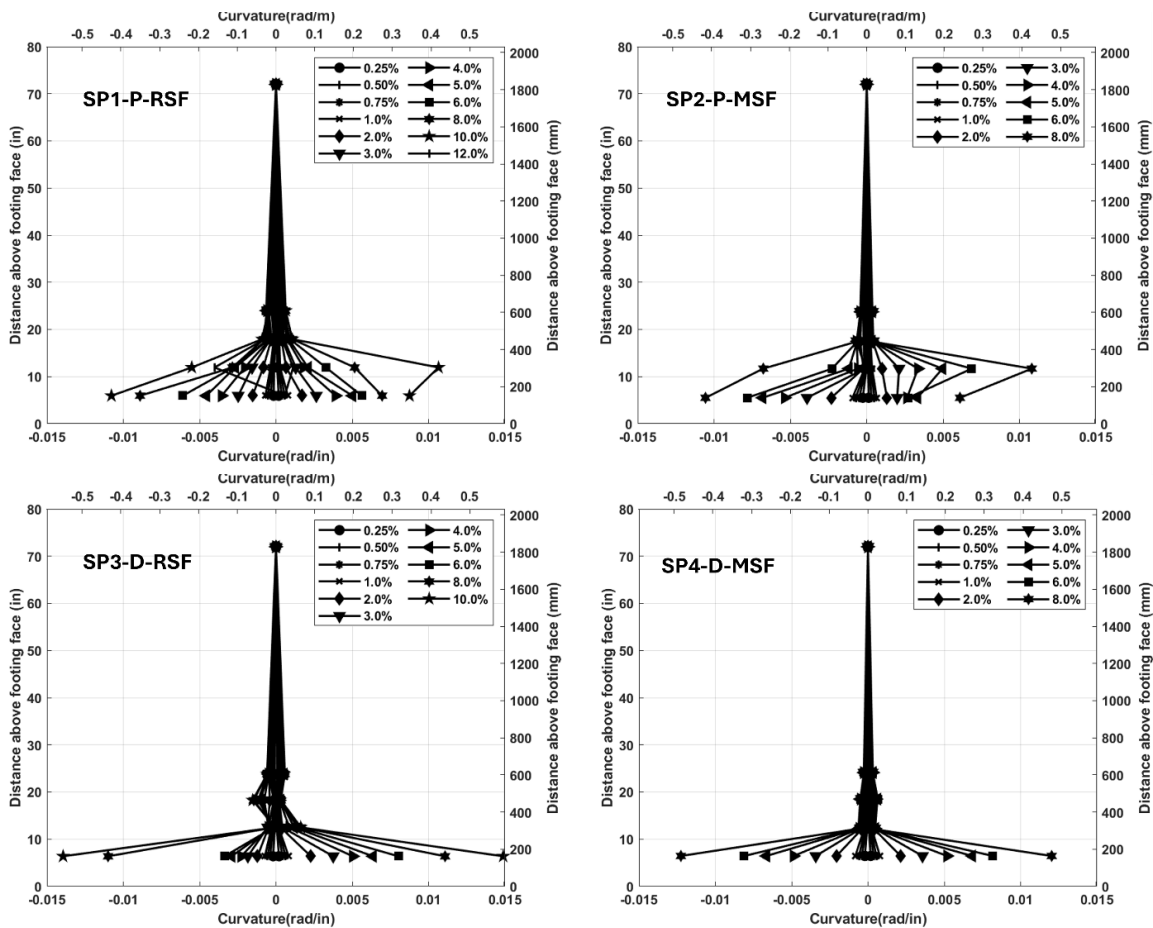
Figure 4-19. Curvature profile of UHPC columns
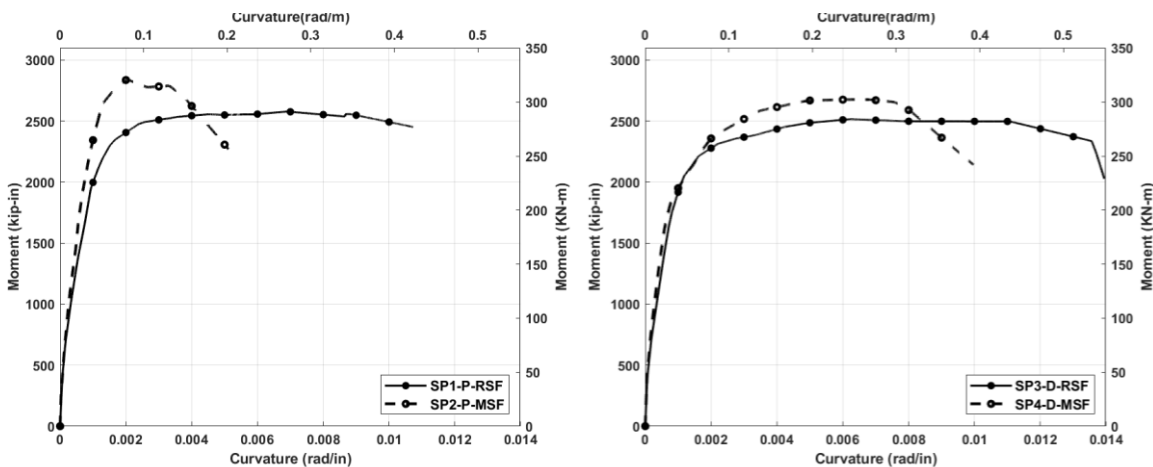
Figure 4-20. Average moment-curvature relationship of tested columns at 6 in (15 cm) above footing

5 SHAKE TABLE TESTS OF ECONOMICAL PRECAST UHPC COLUMNS WITH DIFFERENT FIBERS TYPES AND SEISMIC JOINT MATERIALS

This chapter is a standalone paper that has already been submitted to the Journal of Composite Structures

Abstract

Ultra-high performance concrete (UHPC) is a rapidly growing solution for rehabilitation of aging infrastructure systems like bridges as well as new construction. However, the implementation of UHPC at the full structural components scale is still challenging because of the associated costs and slow development of design guidelines. Moreover, and even within the research community, there is only limited number of studies that focused on structural seismic applications specifically. Thus, this study fills a major knowledge gap and focus on the dynamic seismic performance of full precast UHPC columns that also exclusively use economical scalable UHPC mixtures with recycled steel fibers. With focus on bridge columns with accelerated bridge construction (ABC) grouted duct connections, three large-scale precast UHPC columns were fabricated at an actual precast facility in California and tested on a shake table under dynamic earthquake excitations. The UHPC columns varied based on the UHPC fibers type (manufactured versus recycled steel fibers), and the grouting material in the ABC joint (conventional grout versus UHPC). The paper presents new data and knowledge on seismic response and plastic hinge behavior of UHPC from dynamic shake table tests, and successfully demonstrate the viability of scalable UHPC with recycled steel fibers for seismic bridges.

5.1   Introduction

Ultra-high performance concrete (UHPC) continues to rise and gain popularity as a robust building material due to its superior mechanical performance and enhanced durability, which can significantly increase the service life of structures [1-3]. A key aspect of UHPC is using finer constituent materials that improve the particle packing density [4] and steel fibers that bridge micro-cracks, improving ductility tremendously [5]. A significant advantage of UHPC is its capability to achieve early-age compressive and flexural strength [6], which can be beneficial for rapid construction and post-disaster retrofitting. Most UHPC applications have been mainly used UHPC as joint material for bridge deck connections and overlays. A recent milestone was the deck rehabilitation project for the Delaware Memorial Bridge, which implemented 4,700 yd^3 (3,600 m^3) of UHPC over the 10,000+ ft^2 (3,050+ m^2) bridge deck [7]. Other major UHPC applications and projects are primarily non-structural applications that not necessarily fully utilize the structural benefits of UHPC. Because of the high compressive and improved flexural performance of UHPC, research studies started looking into large structural UHPC applications for bridge superstructures such as prestressed I-Girders [8]. Even though studies have shown that UHPC has a great potential for structural bridge applications, its

limited availability, high cost, and slow development of formal design guidelines for UHPC are some of the main reasons restricting large-scale adoption and implementation.

Whether the focus is bridge structures or buildings, UHPC columns are exemplary candidates for showcasing the superior mechanical properties of UHPC and major compressive strength benefits. Recent studies have explored axial UHPC columns for instance, mostly for buildings and to less extent in bridges or seismic applications. Three different examples of such studies are as follows. Aboukifa and Moustafa [9] investigated the structural behavior of nine square UHPC columns (with 28 cm $\times$ 28 cm sections and 2-5 m height) under pure axial columns. Their study demonstrated the impact of reinforcement detailing and slenderness ratio on the axial capacity of UHPC columns. Sugano et al. [10] performed cyclic testing of small UHPC columns with 1.0 m height and 20 cm $\times$ 18 cm cross-sections. The tests showed that additional lateral reinforcement provides higher displacement, and adding 2% of fiber enhances the lateral force and displacement. Ichikawa et al. [11] also tested the applicability of UHPC hollow segmental jackets at the plastic hinge section of seismic bridge columns. The response of the column showed a rocking mode behavior and revealed no significant spalling and crushing in the plastic hinge zone due to the effects of fibers in the UHPC. The aforementioned examples, among others that are not listed here, have confirmed the significant improvement of structural response of columns for axial and lateral loading, but have been limited to simple loading scenarios like pure centric axial loading, or very small-scale, or even partial UHPC columns only for lateral loading applications. Therefore, there is an urgent need for more UHPC columns testing to address one or

more of the current needs such as using larger-scale models, precast production, seismic applications, and equally important, emerging and economical UHPC mixtures implementation for meaningful structural applications.

On the economic and ecological developments, many studies have explored ways to reduce the cost of UHPC using recycled materials [12-13]. One approach was to use recycled steel fibers (RSF) as an alternative to manufactured steel fibers (MSF). Figure 5-1 shows the visual comparison between RSF and MSF (which are the fibers types used in this study). RSF, typically derived from worn-out tires in landfills, are extracted using standard recycling methods such as mechanical shredding and pyrolysis [14]. Unlike MSF, raw RSF are non-uniform with variations in length and diameter, and are inherently contaminated with some rubber residue depending on the degree of the recycling mechanism. Because of these unique characteristics of RSF, studies have shown that incorporating RSF can affect concrete fresh and hardened properties. High fiber dosage and aspect ratio of RSF can affect the workability of fresh UHPC concrete [15]. However, reducing fiber dosage and lower aspect ratio can negatively affect the tensile and flexural performance of UHPC [16-18]. Hence, RSF fiber dosage and aspect ratio are crucial to attaining a workable UHPC with sufficient tensile performance. Aside from aspect ratio and dosage, rubber presence in RSF has been shown to reduce the compressive strength of UHPC [18], but can improve properties such as splitting tensile and fracture energy [19]. Also, Habib et al. [20] showed that incorporating portions of rubber particles in concrete improves the damping ratio significantly, which can be a good energy dissipator for structures subject to high dynamic loading. Overall, RSF

presents good properties that can be leveraged for structural applications and ultimately be cost-effective and sustainable. However, studies are yet to be conducted on RSF for large structural applications, specifically for bridge columns, which is another knowledge gap filled in this study.

A promising application of RSF is exemplified for accelerated bridge construction (ABC). In ABC, bridge superstructures are prefabricated at a typical precast plant and are delivered on-site for assembly. ABC has more advantages than cast-in-place as it reduces the cost, construction time from shoring and casting, and traffic delays from lane closures. Although ABC provides numerous advantages in construction techniques, ABC joint connections are particularly concerning, especially for regions with high seismic activity. Over the past two decades, several ABC connections, such as pocket and grouted duct connections, have been developed and proposed for both column-to-footing and column-to-cap beam connections [21-23]. However, previous work investigated mostly normal strength concrete (NSC) columns, and UHPC has been primarily used only for connections. Only few studies investigate full UHPC seismic columns. For example, Aboukifa and Moustafa [24] investigated small-scale UHPC columns under combined axial and lateral using high-steel reinforcements [24]. The study showed that the seismic plastic hinge does not show visible concrete spalling, and tensile rupturing of the reinforcement is the main failure mode. Collectively, previous studies provided only general overview and preliminary investigation of the behavior of UHPC in seismic bridge columns. However, most of the tested columns used were relatively smaller in scale, no precast or ABC connections were used with full UHPC columns, economic

aspects of UHPC mixtures were not introduced, and finally, previous studies considered mostly quasi-static loading with a lack in comprehensive dynamic testing.

Based on above, there is a need to test large-scale precast UHPC columns using ABC connections for dynamic behavior, while ideally incorporating emerging economical UHPC mixtures. To fill these gaps and expand the knowledge on UHPC in bridge columns, this study investigates the dynamic behavior of economic UHPC precast columns with both MSF and RSF and with ABC grouted duct connections that also differ in the grouting material. Our specific objectives are to: (1) demonstrate and implement economical UHPC with local and recycled materials for large-scale mixing at actual precast plant in California; (2) fabricate and test three large-scale UHPC bridge columns with ABC grouted duct connections at a uniaxial shake table under increasing earthquake excitations; and (3) assess the global and local behavior and seismic response of UHPC columns with MSF and RSF and connections using UHPC and conventional grout. For the test specimens, NSC precast footings were also fabricated at a precast plant in Nevada and assembled with the UHPC columns at the fabrication yard of the Earthquake Engineering Laboratory of the University of Nevada, Reno, where the shake table testing was also performed.

5.2   Experimental Program Development

An overview of the experimental program is provided in this section to present test specimens and variables, specimens fabrication and assembly, companion material properties, and shake table test setup and instrumentation.

5.2.1 Test Matrix and Specimen Detailing

Three UHPC columns with ABC grouted duct connections were considered in this study with details summarized in Figure 5-2 and Table 5-1. Specimen 1 (SP1-MSF) is the reference column with UHPC MSF and UHPC-filled ducts in the joint. Specimen 2 (SP2-RSF-G) and Specimen 3 (SP3-RSF) use the RSF UHPC in the columns with a joint filling material conventional grout and UHPC with MSF, respectively. Figure 5-2 shows schematically the reinforcement details which is same for all three UHPC columns. The columns had a height of 62 in (158 cm) and a diameter of 16 in (41 cm). A loading head with a dimension of 20 in × 20 in × 20 in (51 cm × 51 cm × 51 cm) was positioned on top of the column. Four PVC pipes were placed at the loading head to attach the specimen to the off-table mass rig (more details provided in the test setup).

Since the UHPC columns are designed with ABC duct connections, the longitudinal reinforcement was extended beyond the height of the column to provide an anchor for the column into the ducts. The reinforcement minimum anchorage length was determined based on Equations 1 and 2. The embedment length calculation in Equation 1 is based on the bond strength of the reinforcement bar and grout, while Equation 2 is based on the bond strength between duct and concrete. The parameter used in the equations are: D_{cm} is the column diameter, d_{bl} is the diameter of the longitudinal reinforcement bar, f_{ye} is the expected yield stress of the reinforcement bar, and f'_g is the compressive strength of the

grout. The calculated embedment length was determined to be 11 in (28 cm) with the measured d_{bl} of 0.75 in (1.9 cm), and the assumption that f_{ye} is 60 ksi (414 MPa), and f_g' is 8 ksi (55 MPa). Although two columns used UHPC for filling connection ducts, the compressive strength of the conventional grout was deliberately used in the calculation to determine the maximum embedment length required. Nevertheless, the embedment length was further increased to 24 in (61 cm) to avoid any issues regarding slippage or pullout.

$$l_e = \frac{0.68 d_{bl} f_{ye}}{\sqrt{f_g'}} \tag{1}$$

$$l_{ad} = \frac{2.25 d_{bl}^2 f_{ye}}{d_d \sqrt{f_c'}} \tag{2}$$

The specimens used precast reinforced concrete (RC) footings of dimensions 72 in × 72 in × 28 in (183 cm × 183 cm × 71 cm). The footing was designed to be a capacity-protected member and was reinforced heavily with a 32 #8 rebars and 40 #3 ties to provide shear resistance. The connection used 10 helical corrugated galvanized steel pipes with a diameter of 2.5 in (6.3 cm) embedded in the footing and mapped to the column reinforcement layout. The footings also included anchors on two opposite sides to provide lifting points for specimens handling.

5.2.2   *Specimens fabrication, UHPC casting, and Assembly*

Figure 5-3 provides an overview of the various specimens construction and assembly stages. The columns reinforcement cages were fabricated and instrumented before placing them into sonotubes. Concrete Dobies were placed around the cage to ensure a clear cover of 0.75 in (1.9 cm). Two UHPC batches were prepared, and the mix design is

summarized in Table 5-2. In this study, a semi-proprietary economical UHPC mixture was used for the first time in a seismic or structural study of this scale. A commercial vendor (CorTuf) supplied the a proprietary UHPC premix that was then mixed with locally sourced sand and cement from ConFab Precast California, who fabricated the UHPC columns for this project. On day of mixing, the moisture content in sand was measured, and the UHPC water content was adjusted accordingly. High-range water-reducing admixtures were used to achieve a low water-to-cement ratio. Regarding steel fibers, MSF with 2% by volume was used for SP1. However, the fiber content by volume of RSF for SP2 and SP3 was reduced to 1.6% as preliminary studies confirmed segregation of fibers if 2% is used.

Two large UHPC batches were produced in a truck mixer, as per typical precast plants practices for conventional concrete, in two separate days in March 2023 that were about one week apart. All the dry components except the steel fibers were placed first. Once the dry components had homogenized, the admixtures and water were streamed in the truck mixer. The components were mixed for five minutes, and the steel fibers were added last from the truck's top gate. Since there are no current practices and specialized equipment yet to disperse steel fibers at this scale, the steel fibers were added as illustrated in the figure. The UHPC was mixed for another five minutes after adding the fibers while the truck moved to the precast bed for casting. Before releasing the UHPC from the truck chute, a sample was taken to do a flow table according to ASTM C1437 and C230 [25-26]. The average spread diameter of UHPC with MSF was around 8.9 in (23 cm). The UHPC with RSF showed fiber clumping in the flow test as shown in the figure.

Nevertheless, the casting of UHPC with RSF was still successful as the loading head and column reinforcement did not block the flow of the UHPC. The average flow test spread diameter of UHPC with RSF was 7.8 in (20 cm). Curing blankets were used to cover the columns top to ensure the heat of hydration is trapped and stay uniform. The columns were cured for three days before stripping of the sonotubes, then later after several weeks, were transported to UNR fabrication yard for specimens assembly.

The footings were cast in August 2023 at Jensen Precast in Reno, Nevada. The footing cage was assembled on-site at Jensen precast and when the formwork sides were installed, the corrugated steel ducts were accurately placed using a locator plate. Conventional concrete was used to cast the footings, and after several weeks, all footings were also transported to our fabrication yard for assembly (see Figure 5-3). The specimens were assembled by pouring grout into the ducts and then the columns were carefully lowered using a forklift. SP1-MSF and SP3-RSF were grouted using UHPC with MSF, while SP2-RSF-G was grouted using conventional grout.

5.2.3   Material Properties

UHPC material samples were obtained and cured alongside the columns at ConFab Precast, then tested later at UNR to determine the compressive, tensile, and flexural strength. Table 5-3 summarizes the average result of each test for day 28 and test date. The compressive strength was determined in accordance to ASTM C1856 [27] after careful preparation of the cylinders [28]. The average compressive strength of UHPC MSF at the test date was 22.1 ksi (152 MPa), while UHPC RSF had 20.1 ksi (139 MPa)

with only 10% difference. Table 5-3 provides also the estimated modulus of elasticity values for UHPC with MSF and RSF. To allow for future studies to consider modeling of the tested columns, full mechanical characterization of UHPC was conducted and briefly reported here for completeness. Sufficient samples were obtained to conduct direct tension and flexure tests of UHPC with both MSF and RSF. The tensile strength was measured using displacement-controlled testing of dogbone coupons with 1 in × 1 in (2.5 cm × 2.5 cm) cross-section using an Instron machine with hydraulic grips. The crack localization point, defined at the maximum tensile stress in this study [29], was calculated to be around 1.68 ksi (11.6 MPa) with 0.41% strain and 2.03 ksi (14.0 MPa) with 0.97% for UHPC with MSF and RSF, respectively. The localized stress and strain of UHPC RSF were higher than UHPC MSF because some RSF were observed to have a higher aspect ratio at the localized crack, which helped achieve higher tensile stress and strain. Conversely, the results of the flexure tests were different as the modulus of rupture of UHPC with MSF of 4.09 ksi (28 MPa) was relatively higher than UHPC with RSF which showed 2.0 ksi (14 MPa) modulus of rupture.

The compressive strength of the grout was also measured to verify whether the embedment length calculated in the earlier design was adequate. Table 5-4 summarizes the maximum compressive strength, strain at maximum, and modulus of elasticity obtained for both grouting materials, i.e. conventional grout and UHPC with MSF produced at UNR during the specimens assembly. The compressive strength of the footing was also determined and shown in Table 5-4. Moreover, the actual yield and ultimate tensile strength of the A706 GR60 reinforcement used inside the UHPC columns

is: 71.3 ksi [492 MPa] and 101.6 ksi [701 MPa] for #3 transverse reinforcement, and 64.2 ksi [443 MPa] and 95.5 ksi [659 MPa] for #6 longitudinal reinforcement, respectively.

5.2.4 *Shake Table and Instrumentation Plan*

The specimens were tested on one of the biaxial shake tables at the Earthquake Engineering Laboratory at the University of Nevada, Reno. Figure 5-4 shows the schematic test setup as well as a photograph of the actual setup for one of the columns at the shake table. A 1.5 in (3.8 cm) grout pad was used to level the footing on the table. Threaded rods were passed and pre-tensioned into the footing to attach the specimens to the table. A rigid link was attached to the specimen through the PVC pipe and connected to the mass rig; a setup that is commonly used at UNR to simulate inertial forces during the dynamic tests. Three 20 kips (89 kN) blocks were placed in the mass rig, which along with 20 kips (89 kN) weight of the rig itself provided a total of 80 kips (356 kN) equivalent mass for the inertial force. A load cell was connected within the rigid link and used to record the inertial force achieved during all tests.

The axial load was generated using two hollow core jacks on the spreader beam. Two high-strength threaded rods were passed inside the jacks and were secured using plates reacted at the base of the footing. Both rods were tensioned to provide a total of 80 kips (356 kN) axial load in the columns during the tests. The equivalent axial load index (ALI), determined as the ratio of the total axial load to the product of compressive strength and cross-section area of the column, was around 2.0%. The axial demands in actual bridges are dictated by the superstructure regardless of columns type, so the 2% ALI for UHPC columns corresponds to 8% ALI for NSC columns with 5 ksi (35 MPa).

The global and local responses of the specimens were captured using different instrumentations. The data were collected from approximately 105 internal and external Data Acquisition (DAQ) channels from the shake table and the specimen. Two accelerometers measuring the North-South, East-West, and vertical acceleration were placed at the interface of the footing and the loading head. An accelerometer was placed on the footing to check how the footing and shake table accelerations compare to confirm that no slippage occurred. Accelerometers were placed at the loading head to measure the acceleration of the column at the top. Four string potentiometers were placed at the corners of the loading head to measure the relative displacement of the column. Four pairs of linear variable differential transformers/transducers (LVDT) were arranged around four sections within the plastic hinge zone to later calculate the curvature of the column. Twenty-four strain gauges were also installed onto the reinforcement before the columns fabrication and Figure 5-5 shows the typical location of such strain gauges in the columns. Lastly, whitewash paint was applied at the surface of the column to facilitate crack monitoring and track of the damage.

5.2.5   *Loading Protocol*

The columns considered herein were intended to be representative large-scale columns to comparatively assess the behavior of new UHPC and connection designs rather than representing an actual prototype bridge. Nevertheless, for selecting the tests ground motion, site location was assumed to be in Galena Creek, Reno, with a soil classification of C and a risk category of II. Based on the site information, the design response spectrum was generated using the ASCE 7 Hazard Tool, and the seismic parameters were

determined as S_{DS} =1.62g and S_{D1} = 0.72g [30]. Moreover, the period of the column was estimated based on the assumption that the specimen is a cantilever with a moment joint at the connection, and in turn, the lateral stiffness was estimated as $3\times(EI)_{crack}/L^3$, where $(EI)_{crack}$ was obtained using MC-BAM, a moment-curvature analysis tool for advanced material [31], and L was the height of the column. The calculated stiffness was found to be 37 kip/in (6.5 kN/mm). The estimated period of the specimen was then calculated using the estimated lateral stiffness along with an equivalent mass from the 80-kip loaded mass rig. The estimated period was found to be 0.10 sec. Using the design response spectrum and the estimated period, the PEER Database was utilized to select the ground motion [32]. Among the candidate ground motions, the 1994 Northridge earthquake ground motion recorded at the Sylmar Converter Station in the 52º direction was chosen because the matching scale factor was almost 1.0, and the acceleration history was fairly symmetric. As such, the selected Northridge ground motion directly represented the 100% of the design-level earthquake (DLE). Eight runs of 25% - 200% (increment of 25%) of the DLE were used for the full loading protocol as illustrated in Figure 5-6. It is just noted that before each ground motion run, a white noise motion with a root mean square amplitude of 0.05g was applied to the specimen to determine the column's period, damping ratio, and stiffness.

5.3   Results and Discussions

This section presents the columns shake table test results in terms of global behavior (damage progression, force-drift relationships, etc.) and the local behavior captured through reinforcement strains and curvature estimates.

5.3.1   *Acceleration Response*

The specimens were excited under uniaxial ground motions in the north-south direction using the previously shown protocol. All columns survived the 150% DLE, or equivalently the maximum considered earthquake (MCE). However, both UHPC with RSF columns reached up to 175% DLE. The acceleration feedback from each run was recorded at different locations in the specimen to better understand the dynamic response. The shake table acceleration (achieved feedback) was also obtained and compared against input ground motion (target) as summarized in terms of the peak ground acceleration (PGA) in Table 5-5. The comparison shows about 0.3% to 21% difference, which is typical in such tests and can be attributed to the mass and dynamics of the shake table itself. However, the differences in the achieved PGA among the specimens were relatively close. To further assess the tests fidelity, the achieved table acceleration was compared to the acceleration history on the footing as shown in Figure 5-7, and the good match confirmed no footing slippage.

The acceleration was also recorded on the loading head and full hsitories for all stetched runs are shown in Figure 5-8. The peak values are also reported in Table 5-5 from each run. As observed, the peak top acceleration values were similar for all specimens, especially when the specimen was still in the essentially elastic range of behavior. Lower peak acceleration values were genrally obtianed at the column's top relative to the input PGA, which is driven by where the specimen initial and softened periods approximeatly fall within the input ground motion spectrum.

5.3.2   Displacement/Drift Response

The absolute displacement time history at the column top was measured by averaging the recorded displacement from the string potentiometers attached to different locations in the loading head. However, since the specimen moved relative to the shake table, the relative displacement was then calculated by subtracting the shake table displacement from the absolute displacement of the column. For more meaningful discussion, the relative displacement at the column top is related to the effective height of the column, 72 in (183 cm), to obtain drift ratios. Figure 5-9 shows the stitched drift ratio time history from all runs for the three columns. As observed, the increasing drift ratio with the increased ground motion intensity was not symmetrical because of the residual drift and permeant damage at the end of each run. Figure 5-9 shows also the summary residual drift after each run for the three specimens. A positive residual drift ratio indicates permanent drift in the south direction, while a negative residual drift indicates permanent drift in the north direction.

5.3.3   Damage Progression and Plastic Hinge Behavior

The cracks after each test run were documented using different colors markers to facilitate the damage progression of the columns. A comprehensive view of the damage progression after three different excitation levels, i.e. 25% DLE, 100% DLE, and the final run causing failure, is shown in Figure 5-10. At 25% DLE, the peak drift ratio of the SP1-MSF column was 0.57%, while SP2-RSF-G and SP3-RSF achieved relatively higher drift ratio of 0.79% and 0.77%, respectively. For such drift demands, no cracks or damages were observed with SP1-MSF, while minor flexural cracks were observed in SP2-RSF-G

and SP3-RSF as shown in Figure 5-10a. The minor damages at 25% DLE indicate that the columns remained essentially elastic.

The drift and residual ratio increased further with the increased ground motion intensity, indicating that the column yielded, with a significant increase noted around the 100% DLE. Figure 5-10b shows that the damage concentrated in the plastic hinge zone. For SP1-MSF, the drift ratio was 4.77% with residual drift of -0.40%. SP2-RSF-G and SP3-RSF reached a slightly higher drift of 4.97% and 4.81% but a lower residual drift of -0.35% and -0.11%, respectively. Comparing the SP1-MSF and SP3-RSF, the drift ratios were similar; however, the residual drift difference was about 114%. The high residual drift difference did not reflect the damages in the plastic hinge zone.

SP1-MSF had a localized crack around 3.0 in (7.6 cm) from interface, while SP3-RSF, although had a distinct localized crack, had multiple flexural cracks within the plastic hinge zone with minor crushing at the interface. The higher residual of SP1-MSF compared to SP3-RSF was of concern as the damage concentration likely occurred at the interface. Likewise, SP2-RSF-G with grout connection had a higher residual drift than SP3-RSF. The higher residual drift of SP2-RSF-G caused more crushing action on the north side of the interface.

The columns continued to achieve a higher drift ratio at 125% DLE. Consistent with earlier runs, SP1 had a smaller peak drift ratio of 6.06% compared with SP2-RSF-G and SP3-RSF that achieved 6.87% and 6.32%, respectively. Moreover, the residual drift of SP1-MSF and SP2-RSF was about -0.91%; significantly higher than the -0.52%. value of

SP3-RSF. The test proceeded with 150% DLE; however, this is when SP1-MSF failed and the tested was stopped following the popping noise that was heard and indicated several reinforcing bars rupture. The peak and residual drift ratios were 9.3% and -5.6%, and Figure 5-10c shows the final damage state of SP1-MSF. No further significant damage aside from minor crushing at the interface of the north section was observed. However, multiple longitudinal reinforcing bars ruptured at the south side at locations close to the interface with footing. In contrast, SP2-RSF-G and SP3-RSF survived the 150% DLE with peak drift of 9.4% and 8.6% and residual drift of -1.9% and -1.5%, respectively.

SP2-RSF-G and SP3-RSF were both tested further under 175% DLE, and this is when the longitudinal reinforcement ruptured and testing was stopped. SP2-RSF-G achieved a peak drift ratio of 13.84% and residual drift of 11.1%. These results were relatively lower for SP3-RSF, which experienced peak drift of 11.1% and residual drift of 6.7%. The high peak and residual drift of SP2-RSF-G can be attributed to the lower bond strength of conventional grout compared to UHPC in the seismic joint, which causes some bond slip failure in the longitudinal reinforcement. However, it is noted that the actual bond slip was not possible to measure in the tests. Figure 5-10c comapres the final damage state of SP2-RSF-G and SP3-RSF. Both columns had minor spalling in the north side of the column associated with UHPC compression crushing. Moreover, the localized cracks developed from earlier runs widened in the south section, and eventually like in SP1-MSF, multiple longitudinal reinforcements ruptured at south sections of the other columns.

5.3.4 Force-Drift Relationships and Response

The force-drift relationship and hysteresis loops were obtained to understand the full behavior and overall performance of the specimens in terms of yielding, ductility, and energy dissipation. Figure 5-11a-5-11c shows the force-drift hysteresis envelope of all the UHPC column specimens. A positive sign drift ratio indicates column movement in the south direction, while a negative sign indicates movement in the north direction. The force-drift hysteresis plots show highly asymmetric behavior in the north direction, that was influenced and pronounced by the high residual drifts after each run. For lower ground motion levels, the hysteretic behavior was nearly linear, as evident with the narrower loops formed. However, as the specimen was subjected to higher seismic levels, the hysteretic loops widened, indicating high energy dissipation in the column. Note that the tests were terminated suddenly when reinforcement ruptured, which explains the final big drops in the plots.

The backbone of the hysteretic envelope of the three UHPC specimens was traced and plotted in Figure 5-11d to compare all three columns. A summary of the response results based on the force-drift relationships is also provided in Table 5-6. The yield point was determined by finding the drift at which the first column longitudinal reinforcement yielded, which is reported to be 0.57% for SP1-MSR; a lower value compared to SP2-RSF-G and SP3-RSF, where first yield occurred at 0.79% and 0.77% drift, respectively. The yield force was around 20.7-22.1 kips (92-98 kN) for the three specimens. SP1-MSF achieved a slightly higher lateral force capacity (~8% higher) when compared with the UHPC with RSF columns. The ultimate drift capacity was identified when the column

peak strength dropped to 80%. The ultimate drift ratio of SP1-MSF was determined to be 7.78%; significantly lower than the 11.98% and 11.13% values of SP2-RSF-G and SP3-RSF, respectively. This difference of about 32-45% renders the favorable drift capacity of RSF columns.

The idealized elasto-plastic curves were also generated to calculate the displacement ductility achieved by each specimen for better comparison against design codes. The curve used an effective yield that was determined by equalizing the area below and above the plastic curve, and terminates at the ultimate displacement value. Figure 5-12 shows the idealized elasto-plastic curve of the three specimens.

The displacement ductility of the columns was calculated from the ultimate and effective yield values and reported in Table 5-6. SP1 showed a relatively lower displacement ductility of 7.6 compared to SP2-RSF-G and SP3-RSF that showed 9.1 and 8.7, respectively. Nonetheless, all three UHPC columns exhibited acceptable seismic behavior with ductility well exceeding the minimum demand of 5.0 according to Caltrans's Seismic Design Criteria [33], for instance.

5.3.5   Column Energy Dissipation

The column's energy dissipation was obtained from the force-displacement hysteresis and shown in Figure 5-13 that shows the cumulative total energy dissipated for all UHPC columns. The energy dissipated was determined by the area enclosed within hysteresis loops. The total energy dissipated for all columns was fairly similar up to the column failure. At rupture, the total energy dissipated by SP1-MSF was 1685 kip-in (190 kN-m),

while SP2-RSF-G and SP3-RSF had 2415 kip-in (273 kN-m) and 2483 kip-in (281 kN-m). The lower dissipated energy from SP1 was expected since the column only reached up to 150% DLE while the other two reached 175% DLE.

5.3.6 *Stiffness Degradation, Period Elongation, and Damping Ratio*

The period and damping of the specimens were determined by subjecting the specimens to white noise motion before each seismic test. The obtained columns acceleration response history from the white noise tests was transformed and processed in the frequency domain using the Frequency Response Function (FRF) to determine the specimen's natural period. The first dominating peak in the frequency domain was recorded as the natural frequency of the specimen. Figure 5-14a shows the natural period of the specimen after each ground motion. All columns had an initial period of around 0.31-0.32 sec. The experimental period of 0.31 sec was re-entered into the PEER ground motion selection tool, and the scale factor was determined to be around 1.01, which was close to the original scale factor used of 1.0. As testing continued with higher seismic intensities and caused damage to the specimens, the stiffness degraded and in turn, the specimens period increased until it reached a constant period of 0.73 sec. The half-power bandwidth method was also used to determine the inherent damping ratio of the specimens. The average damping ratio of SP1-MSF, SP2-RSF-G, and SP3-RSF was determined to be 2.02%, 2.63%, and 2.31%, respectively. The slight increase in the damping value of RSF columns can be attributed to the rubber crumps present with the raw RSF.

The stiffness of the columns was also calculated from the white noise tests, but directly from the best-fit linear approximation within the 10-30% region of the force-displacement response measured in those low amplitude white noise tests. Figure 5-14b shows the trend of column stiffness degradation as relates to the peak observed drift ratio from the corresponding seismic tests. The initial stiffness of all columns was estimated to be around 75-78 kip/in (13.1-13.7 kN/m). The trend in Figure 5-14b shows that 50% of UHPC columns stiffness is lost around 2% of drift ratio. The comparable initial stiffness, as well as similar period, for all three UHPC columns confirm that using RSF does not affect the flexural stiffness of seismic UHPC bridge columns.

5.3.7 *Reinforcement Strain Response*

The peak reinforcement strain values were obtained and plotted to capture strain profile within the plastic hinge zone using four sections as shown in Figure 5-15. Strain gauges were placed on longitudinal rebars at 6 in, 12 in, 18 in, and 24 in (15.2 cm, 30.5 cm, 45.7 cm, and 61.0 cm) relative to the footing interface, i.e. sections 1, 2, 3, and 4 as designated above in Figure 5. As the input ground motion increased, some strain gauges were damaged, and only the prior strain readings were reported. Figure 5-15 shows the strain profile in one of the longitudinal rebars in each column. After the initial run, the longitudinal reinforcement was close to yielding, and after the 50% DLE motion, the strain values significantly increased. SP1-MSF recorded a high localized strain of more than 2% at section 1, with no significant additional strain recorded at sections 2-4. The low strain recorded above section 1 was reflected by the minimal cracks formed in the exact location. Unlike SP1-MSF, high post-yield strains were observed throughout

Sections 1-3 of SP2-RSF-G and SP3-RSF. This fairly distributed strain along 12 in (30 cm) of the longitudinal rebars was manifested in the multiple localized cracks in this region.

Although there are no formal design guidelines for detailing transverse reinforcements in UHPC, previous research suggests that proper confinement is still critical, and only a certain degree of confinement is provided by steel fibers [34-35]. To gain further insight, Figure 5-15 shows also the maximum strain achieved in the transverse reinforcement at locations around sections 1-4 on the north and south sides of the column. Most of the strain activity was observed at the north side of the column, which can be attributed to the high drifts recorded in that side. For SP1-MSF, no yielding was observed in the instrumented sections of the spiral throughout all the tests. High strain concentration in the longitudinal rebars around the interface region with no buckling within the plastic hinge zone caused the transverse reinforcement to be less engaged. However, this observation differs from SP2-RSF-G and SP3-RSF since yielding was recorded around sections 1 and 2. The yielding of transverse reinforcement agrees with the visually observed crushing and minor spalling on the north side of the RSF columns; both indicating some local buckling of the longitudinal reinforcement. Overall, no rupturing of transverse reinforcement was noted in any of the columns, and with the minimal spalling seen, both MSF and RSF are shown to help keep the columns intact within the plastic hinge zone.

5.3.8   *Moment-Curvature Response*

The curvature response was determined to further explain the high drift capacity and high reinforcement strain at the column/footing interface observed in RSF UHPC columns. The curvature of the column was estimated using LVDTs at again, similar locations as the strain gauges. Figure 5-16 shows the curvature profile of all columns at four different sections within the plastic hinge zone. SP1-MSF showed high curvature at section 1, i.e. 6 in (15 cm) above the footing interface, and low curvatures were recorded at other sections of the column. High curvature was also observed at section 1 of SP2-RSF-G and SP3-RSF; however, unlike SP1-MSF, significant curvature was recorded at sections 2 and 3 of those RSF columns.

Since high curvature was recorded at section 1 in all columns, the moment-curvature behavior of this particular section was explored. The moment-curvature behavior was determined based on the average backbone of the positive and negative moment-curvature hysteresis. Note that the moment was calculated using the lateral force achieved in the rigid link multiplied by its distance to section 1. Figure 5-16d shows the average moment-curvature of the three tested UHPC columns and key results of the moment capacity along with peak estimated curvature are summarized in Table 5-7. SP1-MSF had a slightly higher moment capacity of about 7% than the UHPC columns with RSF. However, SP2-RSF-G and SP3-RSGF exhibited a significantly higher curvature capacity than SP1-MSF with an increase of about 48.5% and 35.2%, respectively.

The high curvature at section 1 significantly influences the overall performance of the columns. The localized curvature around section 1 for SP1-MSF can be attributed to the

capability of MSF bridging micro-cracks. Since MSF minimized the formation of cracks in the UHPC, the development of typical plastic hinge behavior at the lower portion of the column was not achieved. The minimal damage in the plastic hinge zone can be visually inferred when the column exhibited a rocking behavior when subjected to the ground motion excitations. Because of this rocking behavior, significant bending stress was concentrated in the weakest section of the column, i.e. the thin cold joint at the interface. The high bending stress in this region resulted in high strain in the reinforcement, which prompted tensile reinforcement rupture without observing any UHPC severe damage in the plastic hinge zone. Therefore, this caused the column to achieve a lesser drift capacity. In the case of SP2-RSF-G and SP3-RSF, the RSF allowed micro-cracks to be developed while maintaining bridging and holding macro-cracks from wide propagation. This resulted in more curvature distribution within the plastic hinge zone at multiple sections, causing the base of the column to crush and develop multiple cracks. Therefore, the strain was also fairly distributed within the considerable sections in the plastic hinge, as already observed from Figure 5-15. Thus, strain concentration at the interface was not as significant, causing columns with RSF UHPC to achieve a higher drift capacity. However, despite having more curvature and strain distribution, the highest strain was still recorded at the interface where the reinforcement eventually ruptured.

5.4   Conclusions

This study investigated the dynamic behavior of economical precast UHPC bridge columns with ABC grouted duct connections. Three scaled UHPC bridge columns with varying fiber types (MSF and RSF) and grouting materials in the joints (conventional

grout and UHPC) were tested at a shake table under uniaxial earthquake excitations. Several conclusions can be drawn from the various phases of this study (including UHPC mixing and precast construction) and test results:

1. Using locally sourced sand and cement and sustainable components such as RSF is shown to be promising for mass production of economical and eco-friendly UHPC as in precast plants settings. Although truck mixing can be adequately used for mixing UHPC, fibers clumping and segregation can be a potential issue in the case of RSF, and future work is recommended to look into better RSF dispersion techniques as well as RFS processing and sorting.

2. Overall, precast UHPC columns with ABC connections are shown to exceptionally meet current seismic design requirements. The three tested UHPC columns survived up to 150% DLE, i.e. MCE level, with the two columns with RSF did not even fail until the 175% DLE. Moreover, all the ABC UHPC columns with either MSF or RSF exhibit good dispalcement ductility that ranged from 7.6 to 9, and in turn, well exceedsthe typical seismic design code requirement of a ductility demand of 5.0 for single-column bents.

3. Upon inspection, the main mode of failure of UHPC columns is tensile rupturing of the longitudinal reinforcement at the column/footing interface. However, the damage pattern within plastic hinge zone varied between the different fibers type. For the UHPC column with MSF, a single major localized crack was observed close to the interface with almost no sign of UHPC crushing or spalling. The UHPC columns with RSF showed different damage patterns with multiple cracks were observed and

spread within the plastic hinge zone along with some minor UHPC crushing and spalling.

4. Further supporting the difference in the damage extent within plastic hinge zone for MSF and RSF UHPC columns, high localized reinforcement strain and curvature were concentrated and obsevred at the column/footing interface in the MSF UHPC, as opposed to more distributed strains and curvatures within plastic hinge in the RSF UHPC columns. Also, only RSF columns showed yielding of the transverse reinforcement.

5. All UHPC columns achieved sufficient total energy dissipation despite the asymmetrical force-drift hysteresis. However, when comparing the UHPC columns with MSF and RSF, the MSF is shown to increase the force and moment capcity by about 8%, while the RSF signifcantly increase the drift capacity of the columns by about 40% on average.

6. From the white noise tests, both MSF and RSF provide same flexural stiffness for UHPC columns. Moreover, the rubber residue in RSF seems to slightly increase the inherent damping of UHPC columns compared to using MSF, which is again another evidence that seismic bridge columns could be an excellent structural application of economical UHPC with raw RSF, and as such, more future work is recommended to exploit the full potential of using RSF in structural UHPC.

5.5   Acknowledgment

5.6   Data availability

The raw/processed data required to reproduce these findings cannot be shared at this time as the data also forms part of an ongoing study.

5.7   References

[1] Shafieifar, M., Farzad, M., & Azizinamini, A. (2017). Experimental and Numerical Study on Mechanical Properties of Ultra High-Performance Concrete (UHPC). Construction and Building Materials, 156, 402–411.

[2] Russell, H. G., & Graybeal, B. A. (2013). Ultra-High Performance Concrete: A State-Of-The-Art Report for The Bridge Community. (Inc. Henry G. Russell, Ed.; FHWA-HRT-13-060). https://rosap.ntl.bts.gov/view/dot/26387

[3] El-Helou, R., Haber, Z., & Graybeal, B. (2022). Mechanical Behavior and Design Properties Of Ultra-High-Performance Concrete. Materials Journal, 119(1), 181–194.

[4] Wang, D., Shi, C., Wu, Z., Xiao, J., Huang, Z., & Fang, Z. (2015). A Review on Ultra High-Performance Concrete: Part II. Hydration, Microstructure, and Properties. Construction and Building Materials, 96, 368–377.

[5] Graybeal, B., & Baby, F. (2019). Tension Testing of Ultra-High Performance Concrete (FHWA-HRT-17-053). FHWA. https://www.fhwa.dot.gov

[6] PCI Concrete Material Technology Committee. (2022). Guidelines for the Use of Ultra-High-Performance Concrete (UHPC) in Precast And Prestressed Concrete. Precast/Prestressed Concrete Institute.

[7] Nault, G., (2023) "UHPC Bridge Implementations since 2019", International Interactive Symposium on Ultra-High Performance Concrete 3(1): 97.

[8] Graybeal, B. A. (2006). Structural Behavior Of Ultra-High Performance Concrete Prestressed I-Girders (Inc. PSI, Ed.; FHWA-HRT-06-115). https://rosap.ntl.bts.gov/view/dot/38701

[9] Aboukifa, M., & Moustafa, M. A. (2022). Reinforcement detailing effects on axial behavior of full-scale UHPC columns. Journal of Building Engineering, 49, 104064.

[10] Sugano, S., Kimura, H., & Shirai, K. (2007). Study of New RC Structures Using Ultra-High-Strength Fiber-Reinforced Concrete(UFC). Journal of Advanced Concrete Technology, 5(2), 133–147.

[11] Ichikawa, S., Matsuzaki, H., Moustafa, A., ElGawady, M. A., & Kawashima, K. (2016). Seismic-Resistant Bridge Columns with Ultrahigh-Performance Concrete Segments. Journal of Bridge Engineering, 21(9), 04016049.

[12] Gholami, E., Afshin, H., Sharghi, M., & Charkhtab Basim, M. (2023). The Effect Of Tire-Recycled Steel Fibers on the Mechanical, Environmental, and Economic

Performance of Ultra-High Performance and Ordinary Concretes Under Steam Curing Conditions. Journal of Materials in Civil Engineering, 35(8), 04023264.

[13] Chen, G., Zheng, D., Chen, Y., Lin, J.-X., Lao, W., Guo, Y., Chen, Z., & Lan, X. (2023). Development of High Performance Geopolymer Concrete with Waste Rubber And Recycle Steel Fiber: A Study on Compressive Behavior, Carbon Emissions and Economical Performance. Construction and Building Materials, 393, 131988.

[14] Liew, K. M., & Akbar, A. (2020). The Recent Progress of Recycled Steel Fiber Reinforced Concrete. Construction and Building Materials, 232, 117232.

[15] Abdolpour, H., Niewiadomski, P., & Sadowski, Ł. (2021). Recycling of Steel Fibres and Spent Equilibrium Catalyst in Ultra-High Performance Concrete: Literature Review, Research Gaps, and Future Development. Construction and Building Materials, 309, 125147.

[16] Romero, A. J., & Moustafa, M. A. (2023). Material Characterization of UHPC with Recycled Fibers and Wires for Future Large-Scale Structural Applications. Third International Interactive Symposium on Ultra-High Performance Concrete. Third International Interactive Symposium on Ultra-High Performance Concrete. https://doi.org/10.21838/uhpc.16719

[17] Zia, A., Pu, Z., Holly, I., Umar, T., Tariq, M. A. U. R., & Sufian, M. (2022). A Comprehensive Review of Incorporating Steel Fibers of Waste Tires in Cement Composites and its Applications. Materials, 15(21), 7420.

[18] Isa, M. N., Pilakoutas, K., Guadagnini, M., & Angelakopoulos, H. (2020). Mechanical Performance of Affordable and Eco-Efficient Ultra-High Performance Concrete (UHPC) Containing Recycled Tyre Steel Fibres. Construction and Building Materials, 255, 119272.

[19] Yang, J., Peng, G.-F., Shui, G.-S., & Zhang, G. (2019). Mechanical properties and anti-spalling behavior of ultra-high performance concrete with recycled and industrial steel fibers. Materials, 12(5), 783.

[20] Habib, A., Yildirim, U., & Eren, O. (2020). Mechanical and Dynamic Properties of High Strength Concrete with Well Graded Coarse and Fine Tire Rubber. Construction and Building Materials, 246, 118502.

[21] Tazarv, M., and Saiidi, M. S. (2014). "Next generation of bridge columns for accelerated bridge construction in high seismic zones." Rep. No. CCEER-14-06, Center for Civil Engineering Earthquake Research, Dept. of Civil and Environmental Engineering, Univ. of Nevada, Reno, NV.

[22] Tazarv, M., & Saiidi, M. S. (2015). UHPC-filled duct connections for accelerated bridge construction of RC columns in high seismic zones. Engineering Structures, 99, 413-422.

[23] Subedi, D., M. A. Moustafa, M. S. Saiidi, (2019). "Non-Proprietary UHPC for Anchorage of Large Diameter Column Bars in Grouted Ducts," Center for Civil Engineering Earthquake Research, Department of Civil and Environmental Engineering, University of Nevada, Reno, Nevada, Report No. CCEER-19-03, May 2019.

[24] Aboukifa, M., & Moustafa, M. A. (2021). Experimental Seismic Behavior of Ultra-High Performance Concrete Columns with High Strength Steel Reinforcement. Engineering Structures, 232, 111885.

[25] " Standard Test Method for Flow of Hydraulic Cement Mortar." ASTM International - Standards Worldwide, https://www.astm.org/c1437-20.html

[26] " Standard Specification for Flow Table for Use in Tests of Hydraulic Cement." ASTM International - Standards Worldwide, https://www.astm.org/c0230_c0230m-20.html

[27] " Standard practice for fabricating and testing specimens of Ultra-High Performance Concrete." ASTM International - Standards Worldwide, https://www.astm.org/c1856_c1856m-17.html

[28] Naeimi, N., & Moustafa, M. A. (2021). Compressive Behavior and Stress–Strain Relationships of Confined and Unconfined UHPC. Construction and Building Materials, 272, 121844.

[29] Haber, Z. B., De la Varga, I., Graybeal, B. A., Nakashoji, B., & El-Helou, R. (2018). Properties and Behavior of UHPC-Class Materials (FHWA-HRT-18-036). https://rosap.ntl.bts.gov/view/dot/37528

[30] ASCE. (2024). American Society of Civil Engineering 7 Hazard Tool Database. Retrieved from https://ascehazardtool.org/

[31] Dhakal, S., & Moustafa, M. A. (2019). MC-BAM: Moment–Curvature Analysis for Beams with Advanced Materials. SoftwareX, 9, 175–182.

[32] PEER. (2014). Pacific Earthquake Engineering Research Center (PEER) Ground Motion Database. Retrieved from https://ngawest2.berkeley.edu/

[33] "Seismic Design Criteria Version 2.0" (2019). California Department of Transportation (Caltrans). https://dot.ca.gov/programs/engineering-services/manuals/seismic-design-criteria

[34] Naeimi, N., & Moustafa, M. A. (2021). Compressive Behavior and Stress–Strain Relationships of Confined and Unconfined UHPC. Construction and Building Materials, 272, 121844.

[35] Aboukifa, M., & Moustafa, M. A. (2022). Reinforcement Detailing Effects on Axial Behavior of Full-Scale UHPC Columns. Journal of Building Engineering, 49, 104064.

Table 5-1 – Test matrix and experimental variables of UHPC columns

Specimen ID	Connection	Column Material	Long. Rft.	ρ_l [%]	Transverse Rft.	ρ_t [%]
SP1-MSF	UHPC MSF	UHPC MSF	10 #6	2.19	#3 spiral at 3" pitch	1.04
SP2-RSF-G	Grout	UHPC RSF	10 #6	2.19	#3 spiral at 3" pitch	1.04
SP3-RSF	UHPC MSF	UHPC RSF	10 #6	2.19	#3 spiral at 3" pitch	1.04

Table 5-2 − UHPC mix constuients and proportions by weight lb/ft^3 (kg/m^3)

Specimen ID	CT 25	Fine Sand	Cement	Fibers	admixtures	Water
SP1	40.0 (641)	52.9 (847)	48.5 (777)	9.8 (157)	6.6 (106)	7.85 (126)
SP2 & SP3	40.0 (641)	53.4 (855)	48.5 (777)	4.9 (79)	6.6 (106)	7.26 (116)

Table 5-3 – Mechanical properties of UHPC column tested at different ages.

Compressive Strength, ksi [MPa]		E_{cyl}, ksi [GPa]		ε_{cyl} [%]		Tensile Strength, ksi [MPa]		ε_{loc} [%]		Modulus of Rupture, ksi [MPa]		δ_{mod}, in [mm]	
Day 28	Test Date	Day 28	Test Date	Day 28	Test Date	Day 28	Test Date	Day 28	Test Date	Day 28	Test Date	Day 28	Test Date
SP1-MSF													
20.3 [139.9]	22.1 [152.3]	5094 [35.1]	5050 [34.8]	0.52	0.55	1.71 [11.8]	1.68 [11.6]	0.32	0.41	4.83 [33.6]	4.09 [28.2]	0.061 [1.55]	0.075 [1.91]
SP2-RSF-G and SP3-RSF													
16.8 [115.8]	20.1 [138.6]	4696 [32.3]	5090 [35.1]	0.46	0.55	1.29 [8.9]	2.03 [14.0]	0.62	0.97	1.94 [13.4]	2.00 [13.8]	0.049 [1.24]	0.051 [1.30]

Table 5-4 – Compression test results of the footing and grouting materials used in the connection

	Compressive Strength, ksi [MPa]		E_{cyl}, ksi [GPa]		ε_{cyl} [%]	
	Day 28	Test Date	Day 28	Test Date	Day 28	Test Date
UHPC Connection	12.8 [88.3]	17.1 [117.9]	5462 [37.7]	6409 [44.2]	0.26	0.32
Grout Connection	N/A	8.4 [58.1]	N/A	3496 [24.1]	N/A	0.32
Footing	6.8 [46.5]	6.2 [42.8]	N/A	N/A	N/A	N/A

Table 5-5 – Recorded PGA and calculated SA for different DLE levels

Ground Motion	PGA, g				Peak acceleration at column top, g		
	Target	SP1-MSF	SP2-RSF-G	SP3-RSF	SP1-MSF	SP2-RSF-G	SP3-RSF
25% DLE	0.16	0.16	0.13	0.13	0.27	0.31	0.28
50% DLE	0.31	0.29	0.28	0.26	0.44	0.48	0.45
75% DLE	0.47	0.45	0.45	0.43	0.51	0.56	0.51
100% DLE	0.62	0.54	0.56	0.52	0.51	0.56	0.50
125% DLE	0.78	0.67	0.72	0.68	0.53	0.58	0.50
150% DLE	0.93	1.10	0.93	0.82	0.40	0.60	0.50
175% DLE	1.09	N/A	1.31	1.15	N/A	0.40	0.51

Table 5-6 – Key results representing the UHPC columns behavior based on force-drift response

Column ID	Yield Point		Peak Point		Ultimate Point		Displacement Ductility,μ_d
	Drift %	Force, kips (kN)	Drift %	Force, kips (kN)	Drift %	Force, kips (kN)	
SP1-MSF	0.57	20.7 (92)	5.60	40.8 (182)	7.78	32.7 (146)	7.56
SP2-RSF-G	0.79	21.5 (96)	6.80	37.7 (168)	11.98	30.2 (134)	9.08
SP3-RSF	0.77	22.1 (98)	10.97	37.9 (169)	11.13	35.0 (156)	8.75

Table 5-7 – Maximum moment and curvature of the UHPC columns at section 1

Specimen ID	Maximum Moment, kip-in (kN-m)	Maximum Curvature, rad/in (rad/m)
SP1-MSF	2674 (302)	0.0103 (0.41)
SP2-RSF-G	2496 (282)	0.0169 (0.66)
SP3-RSF	2482 (280)	0.0147 (0.58)

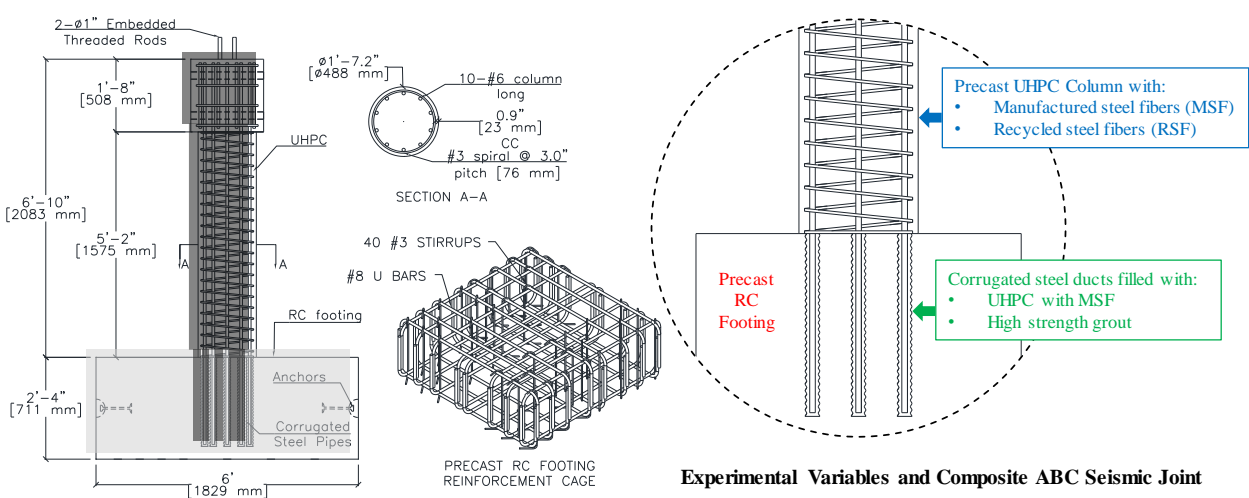**Figure 5-1**. Comparison between RSF and MSF

Figure 5-2. ABC UHPC columns dimensions, reinforcement, and composite joint details

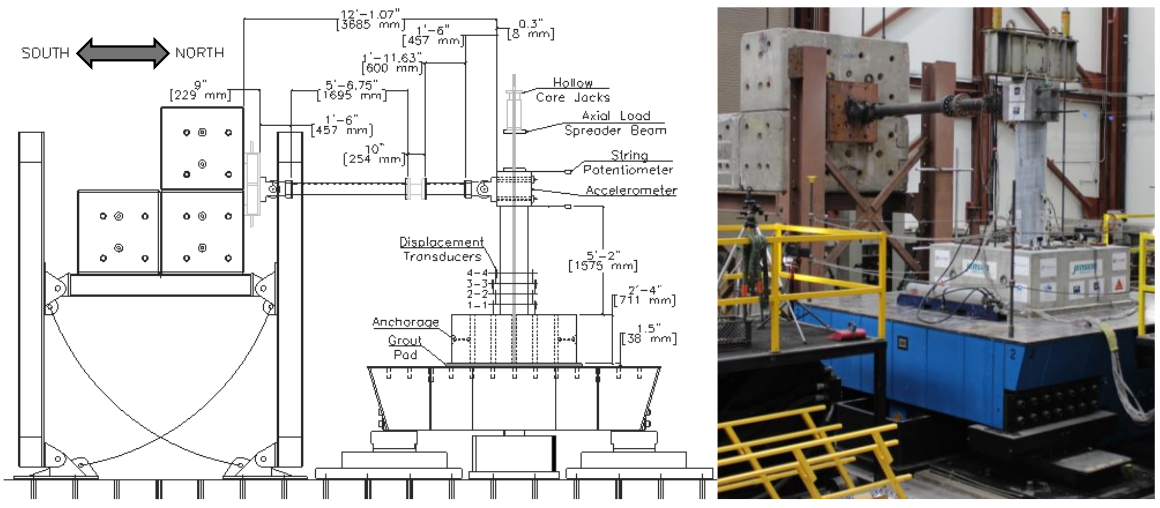**Figure 5-3**. Fabrication, casting, and assembly of UHPC ABC columns

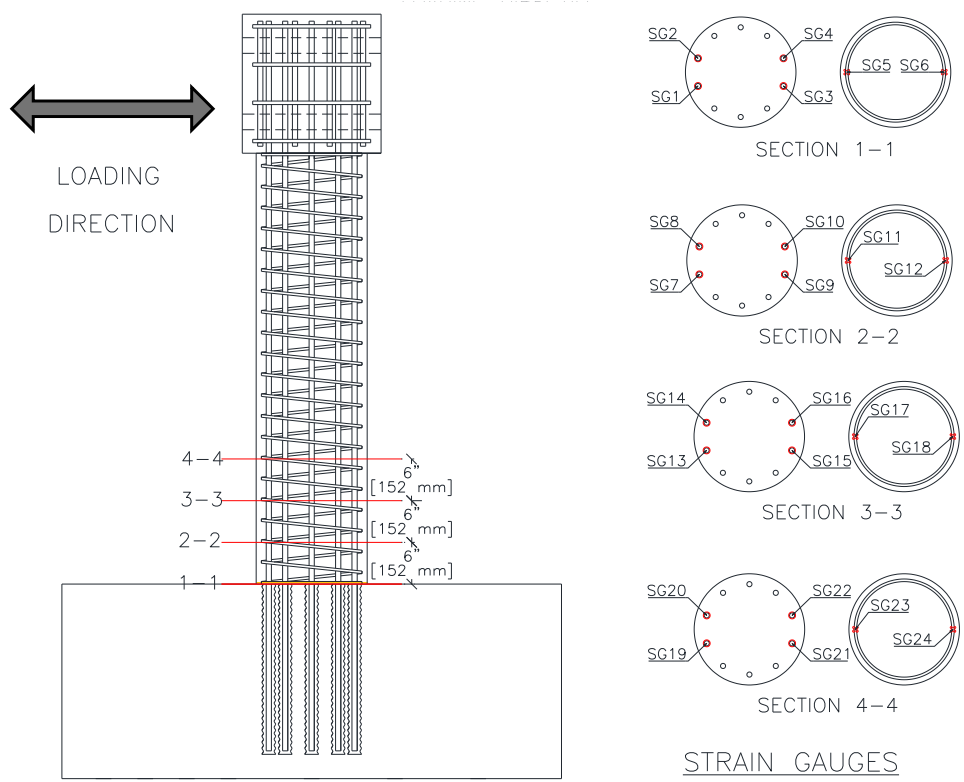**Figure 5-4**. Schematic illustration and actual photograph of shake table test setup

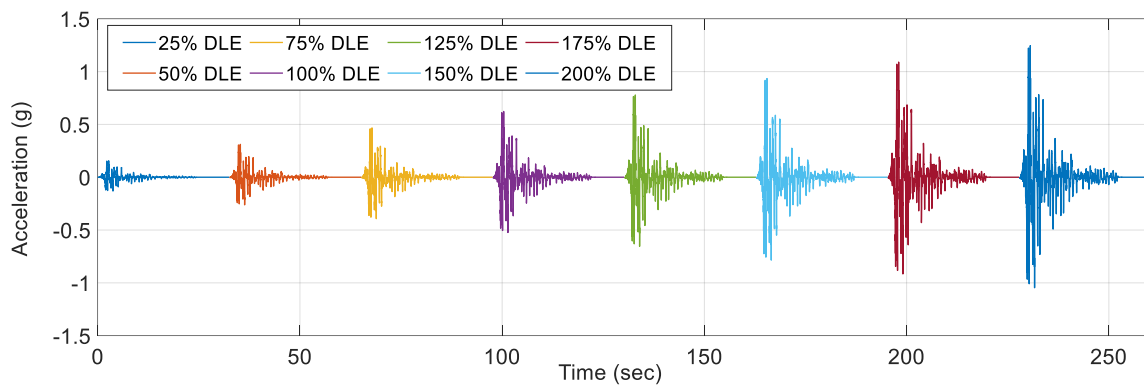**Figure 5-5**. Strain gauges location placement at the longitudinal and transverse reinforcement

Figure 5-6. Stitched loading protocol for shake table tests based on Northridge earthquake ground motion
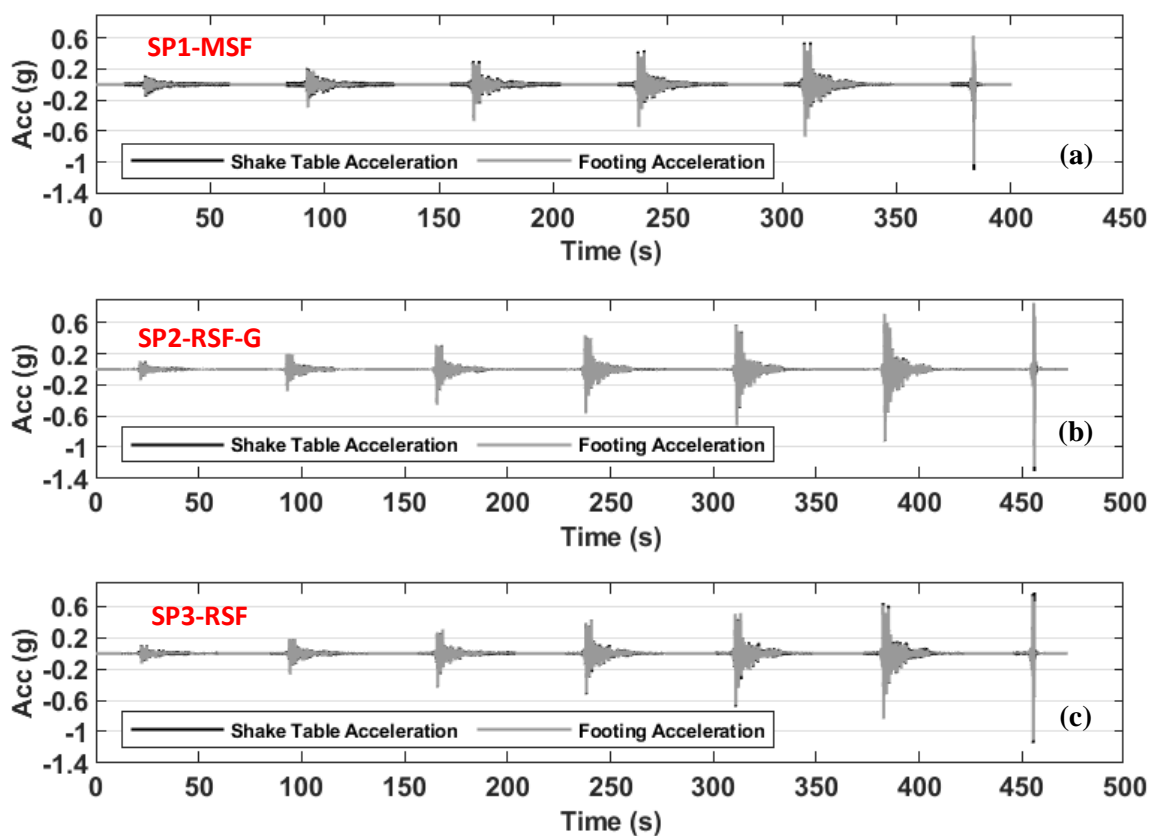
Figure 5-7. Comparison between the shake table and footing acceleration
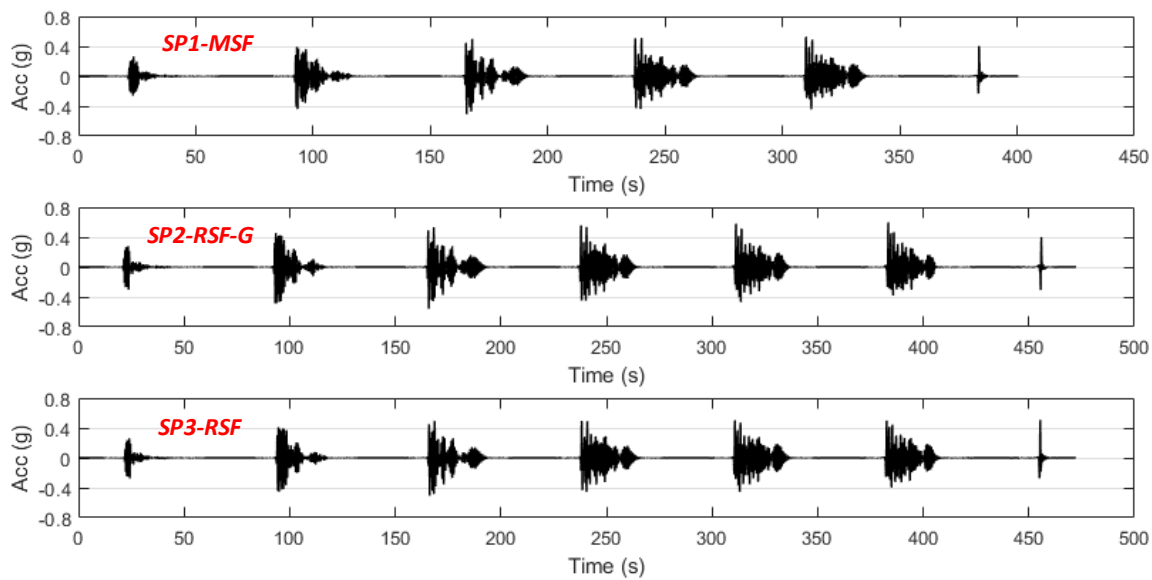
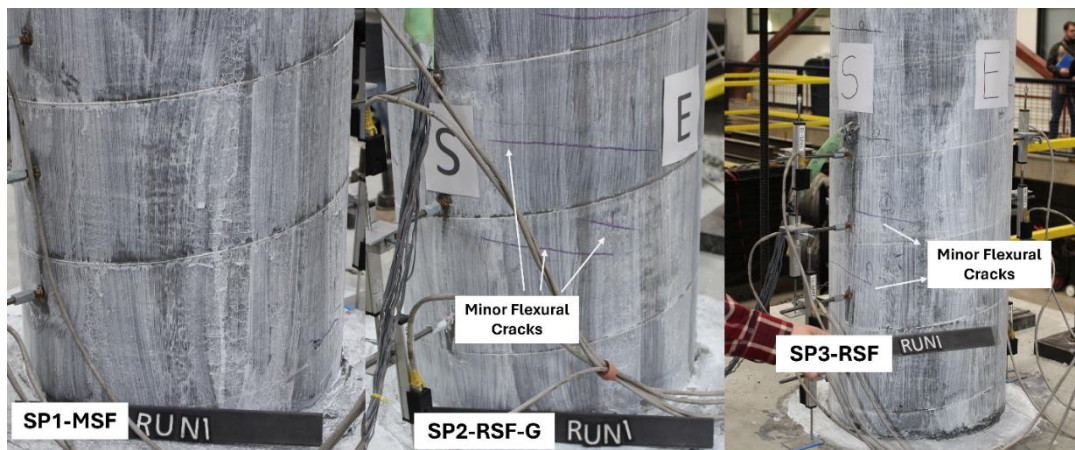**Figure 5-8**. Acceleration time history at the column top obtained for all specimens at all runs
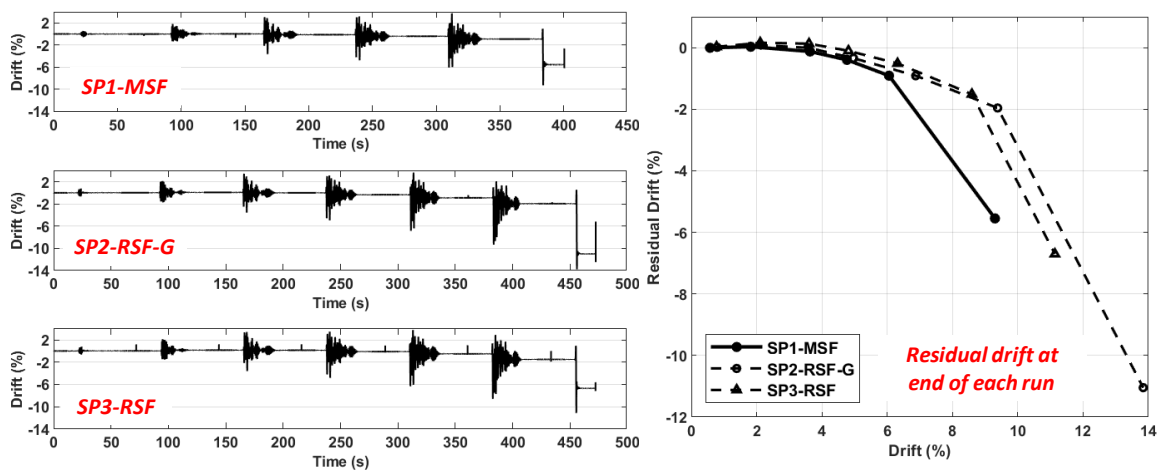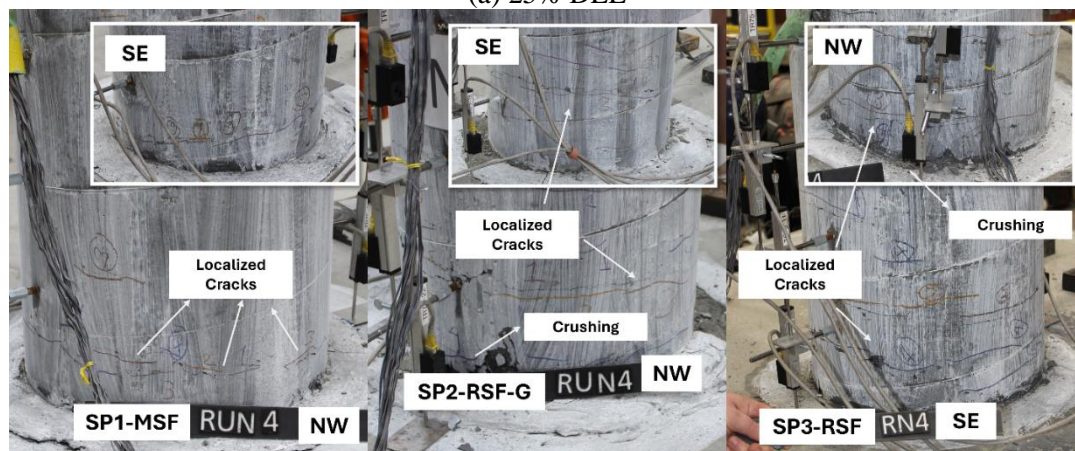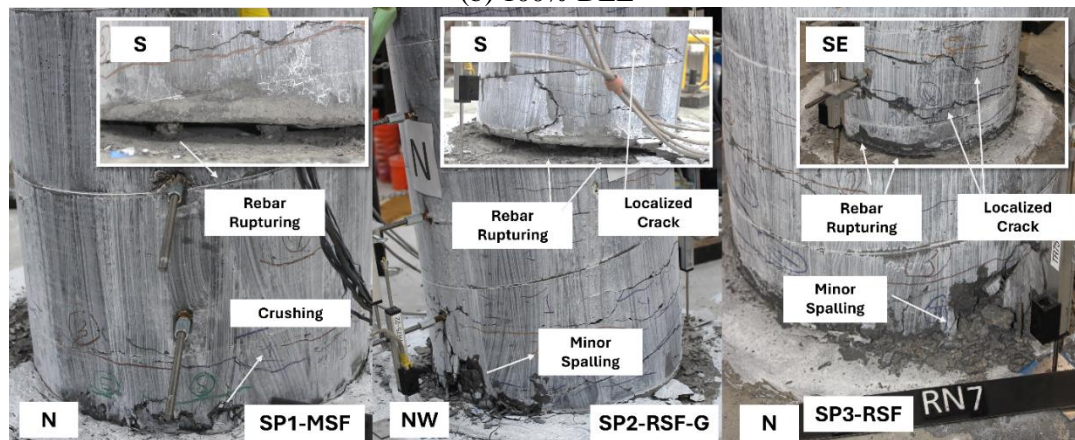

Figure 5-9. Drift ratio time history and residual drift ratio at the end of each run for all UHPC columns

(a) 25% DLE

(b) 100% DLE

(c) Final run (150% or 175% DLE)

Figure 5-10. Photographs of the progression of damage and final damage state for all columns
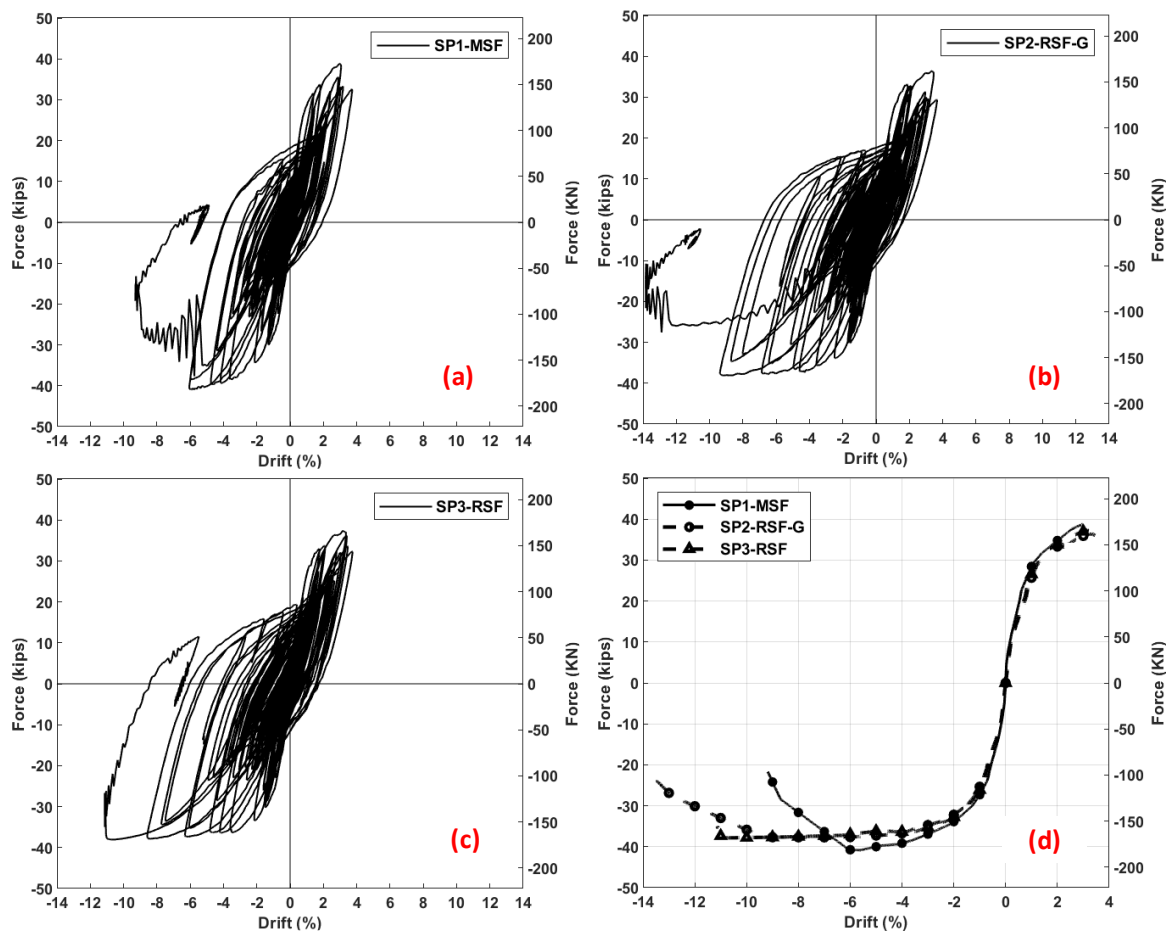
Figure 5-11. Force-drift hysteresis relationships for: (a) SP1-MSF, (b) SP2-RSF-G, (c) SP3-RSF, and (d) envelope comparison of all three specimens together
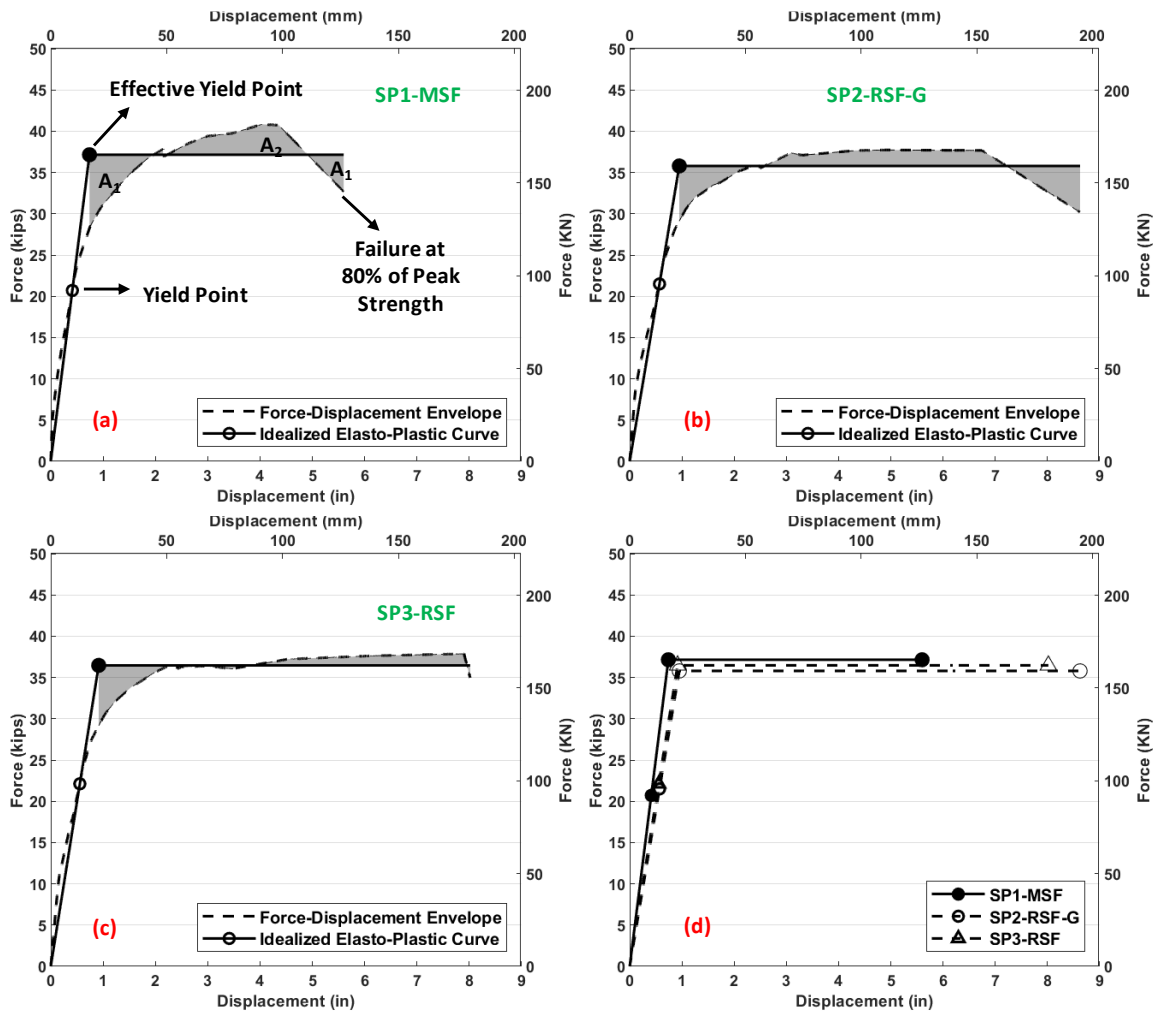
Figure 5-12. Idealized elastoplastic curve based on the average backbone force-displacement curve
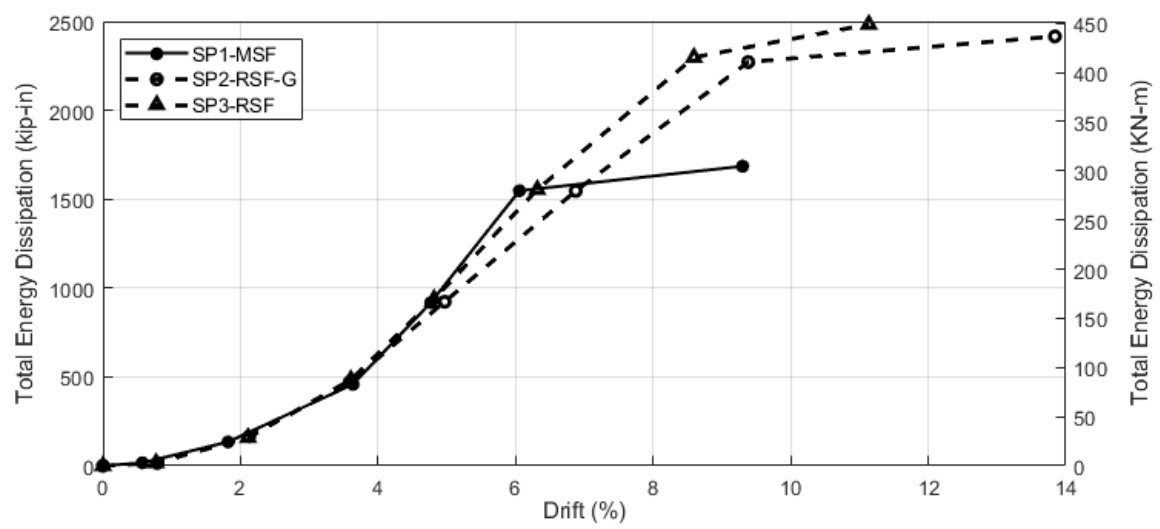
Figure 5-13. Cumulative total energy dissipation of the column.
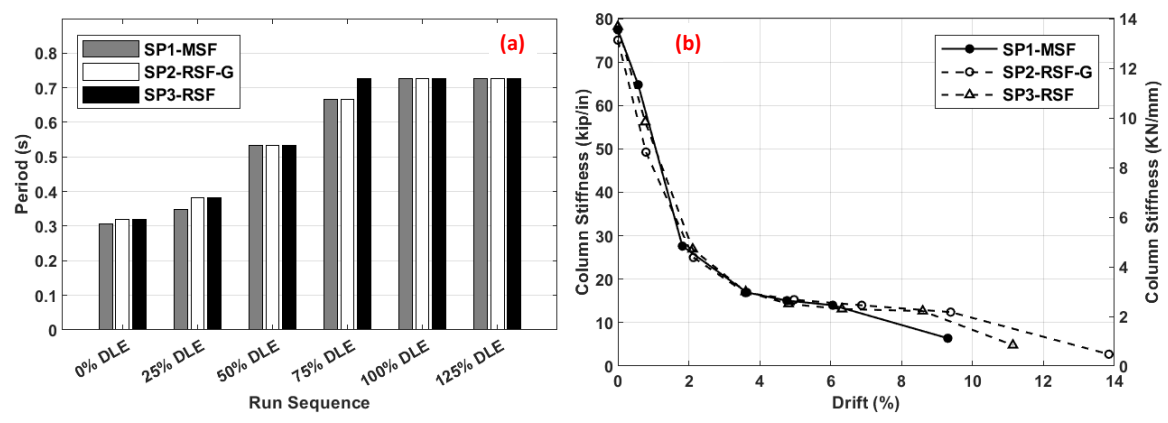

Figure 5-14. (a) Estimated specimens period and (b) column stiffness as obtained from white noise tests
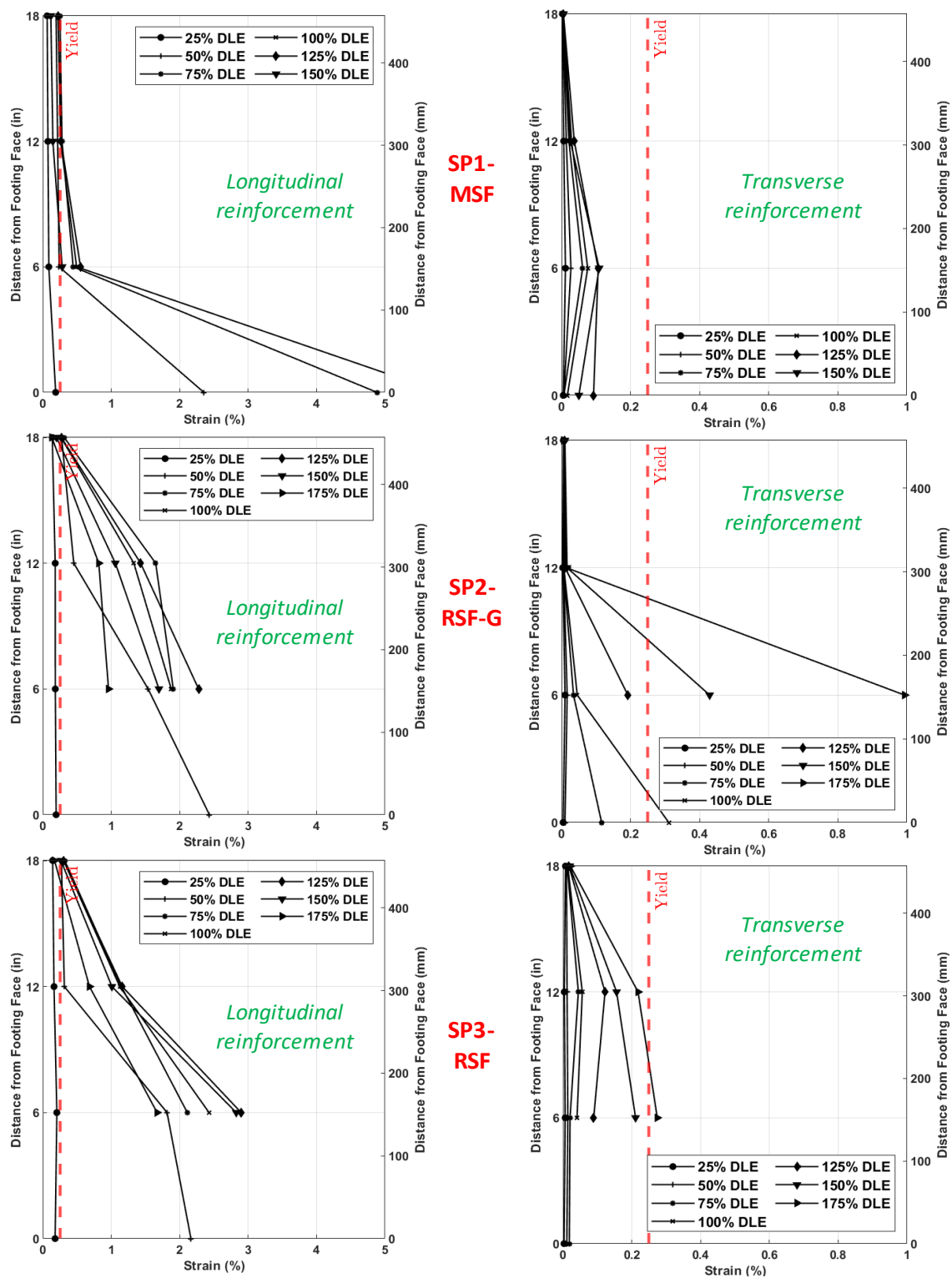
Figure 5-15. Strain profile in selected longitudinal and transverse reinforcement within plastic hinge zone
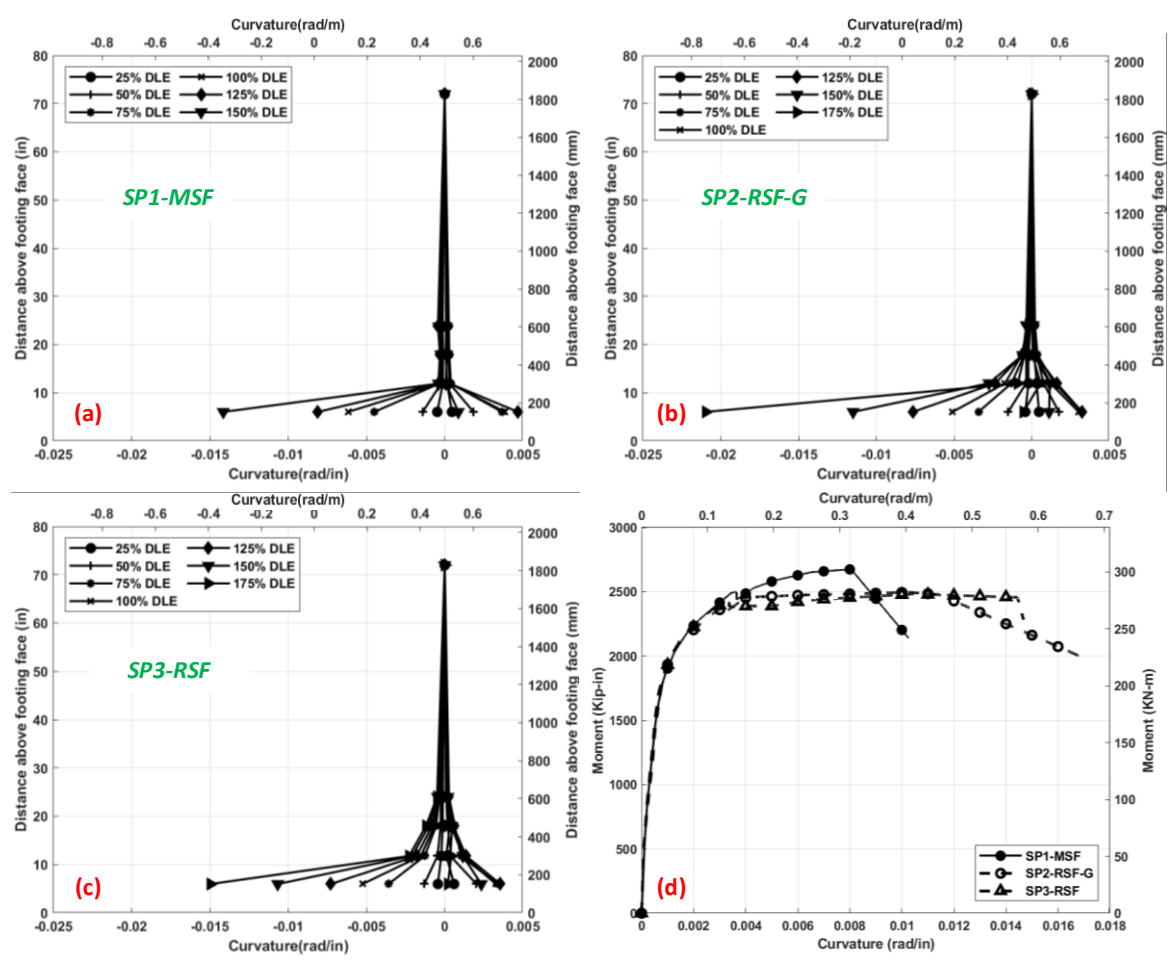
Figure 5-16. (a-c) Curvature profile of each column and (d) moment-curvature of the column at segment 1.

6 SUMMARY, CONCLUSIONS, AND RECOMMENDATIONS FOR FUTURE WORK

6.1 Summary

The utilization of UHPC for large-scale precast applications has been a subject of growing interest because of its inherent superior mechanical properties and durability, which aims to improve the resiliency and longevity of future infrastructure against increasing natural hazards and extreme events. Nevertheless, the high cost of UHPC, along with its high carbon footprint, presents challenges for production at scale for purposes of full precast UHPC components or structures, and efforts to improve the cost of UHPC have been a major research focus in the past decade. To continue along these lines, this doctoral study seeks to develop an economical and eco-friendly (eco^2) UHPC for the next generation of precast structures. The specific research objectives are to (1) conduct a material characterization of recycled steel fibers (RSF) with varying aspects and fiber ratios in eco^2-UHPC and explore the scalability of such fibers with different mixing techniques, (2) examine the axial performance of full-scale eco^2-UHPC columns with wide-range of locally sourced and sustainable components like RSF, (3) implement large-scale truck mixing of eco^2-UHPC and demonstrate its validity for ABC bridge columns that use eco^2-UHPC with MSF and RSF and different ABC connections and tested under combined axial and lateral cyclic loading, and (4) perform shake table testing of eco^2-UHPC scaled columns with ABC grouted duct connections to understand

the dynamic behavior of UHPC columns. Each research objective is presented as a separate paper, but a brief overview is provided in the following paragraphs.

To demonstrate the feasibility of eco^2-UHPC, a series of 13 UHPC material batches were produced incorporating two distinct types of RSF with varying fibers characteristics. The RSF types possess varying fibers aspect ratio, which is shown in this work to be a key factor in influencing the UHPC fresh and hardened properties. Both RSF types were analyzed at different fiber ratios and contrasted with UHPC with typical manufactured steel fibers (MSF). A full material characterization was conducted in accordance with existing specifications and studies for testing UHPC, specifically to characterize compressive, tensile, and flexural behavior. Next, full material characterization was developed, focusing on locally sourced aggregate and cement. In total, 13 batches were produced by modifying the aggregate source and gradation, moisture levels, cement type, mixer type, and curing method. Similarly, the compressive strength gain, direct tensile, and flexural performance of each batch were evaluated. The results of these tests were used as guidelines for developing mixes for production scale mixing and batching.

To assess the performance of eco^2-UHPC, five full-scale axial columns, varied in reinforcement ratio, fiber type, and fiber ratio, were fabricated at UNR fabrication yard using a small production IMER 360 Mortarman high-shear mixer. This resulted in five batches for each UHPC column, and casting took over two days. The columns were left to cure for two weeks before removing the formwork and were then transported to the PEER Laboratory at UC Berkeley, where they were tested using a 4000-kip big press machine. The columns were loaded axially at 1 kip/sec, and the test was stopped after the

column failed. The force-deformation was captured using a load cell and LVDTs attached to rods of different heights along the column. The strain was recorded using multiple strain gauges placed at select sections of the transverse and longitudinal reinforcements.

The second phase of the large-scale experimental campaign was conducted using seven eco^2-UHPC columns with different ABC connections. Unlike the axial columns, the specimens were fabricated in a full-production precast facility in California where 52-ft^3 truck mixers were used for producing the UHPC with different fibers types. The column specimens were cast in two batches, initially casting UHPC with MSF followed by UHPC with RSF. Likewise, the footings were fabricated at a local precast facility in Sparks, Nevada, and were cast in a regular pan mixer using conventional concrete. The specimens were transported to the EEL fabrication yard and were assembled using proper grouting materials like UHPC for the different connections. Two sets of identical columns were tested under quasi-static cyclic testing to compare the structural response of UHPC columns with MSF and RSF and assess the performance of the ABC pocket and grouted duct connections for this application. The columns were loaded at an increasing drift ratio, and the test was terminated when sufficient rupturing reinforcement was observed.

Moreover, three columns were tested using one of the biaxial shake tables at EEL with the objective of investigating the dynamic response of UHPC columns during earthquake ground motion. Specifically, the aim was to compare the response of UHPC columns with MSF and RSF, while also observing the influence of different grout materials in the connections. The 1994 Northridge Earthquake Sylmar Converter Station was utilized to

adopt the testing ground motion for the columns, with the ground motion incrementally increased until the column reached its ultimate capacity. The performance of each specimen was captured through heavy instrumentation, collectively obtaining important information such as drifts, force, acceleration, period, curvature, etc. Overall, design and detailing recommendations were developed based on the experimental tests as enumerated in the following section.

6.2   Key Findings and Conclusions

After conducting comprehensive experimental tests, the conclusions from this doctoral study were presented individually in Chapters 2 through 5. However, an overview of the major key findings and conclusions are collected and summarized here for completeness:

- Small and large production-scale mixing of eco^2-UHPC was successfully demonstrated using different mixing equipment; however, RSF with high aspect ratio must be carefully handled either by using high-shear mixers or use further processing and sorting to allow for higher fibers dosage without fiber clumping and segregation.

- Incorporating locally sourced aggregate and cement in eco^2-UHPC showed acceptable workability and mechanical properties. Only minor adjustments might be needed to utilize recently proposed design equations for this class of UHPC. For example, a K_1 factor of 0.8 is proposed to use instead of default value of 1.0 for this UHPC type to apply the new AASHTO guide specification equation for predicting the modulus of elasticity of UHPC.

- The aspect ratio of RSF is a crucial factor in eco^2-UHPC. A lower aspect ratio can improve workability but negatively affect tensile and flexural performance. A higher aspect ratio can yield better flexural performance but can lead to fiber segregation, especially with a high fiber ratio. Thus, RSF UHPC has to be engineered based on the specific target application.

- The UHPC RSF has comparatively lower first cracking strength than the UHPC MSF, which leads to an overall decrease in localization strength. Furthermore, low aspect ratio RSF can lead to lower strain localization, but high aspect ratio RSF can improve this aspect.

- Adequate transverse reinforcement is still required and recommended for the confinement of UHPC columns under pure axial loading. However, raw RSF can be readily used as an alternative to MSF for axial columns, as there is no significant difference in the compressive behavior or axial load strength. Meanwhile, decreasing the fiber ratio to 1.0% by volume is another cost-saving approach that has a minor impact on the overall axial load strength.

- Regardless of the type of ABC connection, UHPC columns with RSF exhibited higher ductility but slightly lower lateral force than their counterpart columns with MSF. This suggests that the UHPC columns with RSF exhibit higher energy dissipation but at the cost of more damage in the plastic hinge zone.

- The presence of fiber bridging micro-cracks helped reduce the damage and crack propagation at the plastic hinge zone of the columns. UHPC columns with MSF showed localized cracks at the plastic hinge zone with almost no sign of spalling

or crushing. However, UHPC columns with RSF showed multiple flexural cracks at the plastic hinge, as RSF allowed micro-cracks to develop while bridging and holding macro-cracks in place.

- The utilization of RSF in precast columns does not have any impact on the flexural stiffness of the column. Overall, RSF in precast columns demonstrated promising results that can be further improved and explored in future infrastructure projects.

6.3   Mix Design and Detailing Recommendations

Based on the construction and experimental work performed in this study, the following mix design and detailing are recommended for future work in UHPC:

- Increasing the fiber ratio of RSF with low aspect ratio is recommended to improve the tensile and flexural strength. Conversely, to prevent the segregation of fibers, the dosage of RSF with high aspect ratio should be limited to 1.6% or less. Conveyors can be employed to ensure an even distribution of fibers in the mixer. Additionally, high-shear mixers may be utilized to disentangle any matted fibers caused by the distorted nature of RSF.

- Locally sourced aggregate, preferably finer grade for better workability, can be employed in developing eco^2-UHPC. Depending on the requirement, cement with high sulfate resistance can be used, but general cement can also be an option. Curing with higher temperatures can accelerate the compressive strength gain at initial days.

- A high-shear mixer is still recommended for the production of eco^2-UHPC. However, truck mixing also provides an opportunity for large-scale mixing, which can be beneficial in the current precast production.

- Adequate transverse reinforcement detailing should be performed for UHPC under axial loading to fully benefit from the superior compressive strength of UHPC.

- RSF with a low aspect ratio can be used for precast columns under pure axial loading. However, UHPC columns subjected to combined axial and bending should incorporate RSF with high aspect ratio to resist macro-cracks formation and minimize damage.

- ABC pocket connections are recommended to use with UHPC precast columns. In general, ABC pocket connections provide the most efficient construction with minimal intervention when columns are assembled into the footings. Furthermore, the continuity of the UHPC column into the footing avoids any cold joint, that can cause strain concentrations and prematurely rupture the reinforcement, and allows for a good strain distribution in the plastic hinge zone.

- Conventional footings can be used for UHPC bridge columns with ABC connections to minimize the overall piers cost. Embedment criteria, as suggested by the current AASHTO specifications for ABC column connections, can be sufficient for UHPC columns. However, the use of UHPC in lieu of conventional grout in the field joints is suggested to minimize bond slip failure.

6.4   Recommendation for Future Work

Despite the heavy experimental work presented in this doctoral study, the scope of the work did not cover everything and there are more research questions to address in future studies. The following list provides suggested topics to be explored for future UHPC experimental tests and analyses that can stem from this doctoral work:

- Additional experimental work is required to evaluate and improve the workability of UHPC with RSF of high aspect ratio. Moreover, a new method for measuring the flowability of high aspect ratio fibers should be explored, as the current flow table equipment causes the fibers to clump and does not allow for fair evaluation of the mixture consistency, workability, and flowability.

- A standard method to determine and predict the crack localization of UHPC should be further studied. Additionally, the relationship of strain localization at the material and structural level should be explored. In fact, there is room for further assessment of current analytical and computational models or develop new constitutive models for various aspects of the mechanical behavior of economic or lower-end UHPC mixtures.

- Debonding of reinforcement in the plastic hinge zone of UHPC columns should be explored to avoid strain localization and potentially improve ductility. Furthermore, quantifying the region of crack localization within the plastic hinge zone can be further investigated.

- Additional experimental work emphasizing reduced transverse reinforcement or exploring the use of high aspect ratio fibers for structural seismic UHPC columns should be considered. Nonetheless, numerical analysis and modeling of UHPC

columns can be explored to calibrate existing macro-models or fiber-element modeling and validate for UHPC structural and seismic applications.

- More experimental tests should be performed focusing on the bond-slip contribution to the column's overall relative drift, particularly for conventional grouted duct connection.